Integrated Project (IP)
Project No. TIP5-CT-2006-031415

Thematic Priority 6:
Sustainable Development,
Global Change and Ecosystems

Recommendation of, and scientific basis for, minimum action rules and maintenance limits

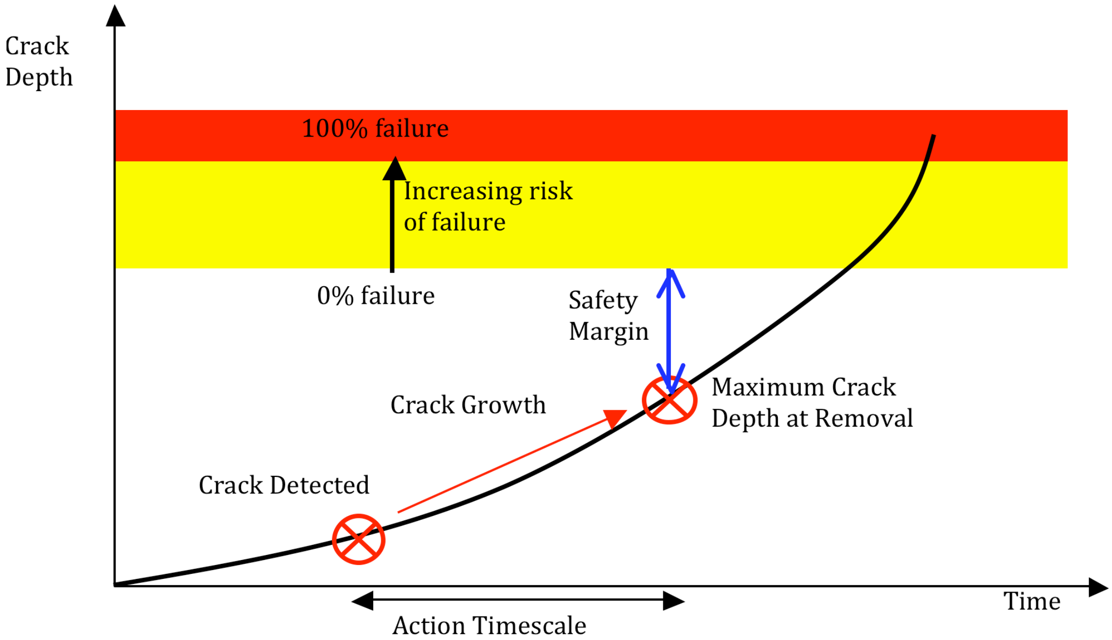

INNOTRACK GUIDELINE

Deliverable report D4.2.6

Table of Contents

1. Contributions

Main contributors to the different chapters are:

Chapter 3:	Rob Carroll, Corus Rail, and Richard Stock, voestalpine Schienen (Rob.Carroll@corusgroup.com, Richard.Stock@voestalpine.com)
Chapter 4:	Zili Li, TU Delft (Z.Li@tudelft.nl)
Chapter 5:	Jens Nielsen, Anders Ekberg and Elena Kabo, Chalmers (Jens.Nielsen@chalmers.se, Anders.Ekberg@chalmers.se, Elena.Kabo@chalmers.se)
Chapter 6:	Francis Franklin, University of Newcastle (F.J.Franklin@ncl.ac.uk)
Chapter 7:	Johan Sandström, Jóhannes Gunnarsson, Elena Kabo and Anders Ekberg, Chalmers (Johan.Sandstrom@chalmers.se, JohannesG@gmail.com, Elena.Kabo@chalmers.se, Anders.Ekberg@chalmers.se)
Chapter 8:	Roger Allen, Corus Rail (AllenDrR@aol.com)
Chapter 9:	Francis Franklin, University of Newcastle (F.J.Franklin@ncl.ac.uk)
Chapter 10:	Anders Ekberg, Jens Nielsen and Elena Kabo, Chalmers (Anders.Ekberg@chalmers.se, Jens.Nielsen@chalmers.se, Elena.Kabo@chalmers.se,)
Chapter 11:	Roger Allen, Corus Rail (AllenDrR@aol.com)
Chapter 12:	René Heyder, DB, and Rolf Dollevoet, ProRail (Rene.Heyder@deutschebahn.com, Rolf.Dollevoet@prorail.nl)

2. Executive Summary

A "Minimum Action", in the context of this guideline, is the least action needed from a responsible track engineer to ensure that the track remains safe, reliable and operational on discovery of a broken or defective rail or weld. There is a massive potential LCC saving in defining optimal minimum action rules since this would mean a minimization of inspection and maintenance while at the same time ensuring reliability and avoiding malfunctions and failures.

The focus of the guideline is on some key topics, briefly summarized in the introduction. The main objective is to give operational guidelines. However, to motivate these, overviews of the topics and research outcomes that these guidelines are based on need to be presented.

To this end, the guideline starts by evaluating the current state-of-the-art with the conclusion that even for the rather similar railways investigated the current minimum actions differ significantly. This indicates a major potential for optimisations and implies that any attempt towards harmonisation has to be based on a solid scientific basis.

The subsequent chapters deal with the following topics:

Chapter 4 – Squats. Guidelines regarding preventive and corrective countermeasures, detection and design against squats are provided. In defining these guidelines, key investigations concern which surface defects that will develop into squats and how such squats subsequently grow.

Chapter 5 – Corrugation. The main result is a scientifically sound, and operationally validated, procedure to define operational acceptance criteria of allowed rail corrugation that accounts for both noise emission and rolling contact fatigue.

Chapter 6 – Wear. Based on testing and simulations, operational guidelines on wheel and rail steel selection, accounting for the influence of weather conditions in wear management, how to carry out wear predictions etc, are provided.

Chapter 7 – Insulated joints. A procedure to define operationally allowed joint dips is presented. In addition guidelines on defining insulating gaps and introducing joint modifications are given based on simulation results.

Chapter 8 gives an overview of the three following chapters that all deal with rail cracks.

In chapter 9 the focus is on small surface cracks and in particular the influence of short-range wheel irregularities on the loading of these. The main result is a guideline for how detailed wheel and rail surfaces need to be characterised in numerical simulations.

In chapter 10 the focus is on larger wheel irregularities, mainly wheel flats. The chapter contains a scientifically sound procedure to prescribe allowed wheel impact loads. Further detailed recommendations for practices to avoid rail breaks are given.

In chapter 11 a probabilistic approach is taken. As compared to the approach in chapter 10 this has the benefit of facilitating an assessment of rail crack growth and rail breaks also in cases when wheel–rail impact forces are not explicitly measured. Further it makes possible an analysis of different "what if" scenarios.

Finally chapter 12 tackles probably the most relevant question from an infra-managers point of view: What is the LCC benefit of implementing the current guideline. As discussed in the chapter it is difficult, close to impossible, to give exact quantifications. However, by examining provided costs for RCF mitigation from DB and ProRail two things are clear: Firstly, there is a potential in massive LCC savings by employing systematic and scientifically sound mitigating actions. Secondly, the consequences of a "laissez-faire" approach are devastating: Not only would a post-active approach that deals with problems when they arise bust maintenance budgets. It would also eventually result in a railway that is unreliable and, in a longer perspective, unsafe.

It is our hope and belief that this guideline will benefit the continuous improvement of design, operation and maintenance procedures of the railway sector towards even more competitive, reliable and cost-efficient railway operations.

3. Introduction and current state-of-the-art

3.1. Background

A "Minimum Action", in the railway context, is the least that the responsible track engineer can do to ensure that the track remains safe on discovery of a broken or defective rail or weld.

All railway Infrastructure Managers (IM's) undertake routine inspection, both visually and using non-destructive inspection techniques, such as ultrasonic or eddy current inspection. Once a defect has been found the question arises whether its severity is an immediate safety risk or a long-term risk. The minimum actions are guidelines worked to by all track engineers and specify the actions to be taken to ensure the integrity of the railway.

If the defect is an immediate safety risk then the requirement can be as severe as immediate blocking the line until it is repaired. With less severe defects the requirements are usually timescales for removing or repairing the defect while carrying out no immediate action. It must be emphasised that these are the minimum actions required and that the engineer must use his own judgement to decide if more severe actions are required depending on local circumstances.

Figure 3-1 demonstrates simply how these actions are implemented to ensure the safety of the railway for a crack in a rail. After initiation, cracks grow as time increases, initially they will be present but will not be discovered by inspection. Only when they have grown to such an extent will they be detected either visually or by non-destructive inspection. On detection the track engineer has to decide if it is a current risk that requires immediate removal or will become a risk in the future. The minimum action rules are used as a guide to this decision, since they specify a timescale in which the defect has to be removed, and during this period the crack will continue to grow until it is removed. The aim of the rules is to ensure a margin of safety remains even at the end of the action timescale.

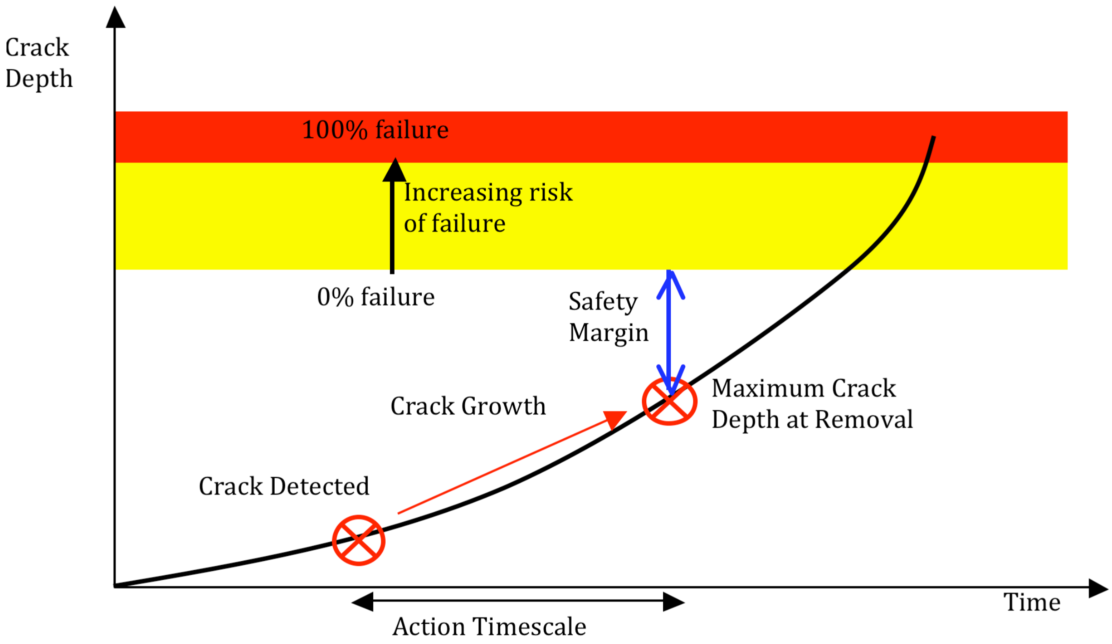

Figure 3-1 Schematic of crack growth and effect of minimum actions

3.2. Current Minimum Actions

All Infrastructure Managers have there own minimum actions, taking into account the maintenance and inspection regimes and the type of traffic of the different railways. These minimum actions are largely based on many years of past experience of defects with little scientific understanding supporting them.

To provide an understanding of current practice of, and variation between, the different IM's involved within the INNOTRACK project, a survey of Minimum Actions for selected defects has been undertaken for Network Rail, ÖBB, Prorail, Banverket and DB; also included are the UIC guidelines. The documents used are included in the Bibliography.

All of the minimum action rules give limits of defects in terms of lengths measured visually or with ultrasonics and/or depths measured using ultrasonic or by eddy current system. There are also often constraints on defects in terms of location in respect to sleepers and joints or welds. The timescales specified can be immediate and are usually applied to mitigating measures such as speed limits or emergency clamps, or they can be for longer timescales. The longer timescale are the maximum time before which a defect has to be removed from track, through repair or rail replacement.

Unfortunately these timescales are unknown for ÖBB. The minimum actions used are for the most intensively used track categories.

The following sections are only summary tables compiled after translation. Some details may have been missed during translation and simplifications have been made to allow easy representation. Only the original document in the original language should be used by track engineers to determine the actions required on discovery of a defect.

3.2.1. Transverse break

Transverse breaks can result from a number of causes including defective welds, tache oval, rail foot corrosion, RCF etc. An example of a transverse break through a weld is shown in Figure 3-2. A summary of the minimum actions is in Table 3-1.

Figure 3-2 Transverse break through an aluminothermic weld

Breaks of this type are often found by visual inspection by maintenance personnel after track circuits have failed or after reports of rough riding by on-train staff. This type of break only applies to vertical transverse breaks and not to beaks at an angle The definition of transverse depends on the IM, Network Rail use a definition of 50mm out of vertical from head to foot of the rail.

For all infrastructure managers the usual action is to immediately stop all traffic. For Prorail and the UIC guidelines the requirement is to carry out a permanent fix before it can reopen. Network Rail (NR), BV, DB and ÖBB allow traffic to resume with speed limits if an emergency clamp can be installed. NR and DB also take into account the position of the break in relation to a joint or weld. Breaks nearer to joints are deemed to be more dangerous than those further away. In contrast ÖBB also take into account the location of the break in relation to sleepers with a lower risk being deemed if the break is over a sleeper, as emergency clamps are not required to keep the line open. For Banverket and Network Rail the separation of the broken rail ends dictates the emergency speed restriction once clamps have been fitted.

Although there are differences between IM's the minimum actions required on discovery of a transverse break are all similar for all IM's.

Table 3-1 Comparison of Minimum Actions for Transverse Breaks

IM	Constraint		Emergency action	Timescale
NR	All	≥75mm	Block Line	Immediately
	Through a weld	≤50mm Gap	5mph[8km/h] (if break is permanently inspected)	Immediately
			20 mph [32km/h] with clamps	Immediately
		50mm < Gap < 75mm	5 mph [8km/h] with or without clamps(if break is permanently inspected)	Immediately
	At or within 1.8m of fishplated joint	All Gaps	Block Line	Immediately
	Within 1.8m of weld	All Gaps	Block Line	Immediately
			5 mph[8km/h] with clamps	Immediately
	1.8 <L< 3m from weld or fishplated joint	All Gaps	Block Line	Immediately
			5 mph[8km/h] with clamps	Immediately
	>3m from weld or joint	≤50mm Gap	5 mph[8km/h]	Immediately
			20 mph [32km/h] with clamps	Immediately
		50mm < Gap < 75mm	5 mph[8km/h]	Immediately
DB	Within 2 ballast bays of joint		Block Line	Immediately
			5 km/h with clamps (if break is permanently inspected)	Immediately
	2 or more ballast bays from a joint		20 km/h with clamps (higher Vmax for longer distance to next joint is defined)	Immediately
			20 km/h (if break is permanently inspected)	Immediately
ÖBB	Mid Sleeper bay		Block Line	Immediately
			10 km/h with clamps or packed under break	Immediately
			60km/h with clamps and packed under break	Immediately
	Over sleeper		10km/h	Immediately
			60km/h when packed with wooden sleeper and clamps	Immediately
BV	Crack Opening ≤ 25mm		70 km/h with clamps	72 hours
	Crack Opening > 25mm		40 km/h with clamps	72 hours
ProRail	All		Block Line	Immediately
UIC	All		Block Line	Immediately

3.2.2. RCF - Squats (UIC712R Code = 227)

Squats are a form of rolling contact fatigue (RCF) that appears as a discrete defect often with a localised widening of the running band. Squats can be observed visually during track walking or ultrasonic equipped trains can find their location. In most cases after discovery, they will then be inspected manually using ultrasound by trained personnel. The summary of the minimum actions for squats is given in Table 3-2. To remove a squat the action can be to replace the rail or to grind down to the bottom of the defect and weld repair. As an indication, Network Rail commonly weld repair squats less than 22mm deep using the Thermit head repair process (with arc repair the depth is less due to the time taken to grind the defect out), anything greater requires the rail to be replaced.

In contrast to rail breaks there is a wide range of parameters specified by the different IM's for intervention on discovery of squats, there is also a large difference in the specified timescales. Of note is that the UIC guidelines are not used or even approximated to by any IM. Although Prorail have similar intervention depths of 10 and 25mm, the timescales are widely different with Prorail being more conservative than the UIC guidelines for cracks between 10 and 25mm but more liberal once a crack is greater than 25mm if emergency clamps are fitted. It is difficult to compare the Banverket requirements as they are based on a comparison to the ultrasonic response from a calibrated 5mm diameter flat bottom hole (FBH) and not an actual depth of crack.

One ambiguity when trying to compare the different documents is what is actually meant by depth of a defect. In most cases this is assumed to be the maximum extent to which it has propagated below the surface. But for non-surface-breaking cracks it can also be interpreted as the location of the defect below the surface.

One surprising difference between the IM's is the speed restrictions put in place once cracks have reached a certain depth. These are plotted in Figure 3-3. The speed restrictions have to be applied once cracks have reached a certain depth and/or length. For ÖBB this is a depth of 10mm and a length of 50mm and the speed limit is 10 or 60km/h depending on the fitting of emergency clamps and supporting the defect by under packing. In contrast DB have an intervention depth of greater than 20mm and a speed limit of 120km/h with a higher speed limit if a different type of clamps is used. Network Rail and Prorail have much lower speed limits of 32 and 40km/h, both at depths greater 25mm.

Table 3-2 Comparison of Minimum Actions for Squats (227)

IM	Length	Depth	Emergency action	Timescale
UIC	L>200mm	or >25mm		2 weeks
			Fit clamps	6 weeks
	50<L<=200mm	or 10<D<25mm		12 months
	<=50mm	or <10mm	Re-inspect	Normal inspection interval
ProRail		>50% (>25mm) head height	40km/h	As soon as possible
			or fit clamps	3 months
		20% (10mm) < D< 50% (25mm) head height		4 weeks
		<20% (10mm) head height		3 months
		No ultrasonic response	Re-inspect visually	6 months
DB	L > 30mm	or: > 20mm	Single squat: 120km/h (160km/h) with clamp (different kind) Multiple squats or squat in conjunction with Head Checks: 20km/h	Immediately
	10mm< L ≤ 30mm	or 10mm< Depth ≤ 20mm	Single squat: Repair Multiple squats: Rerail	Before next inspection
	<10mm	No eddy current or ultrasonic response	Repair weld	
NR	Length > 50mm	>25mm Deep	20mph [32km/h] & Clamps	Rectify within 7 days
		15 < D ≤ 25mm	Fit clamps	7 days
		10 < D ≤ 15mm	Fit clamps	13 weeks
		1 < D ≤ 10mm	Fit clamps	13 weeks
		No ultrasonic response	Fit clamps	13 weeks
	Length ≤ 50mm	>25mm Deep	20mph [32km/h] & Clamps	7 days
		15 < D ≤ 25mm	Fit clamps	7 days
		10 < D ≤ 15mm	Fit clamps	13 weeks
		1 < D ≤ 10mm	Re-inspect at normal frequency	

ÖBB	>50mm	>10mm	Block line	Immediately
			10km/h with clamps or under packed	
			60km/h with clamps and under packed	
	Mid sleeper bay			
	<50mm	<10mm	30km/h	
			100km/h with clamps and under packed	
	Over sleeper			
	<50mm	<10mm	30km/h	
			100km/h with clamps	
BV	Any length	Detection amplitude ≥5mm ϕ FBH, depth ≥10mm		1 month
		Depth less than above		Re-inspect
	L ≥ 100mm	No ultrasonic response		1 month
	L < 100			Re-inspect

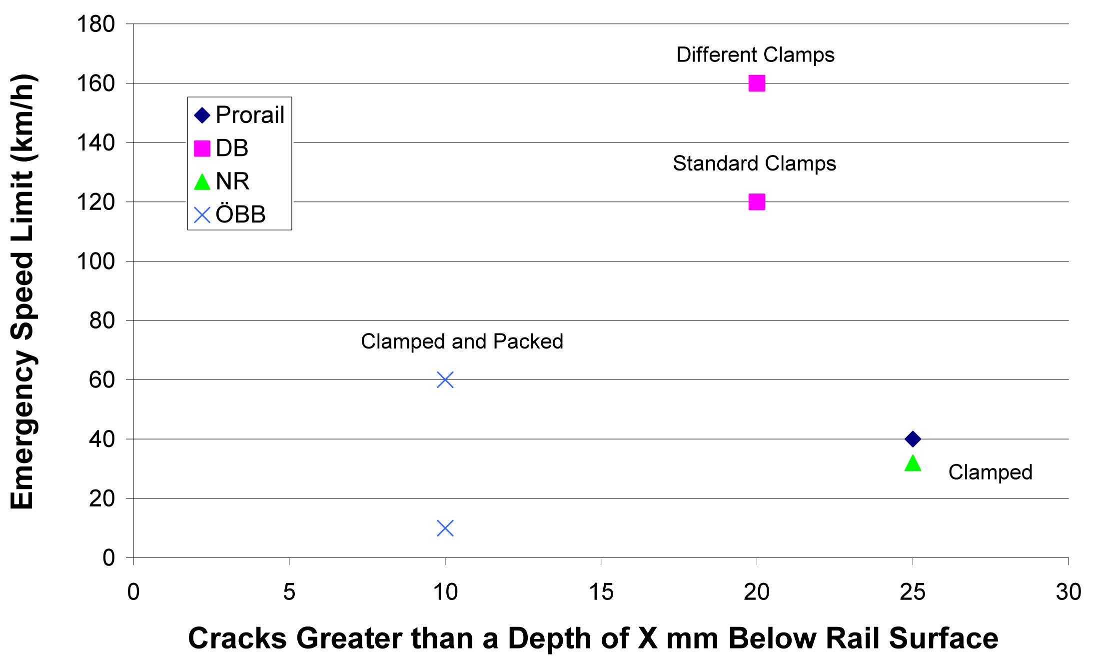

Figure 3-3 Comparison of emergency speed limits for clamped single squats

The minimum actions reported are for single squats, more severe restrictions are in place for multiple squats or squats associated with other types of defects in the same area. An example of the difference is shown in Table 3-2 for DB.

The wide differences in the minimum actions, applied on discovery of squat defects, is an example of the differences between the IM's for a range of other defects including bolt hole cracks(135), tache ovales (211), horizontal and vertical crack in welds (411, 412, 421, 422) etc.

Although there are differences in the form of traffic carried, inspection regimes and track structure between the IM's, it is hard to justify the observed range in minimum action rules. Although no data are available, the crack growth rates of squats under standard mixed traffic conditions in Europe would be expected to be similar for all the IM's involved in the Innotrack project.

3.2.3. RCF – Head checks (UIC712R Code = 2223)

Head checks are a form of Rolling Contact Fatigue that appears on rail as a series of cracks along the running band inclined to the gauge corner, Figure 3-4.

Figure 3-4 Head Checks

Head checks are initially found by visual inspection or by eddy current systems mounted on trains. Once found a follow up investigation is carried out by manual ultrasonic and/or eddy current inspection. The minimum actions are summarised in Table 3-3.

The complexity of the actions required for different railways means that it is hard to make a significant comparison but the thing to conclude from them is the difference in the approach by the IM's.

DB are the only IM who currently use an eddy current system to characterise the depth of cracks, when visual inspection finds cracks over a certain length, to determine when action should be taken. All other IM's use visual inspection to classify the severity of defects, backed up ultrasonic inspection to indicate the depth.

Banverket only specify that the rail should be replaced if the cracks are visible and there is a significant ultrasonic response. In contrast Network Rail are much more prescriptive and have limits based on categorisation of surface crack length and also the ultrasonic response at the centre and gauge corner of the rail as to when rail grinding or renewal should take place. The other IM's lie in between the two extremes.

Table 3-3 Comparison of Minimum Actions for Head Checks (2223)

IM	Length	Depth	Emergency action	Timescale
BV	*Visual*	*Ultrasonic*		
	Visible	≥5mm FBH		1 month
DB	SCL ≤ 20mm		Eddy Current Inspection	4 weeks
	SCL > 20mm		Eddy Current Inspection	2 weeks
		Eddy Current D < 0.5mm	Grind	18 month
		0.5 <D< 1.5mm	Grind	12 month
		1.5 <D< 2.7mm	Grind	3 month
		>2.7mm without UT response	Re-rail Re-inspect with UT after 3 months max V = 0.7 x locally allowed V	6 months
		>2.7mm with UT response	Re-rail 20km/h	6 weeks
ProRail	*Visual*	*Ultrasonic*		
	SCL < 10mm		Re-inspect visually	6 months
	10 < SCL < 19mm		Re-inspect visually	6 months
	20 < SCL < 29mm		UT inspection	2 months
	SCL > 30mm		UT inspection	24 hours
		>50% of head (>25mm)	40km/h	Immediately
			Clamps	3 months
	More than 1 crack within 1.2m	>20% (>10mm)	40km/h	Immediately
		20% (10mm) <D< 50% (25mm)		4 weeks
			Clamps	3 months
		6% (3mm) <D< 20% (10mm)	Re-inspect visually	3 months
		<6% (3mm)	Re-inspect visually	6 months

ÖBB	*Visual*			
	SCL< 25mm		Plan for rail grinding (R200 before R350HT)	
	25 <L< 35mm		Plan for rail grinding (R200 before R350HT) and intensify inspection	
	>35mm - Not on centre of head		Special ultrasonic testing at least quarterly. Plan for rail grinding/change	
	>35mm - Over centre of head	Mid sleeper bay	Block Line	Immediately
			10 km/h with clamps or under packed	Immediately
			60km/h with clamps and under packed	Immediately
		Over sleeper	10km/h	Immediately
			60km/h when packed with wooden sleeper and emergency clamps	Immediately
UIC	Centre head	>5mm		2 weeks
	Gauge corner	>20mm		2 weeks
		5 <D≤ 20mm		12 months
		≤ 5mm		Re-inspect
NR	*Visual*	*Ultrasonic*		
	Surface Crack Length < 20mm	No ultrasonic response	Re-inspect	26 weeks
		0 < Full Screen Height ≤25%	Fit Clamps	13 weeks
		25 < FSH ≤ 50%	Fit Clamps	4 weeks
		>50% Full Screen Height	20mph [32km/h] & Clamps	36 hours
		>50% Full Screen Height with 6dB gain added	20mph [32km/h] & Clamps	36 hours
	20mm ≤ SCL < 30mm	No ultrasonic response	Re-inspect	8 weeks
	SCL ≥ 30mm	No ultrasonic response	Re-inspect	4 weeks
	SCL ≥ 20 mm	0 < Full Screen Height ≤25%	Fit clamps	13 weeks
		25 < FSH ≤ 50%	Fit clamps	7 days
		>50% Full Screen Height	20mph [32km/h] & Clamps	36 hours
		>50% Full Screen Height with 6dB gain added	20mph [32km/h] & Clamps	36 hours
	*if action not carried out within timescale impose 40mph speed restriction			

The planning of train based grinding is based on the depth of cracks found. In all cases after the cracks have extended a certain distance grinding is no longer permissible and rail replacement is the only option. ÖBB are interesting in that the planning of grinding is also dependant on the rail grade with grade R200 to be carried out before R350HT. This is justified on their experience, which has demonstrated that cracks of the same surface crack length (SCL) propagate to a greater depth in softer rails.

3.3. Conclusions

The overview of the current Minimum Actions used by different IM's shows that there is a considerable difference in their approach to defects. For the same type of defect, such as a squat, there is a wide range of timescales and emergency actions required, even taking into account the uncertainty in comparing crack lengths and depths as a result of the differences in inspection (especially ultrasonic) regimes. With a mixed traffic railway, such as those operated by the IM's within the Innotrack project, it would be expected that growth rates of defects will be similar, even when taking into account the different types of vehicles, track support stiffnesses, rail grades and profiles etc. Therefore the wide range of minimum actions encountered within Europe can be seen as a result of historic experience with little science supporting it.

It can therefore be seen that there is a requirement for a more solid scientific basis to be put in place behind the minimum actions to ensure the railway remain safe but also to allow a move towards preventive rather than reactive maintenance. This report summarises the work carried out in Innotrack WP4.2 to provide a scientific basis for minimum actions. The work is split into two themes, the first is by carrying out detailed modelling to understand how different types of defects initiate and grow under a range of loading conditions. The second is to predict when a crack reaches a critical size that may result in rail failure under real world conditions. It is through using the information from both approaches that new Minimum Actions can be proposed.

3.4. An overview of defects considered in this guideline

3.4.1. Squats

Appearance

Fully developed squats have the appearance of shallow surface depression on the running band often in combination with a V-shaped crack (Figure 3-5). Several infrastructure owners have categorized the squats according to their size into three classes (Nework Rail, ProRail...) (Figure 3-6). Squats can often be mistaken with wheel burns – wheel burns always appear in pairs opposite to each other (Figure 3-7) Squats can be found as single events or in an epidemic form randomly distributed over a longer track segment on both rails. No rail grade dependence was found so far. For more information see [3.9], [3.10] and [3.11].

Figure 3-5 Typical full grown squat with V shaped crack

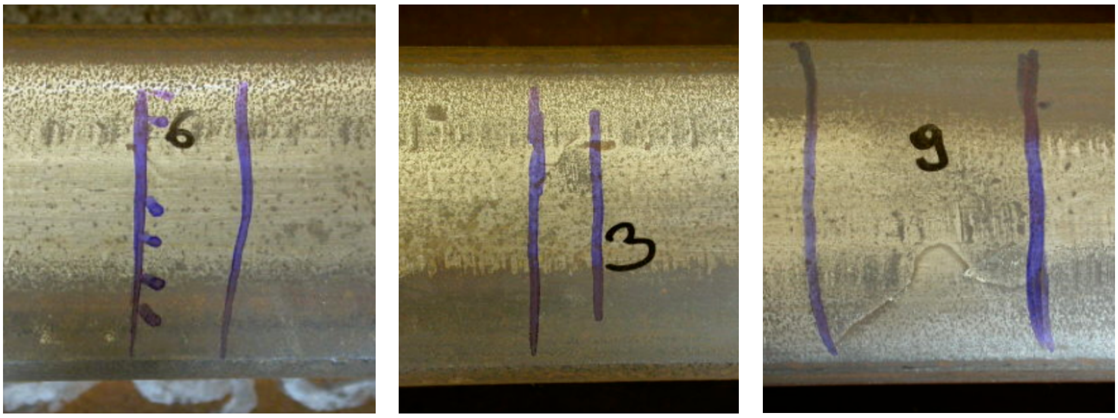

a b c

Figure 3-6 a) Class 1/A, b) Class 2/B, c) Class 3/C

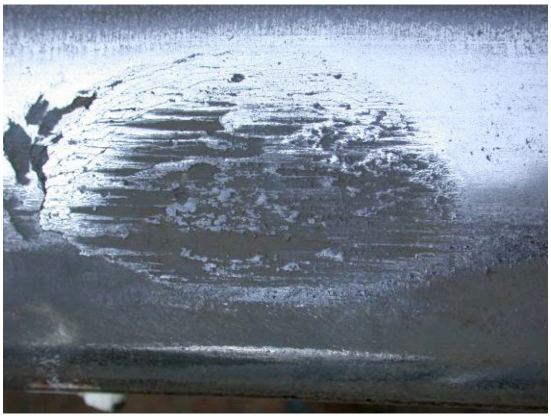

Figure 3-7 Typical wheel burn

Significance

High – Squats are the major RCF problem in Europe and all over the world especially in mixed and light-rail traffic conditions. Squats will not only damage the rail but also cause major track deterioration if not treated/removed in an early stage.

Countermeasures

- preventive grinding / high speed grinding
- repair welding
- rail exchange

3.4.2. Corrugation

Appearance

Periodic irregularities on the rail surface with wavelengths between 10mm and 1.5m (example picture 4). They can appear in tangent track or in curves either on the high rail or on the low rail. According to their appearance and location there exist several sub-types [3.12].

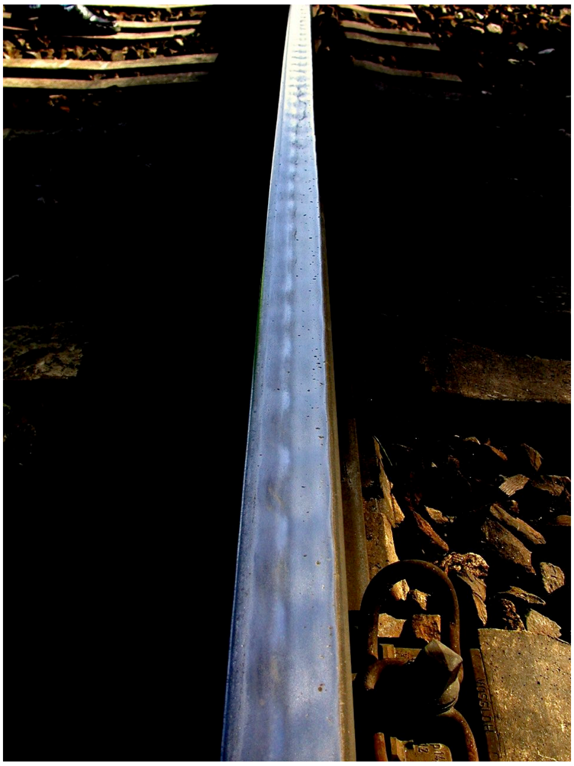

Figure 3-8 Short pitch corrugation

Significance

High – Corrugation is a major problem all over Europe and all over the world. Besides track deterioration (due to dynamic forces acting on fastening systems, sleepers, etc.) corrugation causes especially in densely inhabited areas a major noise problem.

Countermeasures

- Rail grinding
- Friction management of the rail (i.e. friction modifiers)
- Sleeper pads
- Wear resistant rail grades
- Optimised fastening systems

3.4.3. Rail wear

Appearance

Material loss due to the rolling/sliding contact between wheel and rail will result in wear of both partners. In the worst case wear will lead to removal of rail material until safety limits are reached and the rail has to be exchanged. In most cases wear will lead to profile adaption of the rail that can have positive effects like reducing the stress state by favouring a conformal contact between wheel and rail. On the other hand wear can also lead to contact conditions that result in increased stresses that will cause rail damage. In combination with already existing cracks these high stresses will cause accelerated crack growth and might lead to rail breakage (especially in combination with long cracks).

Besides natural wear artificial wear produced by grinding can have the same effects. Main reasons for grinding are on the one hand reprofiling and on the other hand removal of surface damage.

Countermeasures

- Rail grinding
- Friction management
- Wear resistant rail grades

3.5. Bibliography

3.1 Network Rail, **NR/L2/TRK/001/B01, Inspection and Maintenance of Permanent Way – Rail Management**, 5/12/2009

3.2 Banverket, **BVS 524.31, Oförstörande provning (OFP) av räler och rälskomponenter**, 2009/10 issue

3.3 Banverket, **BVS 586.10** including supplement **BVK 2005.012**

3.4 ProRail, **Richtlijn RLN00063**, Klasse-indeling spoorstaafgebreken + ver-volgacties en normering ultrasoon onder-zoek, 4/10/2004

3.5 DB, **821.2007, Zerstörungsfreie Prüfung von Schienen**, 1/4/2007

3.6 ÖBB, **B 12, Behandlung von Schienenfehlern**, 30/10/06

3.7 Auer, F. & Wöhnhart, A., **ÖBB, Info 07 - Head Checks**, 29/6/2008

3.8 UIC, **725R, Treatment of Rail Defects**, 1st Edition, June 2007

3.9 UIC, **712R, Rail defects**, 4th Edition, January 2002

3.10 INNOTRACK Deliverable D4.2.4, **Improved model for loading and subsequent deterioration due to squats and corrugation**, 37 pp (and 7 annexes, 7+10+9+10+8+8+26 pp), 2009

3.11 Li, Z, **Squats on rails**, to be published in *Wheel/rail interface handbook*, eds Roger Lewis & Ulf Olofsson, ISBN 1 84569 412 0

3.12 Li, Z, Xin Zhao, Coenraad Esveld, Rolf Dollevoet and Marija Molodova, **An investigation into the causes of squats – correlation analysis and numerical modeling**, *Wear*, vol 265, pp 1349 – 1355, 2008 (doi:10.1016/j.wear.2008.02.037)

3.13 Weidinger P, **Rauhigkeit im Rad-Schiene System**, Diploma Thesis, 2008

3.14 Grassie, S.L., **Rail corrugation: characteristics, causes, and treatments,** Proc. IMechE Vol. 223 Part F: J. Rail and Rapid Transit, p581-596

4. Squats

4.1. Background

Squats were first reported in the 1950s in Japan where they were described as the 'black spot' [4.1–4.3]. In the 1970s they became known in the UK [4.4]. In other European countries they were reported later [4.5, 4.6]. Definitions of squats can be found in [4.7–4.9]. Squats have in recent years become an important rolling contact fatigue (RCF) problem for railways, such as ProRail [4.6, 4.10].

Research on squats has been carried out over the past decades. In [4.11] Clayton presented a research programme of the British Rail Research, the goal of which was to develop a failure model based on small scale laboratory test; some results were reported in [4.11] and [4.12].

In 1987 the European Rail Research Institute (ERRI) started the D173 Rolling Contact Fatigue Programme, an overview of which can be found in [4.13]. Squats were investigated in this programme; some of the results were summarized by Cannon and Pradier [4.13]. The major work on squats was on crack growth as presented by Bogdanski *et al* [4.14]. Bogdanski and his colleagues have since then published a series of works related to cracks in squats, especially in relation to fluid entrapment, with the latest being [4.15].

Kondo *et al* [4.16] presented the history of the Shinkansen rail surface shelling in Japan, which was also squat related, and discussed causes, growth and detection. Grinding was the countermeasure. Some recent work on the squats in Japan was reported by Ishida *et al* [4.17], in which the initiation mechanism and the effect of grinding were discussed. Other works on squats can be found in [4.18–4.21].

4.2. Characteristics of squats

4.2.1. Characteristics of moderate and severe squats

Descriptions of squats given in [4.7–4.9] differ to certain extent from each other. For instance [4.7] describes only the later stage of squats, i.e. those with cracks, while in [4.9], the development of squats is divided into 3 stages, namely light, moderate and severe, see Figure 4-1.

Figure 4-1 *Classification of squats in the Netherlands [4.9]. Arrows indicate traffic direction. (a) light squats, (b) a moderate squat, (c) a severe squat.*

The definitions in [4.7–4.9] have the following two characteristics in common: One of the most striking visual characteristics of squats is their lung-like shape – a moderate or severe squat always consists of two lung-like depressed halves, of a shape which looks like a permanent deformation indented by somebody sitting, or squatting on the rail, see Figures 4-1(b) and 4-1(c).

Another characteristic feature often associated with squats is the V, U or Y shaped cracks, some of which are illustrated in Figures 4-1(b) and 4-1(c). It is believed that the cracks initiate in the surface [4.11, 4.13, 4.16, 4.21], and grow to a depth of about 3 to 6 mm, before they branch downward transversely [4.7, 4.11, 4.16, 4.21]. In [4.4] and [4.8] explanations are given about how cracks of squats initiate from periodic indentations of an interval of the wheel circumference and how squats grow from surface cracks.

These two characteristics, among other, are typical of squats in the intermediate and late stages of their development.

In Figure 4-1(a) two examples of small rail top defects are given: the one in the middle is relatively large, and is supposed to have already a crack as illustrated on the left side. The defects on the right side in the blue circle are some indentations. These kinds of defects are supposed, based on observations of the Dutch railway of thousands of squats, to be among the initiation sources of squats which later look like what is shown in Figure 4-1(b) and 4-1(c). They are therefore called light squats according to [4.9].

4.2.2. Characteristics of growth process and critical size of light squats – focus of the present work

Two questions arise with the definition of light squats as illustrated by Figure 4-1(a): What is the critical/threshold size of defects like those of Figure 4-1(a), above which such defects can grow into a moderate squat, and subsequently into a severe one? And how a defect of arbitrary shape like those of Figure 4-1(a) grows into the typical lung-like shape shown in Figures 4-1(b) and 4-1(c)?

The first question concerns basically the quantitative definition of light squats: A small defect can be called a light squat only when it is larger than a critical size, because observations and experience tell us that small irregularities such as grinding marks do not grow into squats. This question therefore concerns the critical size characteristic of light squats.

The second question concerns the process with which light squats develop into moderate and severe squats. It may be called the growth characteristic of squats.

From an infra management point of view these two characteristics of light squats are important for the reasons of safety and life cycle costs: It is safer and much more economic to find/detect squats at the earliest possible occasion to remove them in time.

These two questions are not addressed by previous research. They are addressed in this work.

Because the second question concerns the growth of light squats, an answer to it was first sought. The answer was given in [4.10] by a squat growth process derived from numerical analysis, see Figure 4-

2. It is validated in annex 1; an example of monitored squat growth is given in Figure 4-3 below.

The growth process says [4.10, annex 1] that a light squat, the A_1 part of squat A of Figure 4-2, will excite at its trailing edge a dynamic contact force of certain wavelength with a series of peaks. Such peaks are repeated at every wheel passage at the same location, causing localized ratchetting. The deformation caused by the first two force peaks, F_1 and F_2, will eventually cause the light squat A_1 and the wave pattern B_1 that follows it to become the two lung-like parts A_2 and B_2 of squat B. Squat B will further grow till the failure of the rail if no remedial action is taken. It is also noticed that the wave pattern after the two squats follows the fluctuation of the contact force.

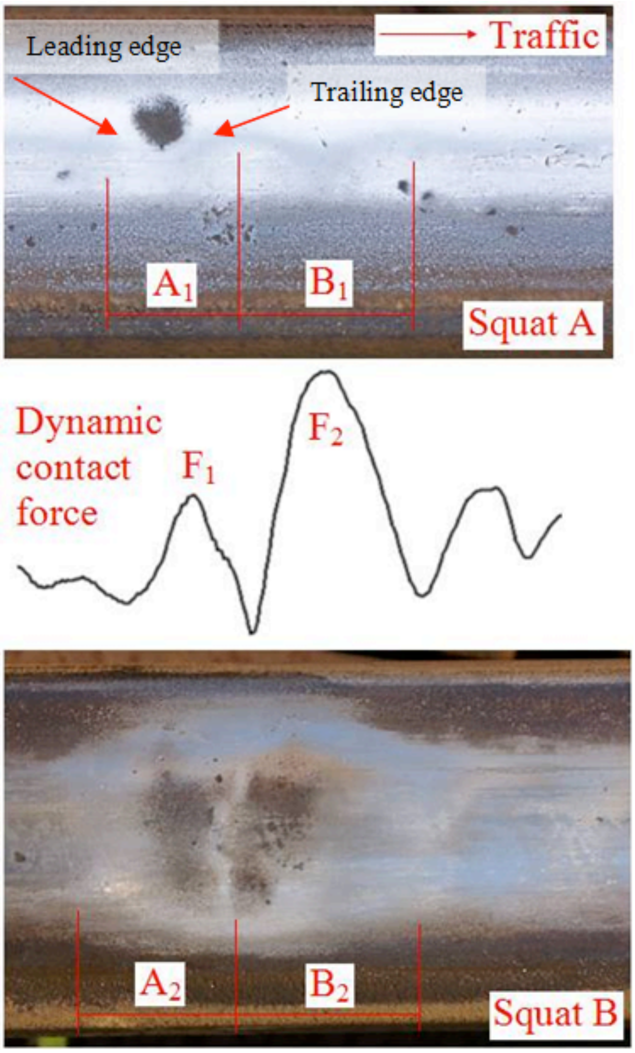

Figure 4-2 *An illustration of the growth characteristic. Squats A and B are two different squats. They are used here for convenience of explanation because of their typical shape and the wave pattern that follows them. Note that it is not necessary that always $F_1 < F_2$.*

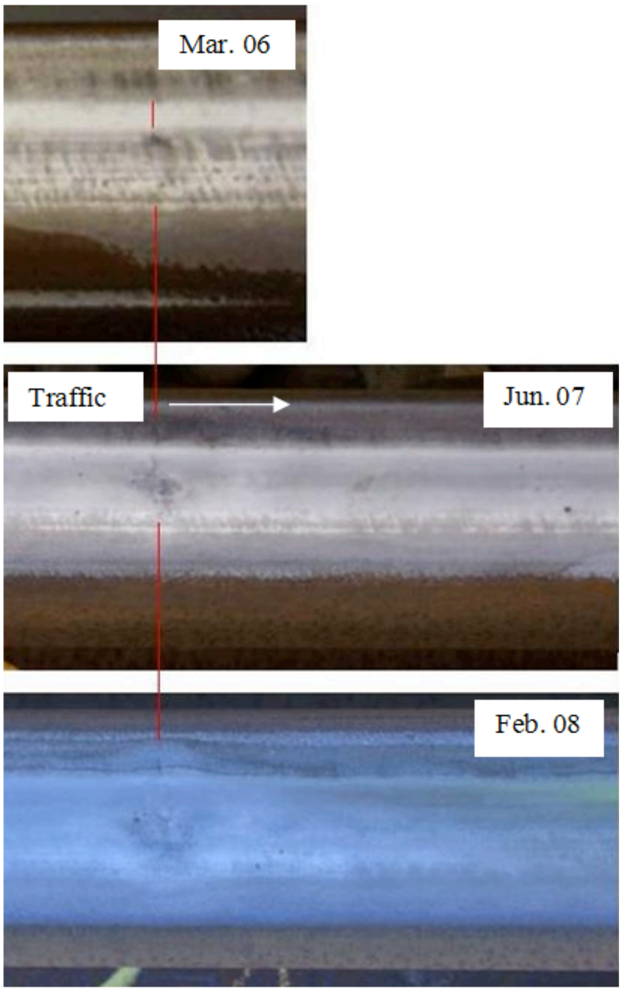

Figure 4-3 *A growing squat with the typical lung-like shape being formed in February 2008. A crack is visible in the middle. It is not clear if there was already a crack in March 2006.*

According to this process the growth of squats is related to high frequency interaction between wheel and rail, the typical wavelength is between 2 – 4 cm, corresponding to a frequency of 950 - 1900 Hz for the typical Dutch main line speed of 140km/h. [4.10, annex 1].

As can be deduced from the dynamic force shown in Figure 4-2, corrugation-like wave pattern may be caused at a certain stage of squat development immediately after squats as can be seen in Figure 4-4(b). The wavelength of the wave pattern is in agreement with that of the dynamic force, i.e. typically 2 – 4 cm [4.10, annex 1]. This wavelength is in the same range as that of short pitch corrugation. This is another characteristic of squats: wavelength characteristic. This characteristic suggests that short pitch corrugation and squats may have something in common.

The short wavelength/high frequency characteristic associated with squat growth has also been confirmed by vertical axle box acceleration (ABA) measurement; see the high energy content encircled by the white oval in Figure 4-5(b). For details please see annex 1. This characteristic may therefore be employed for the detection of light squats by ABA. Such a possibility is discussed in annex 2. Note that in [4.7] it is mentioned that the means of detection of squats are visual inspection and ultra-sonic testing. Visual inspection by walking along the track is unsafe and is gradually disallowed. A current alternative is visual inspection of a video record of the track, which is inefficient and costly because of the needed human resources. Ultra-sonic testing can only reliably detect squats with cracks deeper than 5 – 7 mm. Rails with such large squats are too large to grind.

It should be pointed out that in the work on squats in the frame of INNOTRACK no crack is considered in the numerical model. This is justified because the focus is on light squats, at which there is usually no crack [annex 1], or only a small crack, but with the influence of the crack on the dynamic characteristics of the system being negligible. This is evidenced by the typical lung-like shape of squats and the associated typical wavelength of 2 – 4 cm. At severe stages of squat development the cracks become significantly large and the system may be significantly damaged/disturbed at fastenings, rail pads, sleepers and ballast. In this case the wavelength will become longer, typically up to 6 cm.

The answer to the second question posed, namely the determination of the critical size, will be presented in section 4.4 [annex 3].

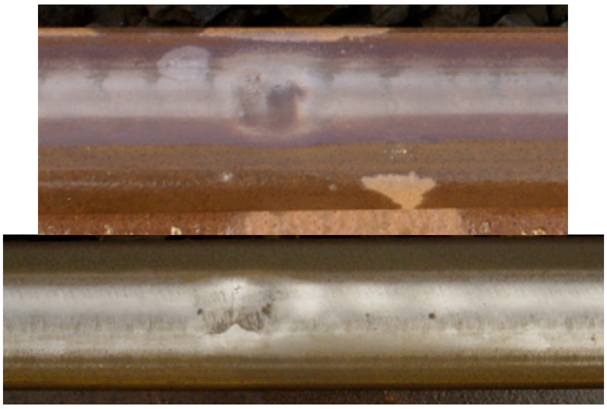

Figure 4-4 *Short pitch corrugation and corrugation-like wave pattern after a squat. The wavelength of the wave pattern is usually in the range of 2 – 4 cm. Traffic is for both cases from left to right. Top: Corrugation caused squats. Bottom: Squat causes corrugation-like wave pattern*

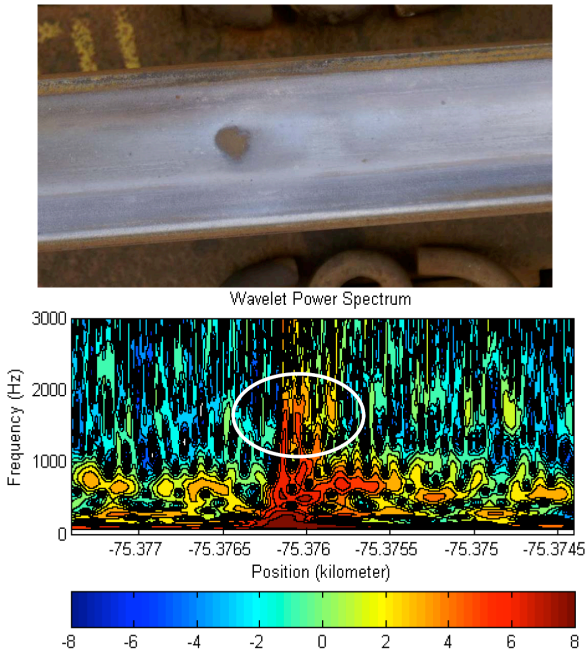

Figure 4-5 *A light squat and the axle box acceleration (ABA) caused by it [annex 1]. Top: The light squat. Bottom: the wavelet power spectrum of ABA*

4.2.3. Characteristics of the numerical analysis of squats

As can be seen from the above analysis squats are a result of accumulated plastic deformation under repeated rolling contact of high frequency wheel-rail interaction. The numerical analysis should therefore include plasticity and the solution should be sought in continuum dynamics of the wheel and the rail. At the same time the influence of the track should also be taken into account. This is the approach employed in this work. To this end, a Finite Element (FE) model for the solution of frictional rolling contact in elasto-plasticity and in continuum dynamics has been developed and validated in annex 4. This approach is applied to the determination of the squat growth process [4.10] and the determination of the critical size of a light squat [annex 3]. The validation of the numerical results of [4.10] is presented in annex 1.

4.2.4. Difference from head checks

Squats and head checks (HC) are the two major types of rail RCF. They differ from each other in several aspects. For example, HC are found on the gauge shoulder and gauge corner, usually on curved tracks, the cracks are (almost) uniformly distributed over a length of the rail. Squats are found on the top of rails, usually isolated and randomly distributed on straight track or gentle curves. HC are associated with a long wave rolling contact, so that the wheel-rail interaction can be considered from contact mechanics point view as being (quasi-) static. Squats occur when wheels roll over local rail top defects; a reasonably accurate solution of the rolling contact problem may need to involve continuum dynamics of the wheel and rail.

It should be noted that when HC are in a late stage, the underlying cracks may come to be beneath the rail top so that the wheel will bump over the underlying HC crack, causing the HC to look like a squat. Such squat-like HC is not considered as a squat in this work.

4.2.5. Initiation sources of squats

Based on the above discussion it becomes clear that any short rail top defects larger than a critical size can cause squats. Such defects can be indentations and short pitch corrugations. Statistically about 33% of squats are caused by such corrugation in the Netherlands, see annex 1. The wave pattern generated by squats mentioned above can be readily distinguished from corrugation, if the traffic is one-directional: At a squat caused by corrugation the waves should be on both side of the squat, see Figure 4-4(a); otherwise the waves occur only after the squat (Figure 4-4(b)).

Squats are often found at welds of continuously welded rails. This may be due to two reasons: One reason is that the heat affected zone (HAZ) causes material inhomogeneity, which may lead to local differential wear or differential plastic deformation, so that local rail top defects arise and squats occur. A solution to this problem may be a reduced HAZ size or improved material homogeneity at the HAZ. Another reason is that the finish geometry of the welds is poor so that rail top defects exist after welding. The solution is tighter control of the finish geometry.

Squats may also occur due to differential wear or differential plastic deformation at a sudden change of stiffness of the structure. This may often be observed at switches and crossings. A case study is presented in [4.22]. Note that usually stiffness change alone is not sufficient to cause a squat; there should usually also be something else wrong with the structure, for instance due to poor maintenance.

Although wheel burns are classified in [4.7] as a different rail top defect from squats, light wheel burns, just like other short rail top defects, can grow into squats. They may only be distinguished as wheel burns from the fact that they usually occur in pair on the opposite rails of a track.

4.3. Parametric influence

4.3.1. Influence of defect size

This will be discussed below in section 4.4 where the critical size is determined.

4.3.2. Influence of traction/braking and unsprung mass

Numerical analysis shows that friction level, and hence tangential force, plays an important role in the magnitude of the von Mises stress and plastic strain. Details are presented in [4.10, annex 1].

The effect of unsprung mass of vehicle is investigated. It is found that in the high frequency domain, the unsprung mass on the axle does not result in an extra dynamic load to the first peak force due to lag in wave propagation. On the other hand unsprung mass close to the contact area, such as the mass of the tyre, can lead to an extra dynamic force, which can be around 12 times that of the additional mass. Details are given in [4.23].

4.3.3. Influence of material inhomogeneity and HAZ of welds

Welds of continuously welded rails, both thermite and flash butt, are vulnerable to squats. Out of a field survey of 65 randomly chosen squats, 11 are found at welds, that is 17% of the total. The high percentage of squats at welds may be explained by two main factors: material strength/hardness and vertical-longitudinal rail top profile. Analyses of the effects of strength and geometry deviation have been carried out, and the inadequacy of existing standards for weld finish geometry is discussed in [4.10, 4.23].

4.3.4. Influence of rail type

Figure 4-6 shows the effects of two different rail types: UIC54E1 and UIC60E1. With all the other conditions being the same, UIC60E1 has smaller dynamic force for both a large and a small squat.

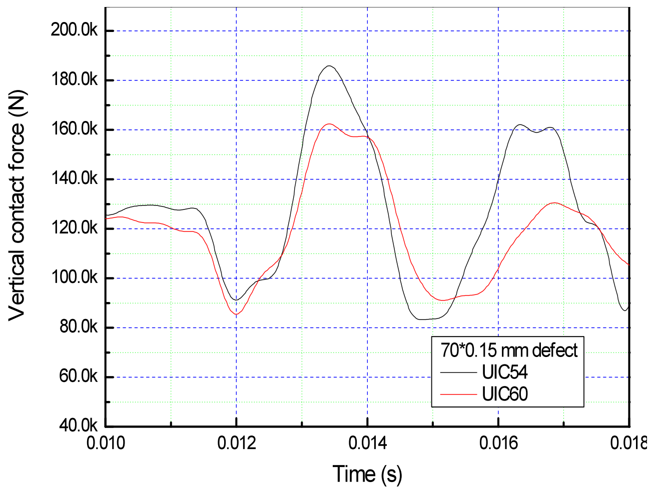

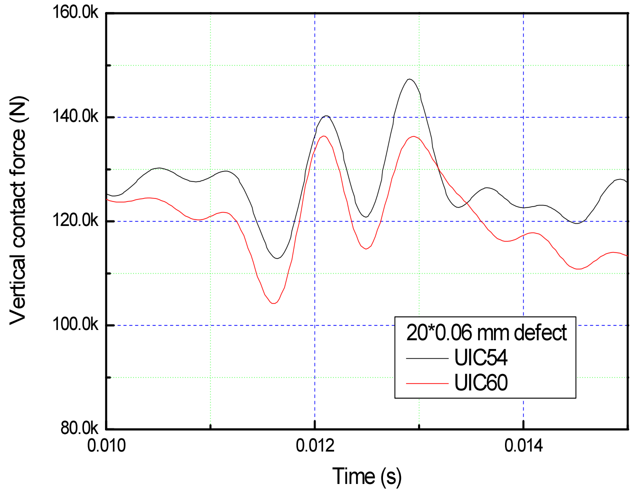

Figure 4-6 Influence of rail type. Top: Dynamic force at a large squat of 70mm long and 0.15mm deep. Bottom: Dynamic force at a small squat of 20mm long and 0.06mm deep.

Here only the vertical contact force is given for the sake of simplicity. The effect of tangential force and stress is equally important. This can be seen in the treatment in section 4.4.

4.3.5. Influence of rail grades

A bi-linear elastic-plastic material model is used in this work. Because squatting takes place when the tensile strength is exceeded, the tensile strength of the rail grades are compared with the maximal von Mises stress to determine the propensity of squat initiation and growth, see [4.10, annex 3]. From this perspective the higher the material strength is, the higher its resistance to squat initiation and growth. It is, however, realized that the formation of squats is influenced by many aspects such as traffic, technical status of the track and maintenance, friction management etc. increasing material strength alone may not be sufficient enough. What is more a benign amount of wear may have a smoothing effect at rail top irregularities so that the chance of squat formation may be reduced. Since material strength is directly related to hardness, wear rate, ductility etc, the optimal rail grade may not be determined by strength only. This is also one of the considerations in annex 3 that the critical size is determined for a range between 6 – 8 mm, not exactly at the numerically determined 6.7mm.

4.4. Critical size for light squats to grow

4.4.1. Motivation

From the point of view of rail infrastructure management, prevention and early correction by timely detection of light squats is most cost effective. It also enhances the safety and availability of the network.

According to the squat growth process postulated in [4.10] and validated in annex 1, a defect causes a dynamic force, which may result in plastic deformation and material hardening. Plastic deformation usually makes the contact geometry more conformal so that the stress will be reduced, if the contact force remains the same. And the hardening will increase the yield stress as long as the tensile strength of the material is not yet reached. Consequently, the stress may be lower at subsequent wheel passages than the increased yield stress, and the material will reach a shakedown state, if the defect is not large enough. The defect will, therefore, not grow into a squat, and it may eventually disappear because of wear. This means that there should be a critical size, only above which a defect can grow into a squat. In other words, a defect can be considered as a squat only when it is larger than the critical size.

Such a critical size has the following significance. Firstly, it can be used as a criterion to distinguish light squats from trivial defects, which will eventually be erased by wear. Currently in the Netherlands squats are classified by visual inspection as being light, moderate and severe, as described in [4.9] and briefly discussed in section 4.2.1. There is not yet a quantitative criterion to determine which defect is a light squat, and which is not. Therefore, false statistics and reporting of light squats may occur. Secondly, it can be employed for automated detection and classification of light squats. So far there is not yet an automatic measurement that can effectively detect light squats. If the critical size is known, it is possible to detect light squats with automated image recognition. The light squats may also be automatically detected with instrumented wheelsets by establishing a quantitative relation between the size of the defects and the pertinent response of the wheelset.

Nevertheless, such a size has not been determined yet.

4.4.2. Determination of the critical size

This work presents a methodology for the determination of such a critical size, demonstrated with its application to typical operation conditions of the Dutch railway as an example. Details are presented in annex 3. The methodology is generally applicable to other operational conditions.

Here below a brief description of the methodology is given.

At a defect of certain size the maximum von Mises effective stress is calculated by employing the rolling contact model described in section 4.2.3. This stress is compared to the tensile strength of the rail material to evaluate its tendency to deform plastically. The von Mises stress can be compared with the tensile stress because surface deformation is considered. In other words the material behaviour under high hydro-static pressure is not considered. Because for the typical Dutch operational conditions the most influential parameters for the stress are the size of the defects, the coefficient of friction (COF, f), and the traction coefficient μ,

$$\mu = F_{\mathrm{L}}/N \qquad (4.1)$$

where N is the vertical contact load and F_L is the longitudinal friction force, $F_L \leq f \cdot N$, parameter variation is performed with them. Figure 4-7 shows how the defects are applied to the rail head, and Figure 4-8 shows the distribution of the maximum von Mises stress.

In this way it is determined that for typical Dutch operational conditions a defect has little chance to grow when its dimensions are smaller than 6 mm in the rolling and transverse direction. Further, the probability of growth is very large if the dimensions are larger than 8 mm in the rolling and the transverse directions. In other words a defect can be classified as a light squat if it is larger than 8 mm. A validation of this critical size is presented in Figure 4-9.

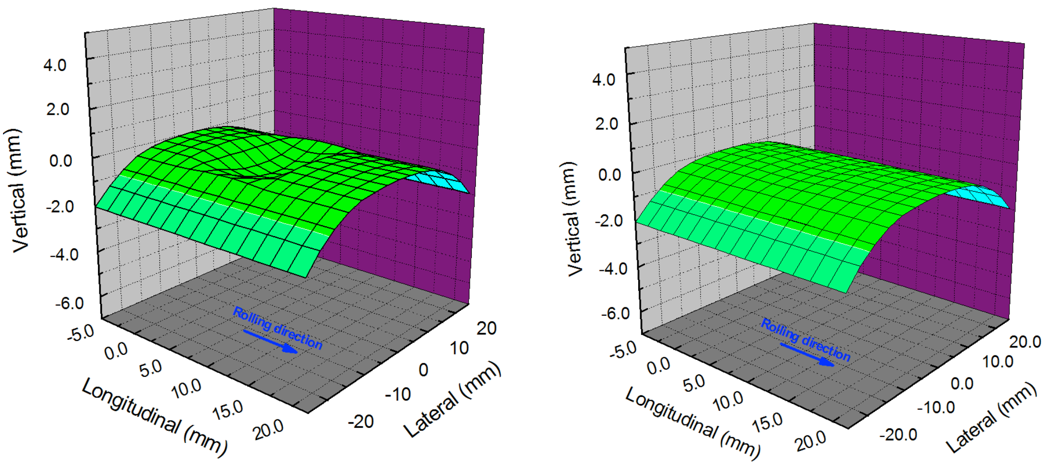

Figure 4-7 *The 3D appearance of a defect when it is applied to the rail head. Note in (a) the magnification is applied only to the defect, not to the rest of the rail top surface, the scale of the ordinate remains therefore unchanged. Left: Defect with 10x magnification in vertical direction. Right: Defect without magnification*

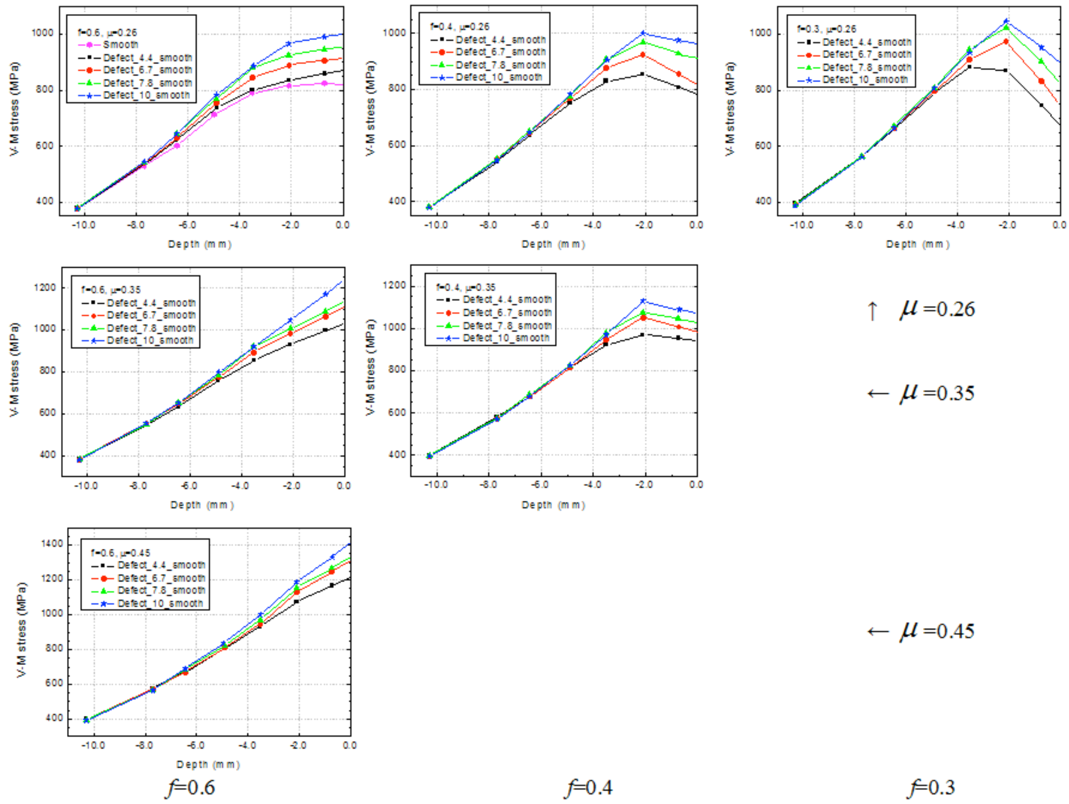

Figure 4-8 The Maximal v-M stress distribution at defects under different friction coefficient (f) and traction coefficient (μ).Origin of the abscissa is at the rail top surface. Depth is measured downward from rail top. The curves in the different color represent different size of the defects. Details are in annex 3.

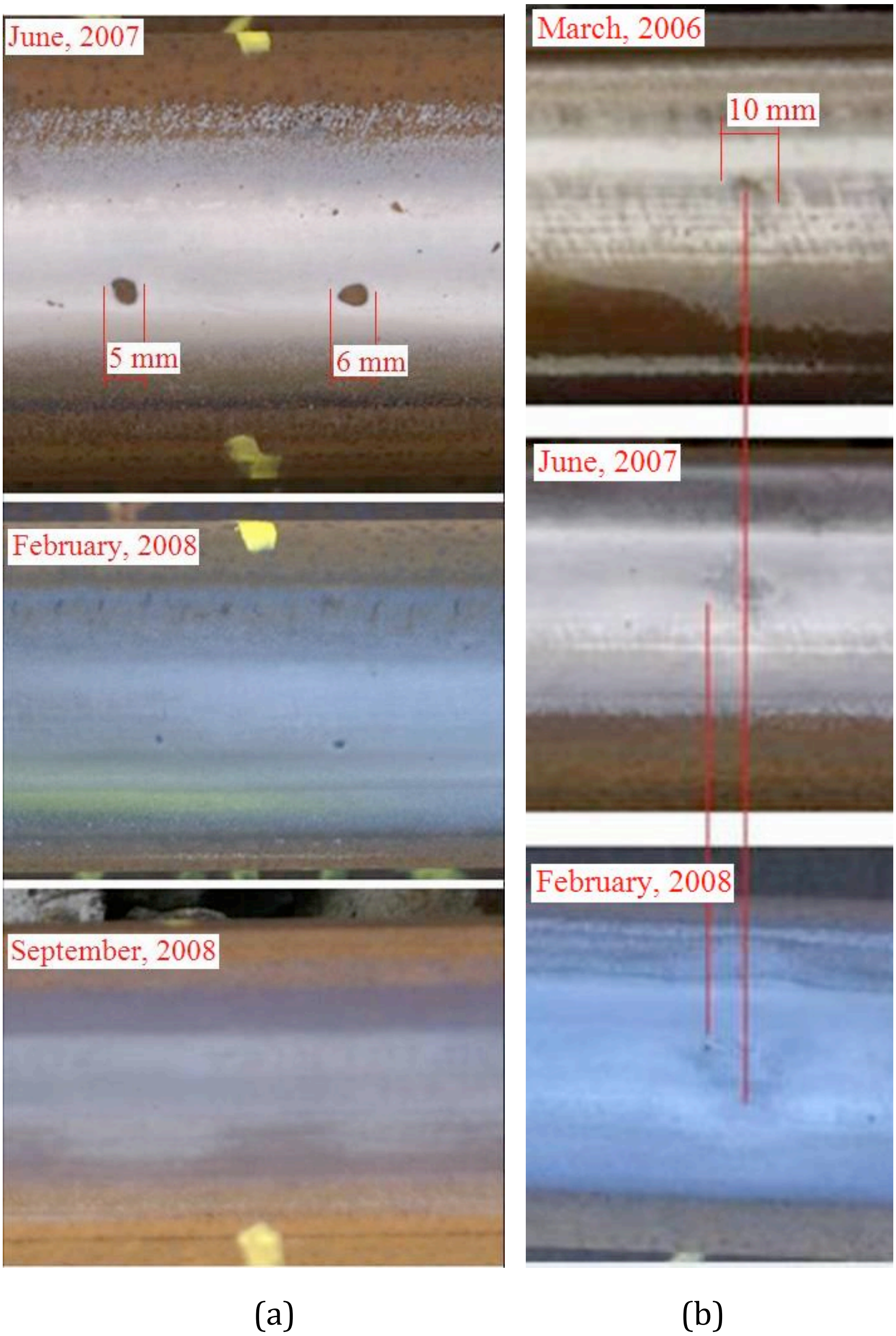

Figure 4-9 Validation of the critical size. (a) two defects of 5 and 6mm were erased by wear, and (b) a defect of 10mm had grown into a moderate squat with the typical V form.

It is noted that in this criterion for squat growth no depth is considered. This is for two reasons. The first is that based on many vertical-longitudinal profiles of rail top measured in the tracks at various defects, the depth of them are larger than 0.05mm, which is the typical compression of a wheel or rail at contact. When a defect is deeper than this value there will be no or little contact at the bottom of the defect and a criterion for the depth is not very meaningful. This is evidenced by the observation that indentations usually have a black bottom. The second reason is that when this criterion is used for visual inspection, it is usually not possible to measure the depth. But this does not mean that the depth of squats is not important. Rather it is very important for planning of rail grinding.

4.4.3. Applicability and limitations

The critical size is derived for indentations, small wheel burns, differential wear or differential plastic deformation. As far as corrugation is concerned, this critical size is not directly applicable because the wavelength of corrugation is larger than 20mm. In this case the depth of corrugation has to be taken into account. Such a critical size may also be derived with the presented methodology. But that should not be necessary since for corrugation there are other criteria; actions should usually have been taken before it has to be treated for squats, though this is currently often not the case.

The above discussed critical size is based on the typical Dutch operational conditions. In view of the wavelength characteristics associated with the growth process of squats discussed in section 4.2.2, and the similarity between the wavelengths of squats and of short pitch corrugation, it may be postulated that the derived critical size may also be applicable to railways similar to those of the Netherlands. This is based on two arguments. The first is that the wavelength of the short pitch corrugation is more or less similar between the railways worldwide. The second, which should actually also be the reason for the first argument, is that the structures of the railways are also similar. Looking at Figure 4-6, the wavelengths of the UIC54 and UIC60 are more or less the same. Of course for an accurate determination of the critical size under individual specific operational conditions the proposed methodology can be used.

One difference in operational conditions is the speed. Its variation is not considered in the present work. A parameter variation study of speed, together with other parameters, such as many of those discussed in section 4.3 should be performed. They are not included in the frame of INNOTRACK due of the complexity of the strongly non-linear and high frequency FE modelling and the long associated computational time.

4.5. Conclusions and recommendations

4.5.1. Major characteristics of squats

The major characteristics of squats are

- The lung-like superficial shape and the V, U or Y shaped cracks for the moderate and severe squats.
- The critical size for squats to grow and the wavelength characteristic associated with the growth process. These characteristics can be employed for classification and detection of light squats, and for maintenance policing and planning.

4.5.2. Corrective countermeasures for moderate and severe squats

With severe squats and most of the moderate squats, rail replacement is often inevitable. With each replacement two new welds will be needed, which is a major disadvantage. As an alternative, a squat can be repaired by first removing the damaged part of the rail head (squat and also the possible crack), and subsequently filling the cavity by welding. This is often applied to parts of switches and crossings. It is very important to guarantee the quality of the welding process and the ensuing grinding to reduce the chance for new squats to occur at the repair welds.

The large dynamic force at squats causes damage to railpads, fastening, sleepers and ballast. They should also be repaired when squats are removed. Otherwise such track short defects may cause squats to re-occur.

4.5.3. Preventive and early corrective countermeasures

Class A squats and some class B squats with shallow cracks can be removed effectively by grinding. In principle squats should be removed at the earliest possible occasion. The characteristic critical size derived in this work provides a criterion for classification and early detection of light squats for LCC reduction.

It should be pointed out that when grinding the non-uniform sub-surface plastic deformation at the squats due to the local high dynamic force should also be taken into account. Otherwise the remaining in-homogeneity in the surface layer of the rail material may promote re-occurrence of squats.

Because squats always grow from small rail top surface defects, preventive and cyclic grinding will greatly reduce their occurrence. Preventive grinding should be applied shortly after new rail is installed. Interval and depth of cyclic grinding should be determined optimally from a life cycle costs point of view, with loading conditions taken into account.

Reducing the width of the heat affected zone of welds to below a critical size should help reduce squats at welds. The methodology presented in this work may be employed for the determination of such a critical size. Improved finish geometry will also help.

Short pitch corrugation as a major initiation source of squats should have been treated according other criteria such as acoustic noise based, before it has to be treated for squat formation.

4.5.4. Automatic detection of light squats

From a maintenance point of view, squats should be detected as early as possible so that predictive and preventive actions can be taken in time to reduce LCC.

Currently the most widely employed automatic inspection for squats is ultra-sonic detection. This method detects cracks and it is reliable only when the cracks are more than 5 – 7 mm deep. Such a depth of cracks is often too late for grinding.

As discussed in section 4.2.2 light squats should be detectable according to their wavelength/frequency characteristic by instrumented wheels or axle boxes. These methods have the advantage to measure or give indication of the magnitude of the dynamic contact force. The tendency of the squats to grow may therefore be assessed based on measurements. This may lead to more accurate detection and classification of squats than visual inspection since the measurement automatically includes not only the influence of the 3D dimension of the squats, but also those of all the other parameters in the system which may promote the initiation and growth of squats. The development of such a system for the detection of light squats, together with the necessary criteria presents a challenge.

4.5.5. Preventive measures by design

The best countermeasures are always those predictive and preventive based on fundamental understanding of the problems and optimal design of the system. As the correlation and numerical analyses have shown that a large amount of squats are related to short pitch corrugation, research on corrugation and on squatting should join hands. Because there have been strong evidences that occurrence of the short pitch corrugation is in one way or another related to some parameters of the track system, it should be possible that one day when the controlling parameters of the short pitch corrugations are identified, short pitch corrugation and squats formation can be controlled by improved design.

4.6. Bibliography

4.1 P. Clayton: *Wear*, 1996, vol. 191, pp. 170-183.

4.2 R. Nakumura, S. Owaku and N. Enomoto: *Rep. Railway Tech. Res. Inst. Jpn. National Railways,* 1965, vol. 6, pp. 34-44.

4.3 A. Ito and R. Kurihara: *Bull. Permanent Way Sot. Jpn.,* 1965, vol. 13 pp. 17-32.

4.4. P. Clayton and M.B.P. Allery: *Can. Metall. Q.*, 1982, vol. 21, pp. 31-46.

4.5 R. Deroche, J.P. Bettembourg, B. Prasil, J.P. Bertrand and C. Juckum: *Rail Quality and Maintenance for Modem Railway Operation,* Kluwer, Dordrecht, 1993, pp. 435-448.

4.6 J. Smulders: *Railway Gazette International,* 2003, June, 439 – 442.

4.7 UIC Code 712, Rail defects, 4th edition, January 2002.

4.8 Rail Damages, the Blue Book of RailTrack, February, 2001, UK.

4.9 Classification of Squats with Examples (in Dutch: Categorie indeling voor Squats aan de handen van Voorbeelden), Squat Handout, Version 2, March, 2004, ProRail

4.10 Z. Li, X Zhao, C. Esveld, R. Dollevoet and M. Molodova: *Wear*, 2008, vol. 265, pp. 1349– 1355, doi:10.1016/j.wear.2008.02.037.

4.11 P. Clayton, M.B.P. Allery, and P.J. Bolton: *J. Kalousek R.V. Dukkipati and G.M.L. Gladwell Ed. Proceedings of the conference on*

Contact Mechanics and Wear of Rail/wheel Systems, Vancouver, British Columbia, July 6-9, 1982, 419-443, University of Waterloo Press, 1983.

4.12 P. Clayton and D.N. Hill (1987): *G.M.L. Gladwell, H. Ghonem and J. Kalousek Ed. Proceedings of the conference on Contact Mechanics and Wear of Rail/wheel Systems II*, University of Rhode Island, Kingston, R.I., July 8 - 11, 1986, 361-378, University of Waterloo Press, 1987.

4.13 D.F. Cannon, H. Pradier: *Wear*, 1996, vol. 191, pp. 1-13.

4.14 S. Bogdanski, M. Olzak and J. Stupnicki: *Wear,* 1996, vol. 191, pp. 14-24.

4.15 S Bogdanski and R. Lewicki: *Wear,* 2008, vol. 265, pp. 1356 – 1362.

4.16 K. Kondo, K. Yoroizaka and Y. Sato: *Wear,* 1996, vol. 191, pp. 199-203.

4.17 M. Ishida, M. Akama, K. Kashiwaya and A. Kapoor: *Fatigue Fract Engng Mater Struct,* 2003, vol. 26, pp. 909-919.

4.18 P.E. Bold, M.W. Brown and R.J. Allen: *Wear*, 1991, vol. 144, pp. 307-317.

4.19 R. Smallwood, J. C. Sinclair and K. J. Sawley: *Wear,* 1991, vol. 144, pp. 373-384.

4.20 M. Busquet, L. Baillet, C. Bordreuil and Y. Berthier: *Wear* 2005, vol. 258, pp. 1071–1080.

4.21 K. Dang Van and M.H. Maitournam: *Fatigue Fract Engng Mater Struct,* 2003, vol. 26, pp. 939-948.

4.22 Z. Li, X. Zhao, R. Dollevoet, and M. Molodova: *Vehicle System dynamics,* 2008, vol. 46 (*Supplement* 1), pp. 237-46. DOI: 10.1080/00423110801935855

4.23 Li Z, Zhao X, Esveld C and Dollevoet R (2007), *Rail Stresses, Strain and Fatigue under Dynamic Wheel-Rail Interaction*. Proceedings International Heavy Haul Conferences 2007 Specialist Technical Session, June 11 – 13, 2007 at Kiruna, Sweden, 389 – 396

5. Corrugation

5.1. Background

In the following, corrugation refers to small amplitude undulations (irregularities, roughness, waviness) with wavelengths in the order of 1 – 10 cm on the running surfaces of wheels and rails. These can induce vibrations that cause rolling noise and high-frequency vertical wheel–rail contact forces that in turn may cause subsurface initiated rolling contact fatigue (RCF) in wheels and rail.

The study concerns tangent track operations on modern tracks (60E1 rails on resilient rail pads and concrete monobloc sleepers with a spacing of 0.60–0.65 m) and speeds in the order of 200 km/h for passenger wagons and 100 km/h for freight wagons. Simulations of train–track interaction are carried out using DIFF [5.1], which incorporates high-frequency interaction up to some 2 to 3 kHz. For details on simulations and measurements performed, the reader is referred to INNOTRACK deliverables D4.2.1 [5.2] and D4.2.4 [5.3].

The formation and growth of corrugation is not a scope of the current guideline. The interested reader is referred to references [5.4, 5.5, 5.6, 5.7].

Current regulations throughout Europe differ between countries and mainly consider the influence on noise generation. In the UIC series of technical and research reports, rail corrugation is included under topic D 185. The European norm EN 15610:2009 regulates measurements of corrugation.

5.2. Corrugation characteristics

The type of corrugation investigated within the frame of INNOTRACK is so-called short-pitch rail corrugation, corresponding to “roaring rail” corrugation using the nomenclature of Grassie and Kalousek [5.7].

The “standard corrugation spectrum” employed in the subsequent analyses is based on measurements with the Corrugation Analysis Trolley (CAT) on three severely corrugated stretches of track between Stockholm and Gothenburg in Sweden (max speed 200 km/h). The roughness levels are in the order of 20 dB (re 1 μm) at wavelengths in the interval 4 – 8 cm. Measurements in Koerle, Germany (max speed 250 km/h) show a similar corrugation spectrum.

The rail corrugation in the wavelength interval 3 – 8 cm is here quantified by taking the mean square of rail roughness levels in the five 1/3 octave bands with centre wavelengths 3.16, 4.0, 5.0, 6.3 and 8.0 cm as

$$\tilde{r}^2_{\text{mean, 3-8 cm}} = \tilde{r}^2_{\text{ref}} \frac{1}{5} \sum_{i=1}^{5} 10^{L_{\text{r},i}/10} \tag{5.2}$$

The corresponding mean roughness level $L_{\text{r,3-8 cm}}$ is obtained as

$$L_{\text{r,3-8 cm}} = 20\log_{10}\left(\frac{\tilde{r}_{\text{mean,3-8 cm}}}{r_{\text{ref}}}\right) \tag{5.3}$$

where r_{ref} = 1 μm. The mean roughness level for the “standard corrugation spectrum” (“Corrugated rail” in Fig 1.1) is 17.7 dB (re 1 μm).

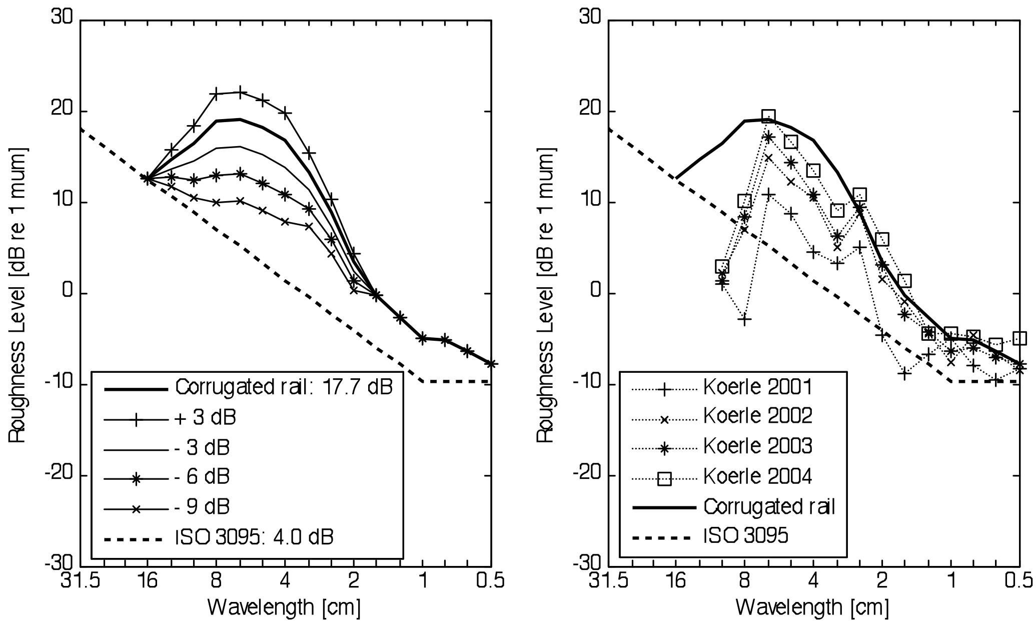

Figure 5-1 Rail roughness level spectra used in the parametric studies (left) and comparison to corrugation spectrum in Koerle (right). From [5.8].

As a comparison, a “smooth” rail is defined in accordance to ISO 3095. The mean roughness level for the ISO 3095 spectra is 4.0 dB (re 1 μm). An increased (decreased) roughness is obtained by adding (subtracting) multiples of 3 dB from the mean roughness level of the

"Corrugated rail". The corresponding roughness spectra are shown in Figure 5-1. Measurements on less corrugated rails show good correlations to these downscaled magnitudes (see [5.8]).

5.2.1. Wheel–rail contact forces

Wheel–rail contact forces during operations on the corrugated rail have been measured with high-frequency sampling as described in [5.9]. A numerical model in DIFF [5.1] has been calibrated against the measured data, see [5.10].

For the cases studied it is found that a major contribution to the wheel–rail contact force lies in the frequency domain 200–1000 Hz. A 90 Hz low-pass filtering (of measured or simulated contact forces) will result in a basically (quasi-)static response, see Figure 5-2.

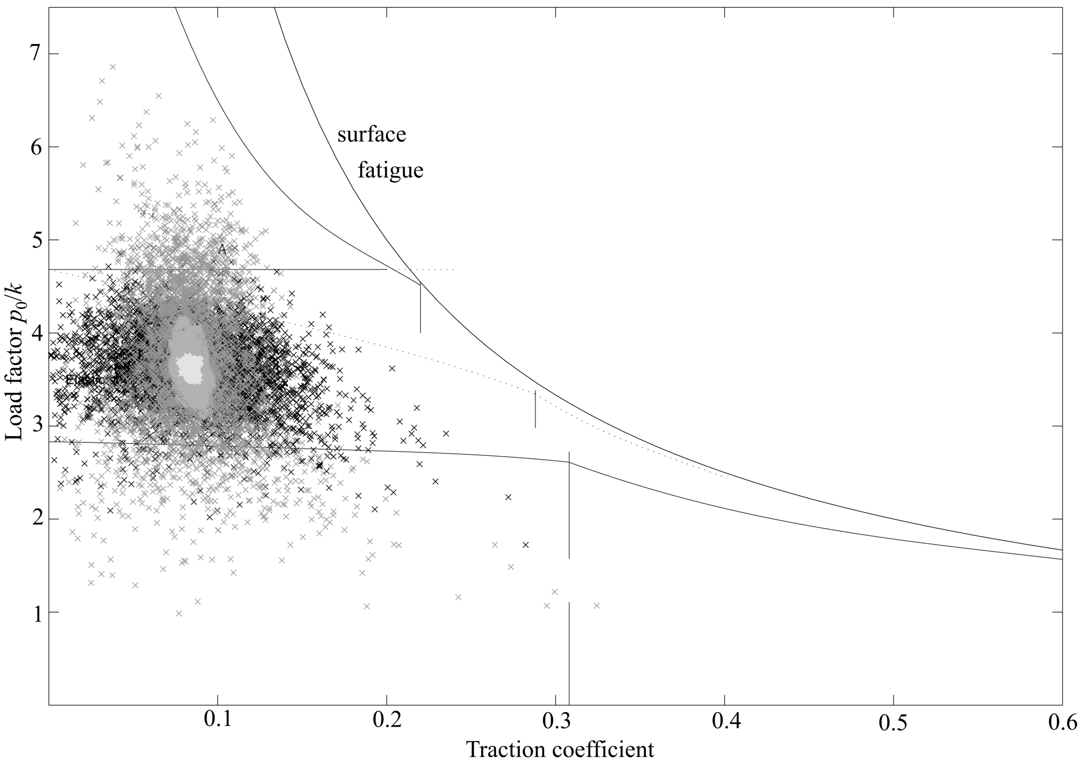

Figure 5-2 Shakedown diagram with response given in terms of scaled contact pressures (p_0/k) versus traction coefficients . The studied case is a powered wheelset at v = 200 km/h on corrugated rails. The wheel–rail friction coefficient is μ = 0.3. Responses using low-pass filter with cut-off frequency at 90 Hz (light grey), 200 Hz (grey) or 1000 Hz (dark grey) are compared to the non-filtered response (black). From [5.11].

5.3. Parametric influence

To quantify the vertical wheel–rail contact force in magnitudes relevant for subsurface initiated rolling contact fatigue (RCF), a fatigue index has been adopted. This index, FI_{sub}, is taken as the Dang Van equivalent stress, which for the current study can be written as

$$FI_{\mathrm{sub}} = \frac{F}{4\pi ab} \tag{5.4}$$

where F is the vertical wheel–rail contact force and a and b the semi-axes of the Hertzian contact.

A reasonable assumption is that there is a risk of subsurface initiated RCF if $FI_{sub} \geq 220$ MPa (see references [5.2, 5.3] for details).

Noise emissions are evaluated using TWINS [5.12] from a model calibrated to field measurements, see [5.8, 5.13]. Sound pressure levels (SPL) are calculated at 7.5 m from track centre and 1.2 m above the rail.

Three vehicle–track configurations are considered. Main parameters are given in Table 5-1.

Details of the simulations are given in references [5.8, 5.13, 5.14, 5.11] along with simulation results for other cases.

Table 5-1 Main parameters of vehicles considered.

Vehicle	axle load [tonnes]	unsprung mass [kg]	wheel radius [m]	axle distance [m]	pad stiffness [kN/m]
X2000 [5.11]	12	1390	0.44	2.9	100
Passenger [5.8]	17	1200	0.44	2.9	120
Freight [5.8]	22.5	1200	0.44	1.8	120

5.3.1. Influence of speed and corrugation magnitudes

In Figure 5-3 and Figure 5-4 the parametric influence of speed on FI_{sub} is seen. Three conclusions can be drawn:

- An increased speed will increase the fatigue impact in terms of higher extreme FI_{sub} magnitudes.

- The increase in FI_{sub} magnitudes due to a certain increase in vehicle speed will be lesser for higher speeds. This trend is very marked for high-speed operations, but hard to distinguish at the moderate speeds of freight operations.

- The more severe the corrugation, the less the influence of vehicle speed on extreme FI_{sub} magnitudes.

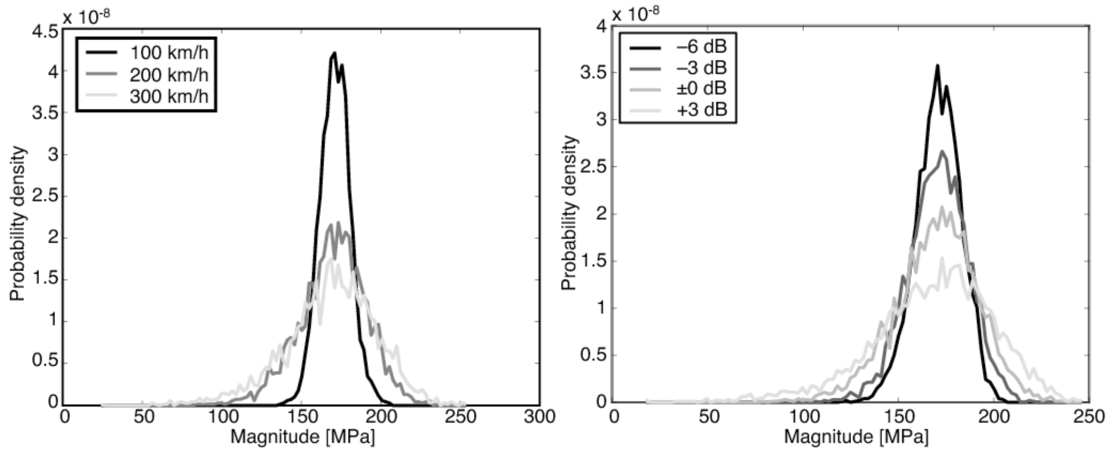

Figure 5-3 Influence of speed (left) and corrugation magnitude (right) on magnitudes of FI_{sub} for an X2000 vehicle. Corrugation magnitudes of ±0 dB correspond to $L_{r,3\text{-}8\ cm}$ = 17.7 dB. From [5.14]

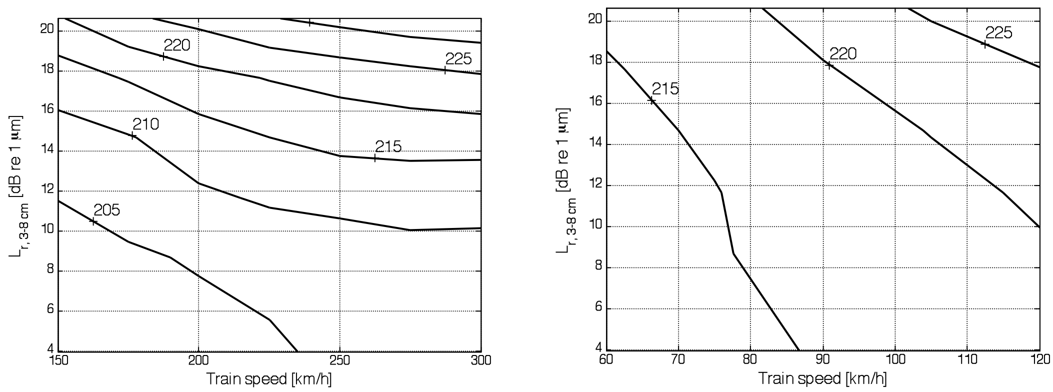

Figure 5-4 Influence of corrugation magnitude ($L_{r,3\text{-}8\ cm}$) and train speed on magnitudes of FI_{sub} [MPa] for passenger (left) and freight (right) vehicles. From [5.13].

Noise emissions are significantly influenced by the roughness of the wheel. In the following this is accounted for by adopting wheel roughness spectra based on measured disc braked passenger wheels and tread braked freight wheels (see [5.13] for details).

Figure 5-5 shows the influence of vehicle speed and corrugation magnitudes on noise emission levels. Similar conclusions that could be drawn with respect to subsurface initiated RCF (in terms of FI_{sub} magnitudes) can be drawn with respect to noise emissions (in terms of SPL), namely:

- An increased speed will lead to increased noise emissions in terms of higher SPL magnitudes.
- The increase in SPL magnitudes due to a certain increase in vehicle speed will be lesser for higher speeds.

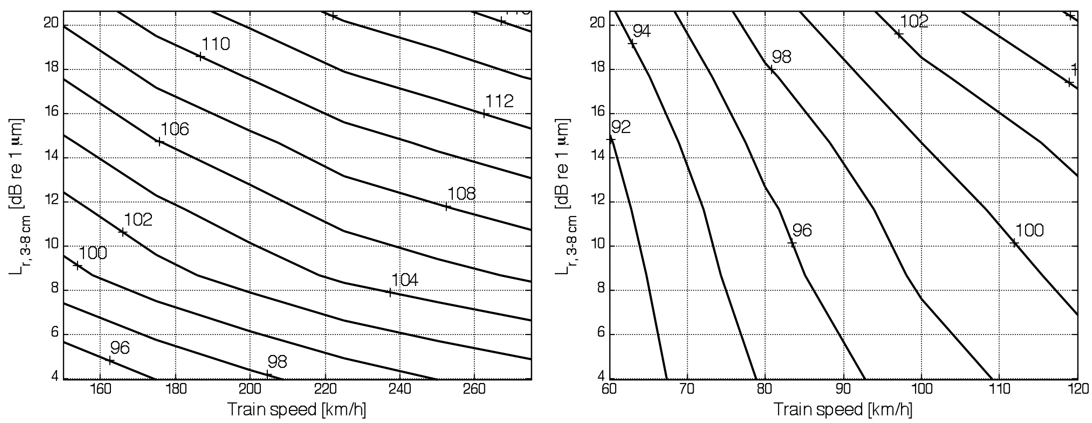

Figure 5-5 Influences of train speed and mean rail roughness level on SPL [dBA]. Response for passenger train (left) and freight vehicle (right). From [5.13].

5.3.2. Influence of un-sprung mass and axle load

As can be seen in the left graph of Figure 5-6, the influence of the axle load is in increasing the mean value of FI_{sub}, but decreasing the scatter. The consequence will be a higher net RCF loading, but a decreased influence of the corrugation. The same trend can be seen when comparing the two graphs in Figure 5-4.

As seen in the right graph of Figure 5-6, the influence of the un-sprung mass on RCF is negligible under the considered conditions.

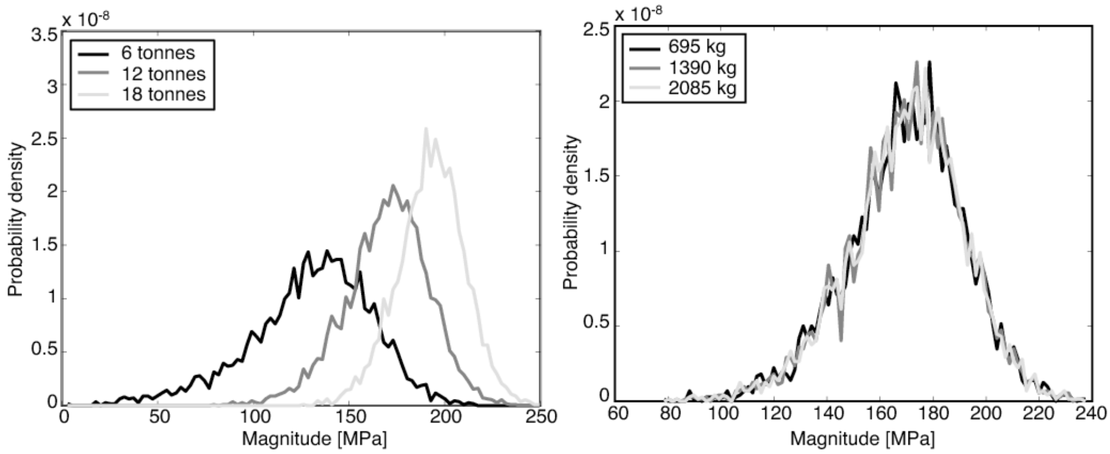

Figure 5-6 *Influence of axle load (left) and un-sprung mass (right) on magnitudes of FI_{sub} for an X2000 vehicle. Speed 200 km/h, $L_{r,3\text{-}8\,cm}$ = 17.7 dB. From [5.14].*

5.4. Operational acceptance criteria

With the help of the numerical models described above, a stringent, scientifically based method of defining operational acceptance levels for corrugation under the studied conditions has been developed, see [5.13]. Based on least square fits of the calculated SPLs [dB(A)] in Figure 5-5, response surface models have been determined to quantify the effects of train speed and mean rail roughness level, see [5.13]. The method is outlined in Figure 5-7.

Given the operational conditions, evaluations of sound pressure levels are carried out for varying magnitudes of corrugation. In addition RCF is assessed by an evaluation of FI_{sub}. Risk of subsurface initiated RCF (in wheels and/or rails) is considered by defining an allowed FI_{sub} magnitude. Rail corrugation magnitudes for which this threshold is exceeded are identified.

The acceptable rail corrugation magnitude is then defined as the highest magnitude for which noise emissions and RCF loadings are acceptable.

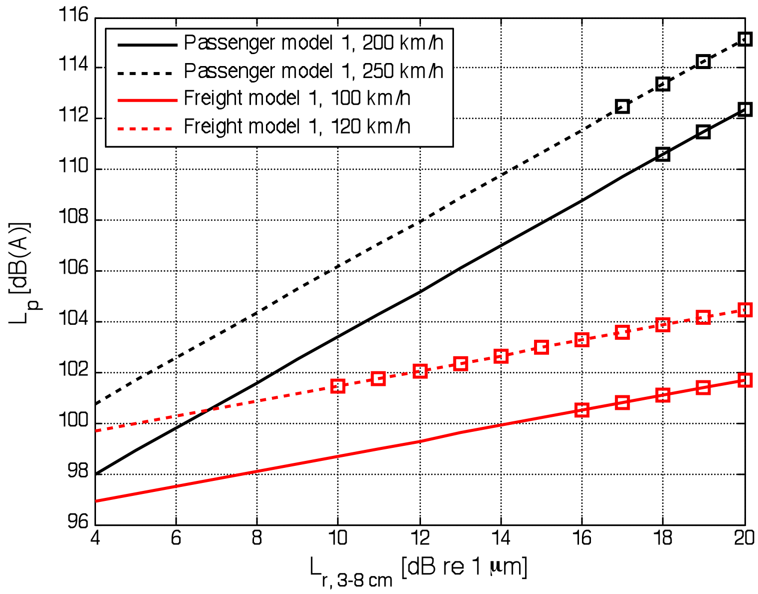

Figure 5-7 Demonstration example of the establishment of operational acceptance limits: influence of mean rail roughness level on SPL at 7.5 from track centre. Operational cases that pose a risk for subsurface initiated RCF are marked with squares. From [5.13].

The definition of acceptance limits can account for risk analyses (e.g. by the chosen limit on allowed FI_{sub} magnitude) and imposed noise restrictions. It can also be adopted in an iterative fashion where, at a first stage, simplified methods and generalized corrugation spectra (such as those provided in this and referenced reports) are adopted. Finally it can be adopted for predictive purposes e.g. when upgrading lines.

5.5. Conclusions and recommendations

The following conclusions and recommendations are valid for (close to) tangent track operations on modern tracks (60E1 rails on resilient rail pads and concrete sleepers) and speeds around 200 km/h for passenger and 100 km/h for freight operations. The conclusions may be valid for other kinds of operations, but this has not been validated in the INNOTRACK study.

5.5.1. Corrugation characteristics

A wavelength spectrum for corrugated rails on modern tracks has been quantified (Figure 5-1). The similarity of spectra evaluated at different locations and allowed speeds (between 200 and 250 km/h) are consistent enough to recommend using the derived spectrum as a standard spectrum for analyses of consequences of short pitch rail corrugation on tangent tracks under the stated conditions.

Scaling of the corrugation spectrum has been defined (Figure 5-1). Corrugation spectra on stretches where corrugation is less developed show sufficient agreement to recommend using the scaled spectrum as a standard for analyses of growing rail corrugation under the prescribed conditions.

Corrugation induces wheel–rail contact force in the frequency domain 200–1000 Hz. Contact force measurements and numerical simulations of corrugations need to consider high enough frequencies to capture these contributions.

5.5.2. Influence of speed, axle load etc on RCF and noise emissions

A given speed increase will increase the maximum RCF loading. (The relative increase is less the higher the speed in high-speed operations. The influence of vehicle speed on RCF loading decreases with increased corrugation magnitude.)

A given speed increase will increase noise emissions. (The relative increase is less the higher the speed.)

An increased axle load will increase the mean value of the RCF loading, but the load scatter due to the corrugation will decrease. Normally the result will be a net increase in maximum RCF loading.

5.5.3. Operational acceptance criteria

Operational acceptance levels for corrugation under the studied conditions are defined in the following manner:

Given the operational conditions including rail and wheel roughness spectra (available in [5.13]), sound pressure levels are evaluated for varying magnitudes of corrugation. RCF is assessed by FI_{sub} evaluation and comparison to an allowed FI_{sub} magnitude. Allowed rail corrugation magnitude is then defined as the highest magnitude for which noise emissions and RCF loadings are acceptable.

Numerical tools to predict wheel–rail interaction and resulting RCF loading and noise emissions for such an assessment exist and have been validated against field measurements.

An example of how to define operational acceptance levels is shown in Figure 5-7 with details in [5.13].

5.6. Bibliography

5.1 Jens C O Nielsen & Annika Igeland. **Vertical dynamic interaction between train and track – influence of wheel and track imperfections**, *Journal of Sound and Vibration*, vol 187, no 5, 825–839, 1995

5.2 INNOTRACK Deliverable 4.2.1 – **Simplified relation for the influence of rail/joint degradation on operational loads and subsequent deterioration**, 22 pp, and 10 appendices, 27+25+10+12+6+8+7+7+25+4 pp, 2007

5.3 INNOTRACK Deliverable 4.2.4 – **Improved model for loading and subsequent deterioration due to squats and corrugation**, 33 pp, and 5 appendices, 7+10+8+26+26 pp, 2009

5.4 Annika Igeland, **Railhead corrugation growth explained by dynamic interaction between track and bogie wheelsets**, *IMechE Journal of Rail and Rapid Transit*, vol 210, no 1, pp 11–20, 1996

5.5 Heike Ilias, **The influence of railpad stiffness on wheelset/track interaction and corrugation growth**, *Journal of Sound and Vibration*, vol 227, no5, pp 935–948, 1999

5.6 Jens C O Nielsen, Roger Lundén, Anders Johansson & Tore Vernersson, **Train-track interaction and mechanisms of irregular wear on wheel and rail surfaces**, *Vehicle System Dynamics*, vol 40, nos 1-3, pp 3-54, 2003

5.7 Stuart Grassie & Joe Kalousek, **Rail corrugations. Characteristics, Causes and Treatments**, *IMechE Journal of Rail and Rapid Transit*, vol 207, no 1, pp 57–68, 1993

5.8 Jens C O Nielsen & Anders Ekberg, **Subsurface initiated rolling contact fatigue and rolling noise – influence of train speed and rail roughness**, Research report 2009:04, *Department of Applied Mechanics, Chalmers University of Technology*, Gothenburg, Sweden, 26 pp

5.9 Per Gullers, Lars Andersson and Roger Lundén, **High-frequency vertical wheel–rail contact forces – field**

measurements and influence of track irregularities, *Wear*, vol 265, pp 1472–1478, 2008

5.10 Jens C O Nielsen, **High-frequency vertical wheel–rail contact forces – validation of a prediction model by field testing**, *Wear*, vol 265, pp 1465-1471, 2008

5.11 Jens C O Nielsen, Anders Ekberg & Roger Lundén, **Influence of short-pitch wheel/rail corrugation on rolling contact fatigue**, *IMechE Journal of Rail and Rapid Transit*, vol 219, no F3, pp 177–187, 2005

5.12 **TWINS (Track Wheel Interaction Noise Software), Theoretical and User´s Manual (version 3.0)**, *TNO Institute of Applied Physics*, Delft, The Netherlands, 1999

5.13 Jens C O Nielsen & Anders Ekberg, **Acceptance criterion for rail roughness level spectrum based on assessment of rolling contact fatigue and rolling noise**, *Proceedings 8th International Conference on Contact Mechanics and Wear of Rail/Wheel Systems (CM2009)*, Florence (Italy), September 2009, vol 2, pp 409–418

5.14 Anders Ekberg, Elena Kabo, Jens C O Nielsen & Roger Lundén, **Subsurface initiated rolling contact fatigue of railway wheels as generated by rail corrugation**, *International Journal of Solids and Structures*, vol 44, pp 7975–7987, 2007

6. Wear

6.1. Background

Rail wear influences both vehicle performance and rail life. Wheel and rail profiles are generally designed to (a) improve vehicle ride quality (for passenger comfort and safety), and (b) reduce rolling contact fatigue (RCF). Loss of material from the rail head (and also plastic deformation of the rail head) are gradual processes, but have the effect of changing the rail profile. When designing a new rail or wheel profile, therefore, a good model of rail wear is required so that changes to the profile over time can be predicted.

Periodic grinding is carried out to maintain the rail, usually to correct the profile but grinding also removes small cracks (and shortens longer cracks). Grinding can be considered as a controlled but severe wear process, removing about 0.2mm depth of material from the rail surface – by comparison, normal rail wear is usually less than 1nm per wheel pass.

A hypothetical example is a railway line, which sees 6 MGT (300000 axles with 20 tonne axle load) every six months, after which there is a regularly scheduled grinding maintenance; consequently, 0.5mm depth of material is removed from the rail during this half-year period.

In practice, wheels do not always make contact at the same transverse location on a rail, although if both wheel and rail profiles are tightly controlled (through frequent inspection and maintenance, i.e., rail grinding and wheel turning) the running band on the rail can be very narrow. Even a small change to the profile can cause a change in vehicle dynamics and lead to contact at a different location, so wear is distributed across the profile.

One method for reducing wear is to use harder steels (or even special coatings), since the general rule is that harder steels wear less and therefore harder wheels and harder rails will maintain their designed profiles longer. One difficulty with this approach is that both wheel and rail profiles need to be designed with this in mind. One of the advantages of softer steels is that locations where the wheel-rail contact causes especially high stresses wear faster and so the profiles adjust more quickly to remove high-stress contacts. Use of harder steels reduces wear but can maintain high-stress contacts for longer.

The combination of lower wear rate and higher stress is dangerous since crack initiation and growth increase; for this reason, harder steels need to be designed to be more crack-resistant as well as wear-resistant.

Another concern with harder wheels and rails is the question: *Do harder wheels wear rails faster?* (And vice versa.) The perceived wisdom is that they do, but anything that affects wear rate will affect profile evolution and consequently vehicle dynamics and thus also the wheel-rail contact, i.e., the whole system is affected by a change in one parameter. The question is non-trivial to answer, and the conclusion once again is that *wheel and rail profile design and maintenance must consider the whole system*.

Twin-disc tests

A series of twin-disc tests (on the **S**heffield **U**niversity **Ro**lling **S**liding testing machine – SUROS) has been performed in InnoTrack with the aims of:

- studying the effect of hardness of one disc on the wear rate of the opposite disc;
- calibrating material hardening and wear prediction models for a selection of pearlitic rail steel grades.

Wheel discs were machined from a VAS R7 wheel. Rail discs were machined from CORUS 260 and CORUS 400 grade rails, and from VA 350 and VA 400 grade rails. Tests were run at a peak pressure of 1500MPa and -1% slip to simulate a driving wheel, for the following three test sequences:

- 5000 cycles dry
- 5000 cycles dry followed by 5000 cycles wet (water-lubricated)
- 15000 cycles dry

Following testing, discs were sectioned and a series of micro-hardness measurements made from the surface to a depth of 10mm. Plastic shear strain was estimated from optical micrographs of the etched microstructure, and combined with the micro-hardness data to create material models for wear prediction. Measured wear rates were used to calibrate the wear model and to study the effect of rail disc hardness on wheel disc wear rate. (See InnoTrack Deliverable D4.2.5 for details.)

6.2. Parametric influences on wear

6.2.1. Effect of hardness

During the cyclic loading of material as a consequence of passing trains, the steel microstructure deforms plastically and, in general, hardens. Metallurgy has an effect on rail and wheel steel hardness and strain-hardening characteristics, and also on wear behaviour and susceptibility to crack initiation, but the correlation between these is not straightforward.

To investigate hardness of the material, test specimens have been sectioned and microhardness measurements taken at different depths on a circumferential cross-section. All discs have shown material hardening characteristics at the surface.

The rail material hardens more when run for more cycles. The softer CORUS 260 steel hardens more at the surface (i.e., at a depth of 50 microns) than the harder VA 350 and CORUS 400 in dry tests, while the other two materials have similar hardening rates. In wet tests, the CORUS 260 deteriorated a lot and is almost always softer than the other two materials when measured from the surface into the depth of material.

The wheel discs had similar hardness values initially. When microhardness was measured after testing, the wheel discs (like the rail discs) had hardened most for 15000 cycles, less for 10000 cycles (5000 dry + 5000 wet), and the least for 5000 cycles dry. After 15000 cycles dry, the wheel disc microhardness at depth 50 microns correlates with the rail disc microhardness at depth 50 microns, i.e., the CORUS 260 was the hardest at this depth, then the VA 350, and finally the CORUS 400 and VA 400, and the corresponding wheel discs matched this order of hardness. However, there is no matching trend after 5000 cycles.

In general, the harder the rail disc material becomes at the surface, the harder the wheel disc material becomes at the surface. Rail disc wear decreases when rail steel hardness increases. In wet tests, wheel disc wear rate drops as rail disc hardness increases. In the system as a whole (i.e., considering both wheel and rail discs), using harder CORUS 400 and VA 400 rail steels lowers the total wear rate.

From a review of the academic literature, there is no conclusive finding that harder rails wear wheels more, or vice versa. In general, harder materials wear less, but material hardness is not the only determining factor of wear performance; microstructure and strain-hardening behaviour are critical factors, and rolling contact fatigue performance is equally important. However, as a fairly general rule:

→ *To reduce system wear, harder steel grades should be used for both wheel and rail.*

6.2.2. Effect of contact load and traction

Deliverable D4.2.5 focused on development of material hardening models of the tested rail steel grades for use in rail wear prediction. The report comprised detailed results from twin-disc tests, a literature survey of the effect of wheel and rail hardness on wear rates, and development of an improved wear model and a simplified wear equation. The wear model, calibrated for CORUS 260 and dry contact, was used to study the effect on rail wear of vehicle characteristics through their effect on the wheel-rail contact. The patch was assumed to be elliptical and the pressure distribution to be Hertzian; in addition, the contact was assumed to be on the top the rail, suitable for straight track, not curves, and the traction to be longitudinal only.

Traction coefficient has a significant effect on the wear rate. For distributed traction systems the traction coefficient may often be about 0.1, i.e., an average wear rate of about 0.75nm/cycle. For locomotives the traction coefficient may be 0.3 or even higher, i.e., an average wear rate of 1.5nm/cycle or more.

→ *There was a very clear linear trend of wear rate against peak contact pressure (for the range of pressures studied).*

→ *Wear equations, giving wear rate for a given pressure and traction coefficient, have been extrapolated which can be used for quick estimation of rail wear.*

The wear rate equation was developed for an elliptic wheel-rail contact patch with a fixed elliptic ratio (longitudinal semi-contact width over transverse semi-contact width) of 1.32, derived for wheel-rail contact on top of the rail head (i.e., appropriate for straight track, not curves). The longitudinal and transverse contact half-widths in [m] are given by:

$$a_L = 1.57 \times 10^{-4} \times \sqrt[3]{F}$$
$$a_T = 1.19 \times 10^{-4} \times \sqrt[3]{F}$$

where F [N] is the normal load, and the peak pressure is:

$$p_0 = \frac{3}{2}\frac{F}{\pi a_L a_T}$$

The wear rate is maximum under the centreline of the wheel-rail contact and drops to zero near the edges of the contact; Figure 6-1 shows this effect for a selection of traction coefficients – clearly wear rate increases as the traction coefficient increases. Wear rate increases also as the normal load (and thus peak pressure) increases. Figure 6-2 shows the predicted wear rates for a range of normal loads – the wear rate varies linearly with the peak pressure. Wear rate increases with time, starting low when the rail is relatively undamaged, increasing asymptotically to a 'steady state' wear rate; Figure 6-2 shows the wear rates averaged over (a) the first 10000 wheel passes, (b) all 100000 wheel passes of the simulation, and (c) the final 10000 wheel passes (which is used to determine the asymptotic behaviour). These results have been used to construct the following simple wear equations.

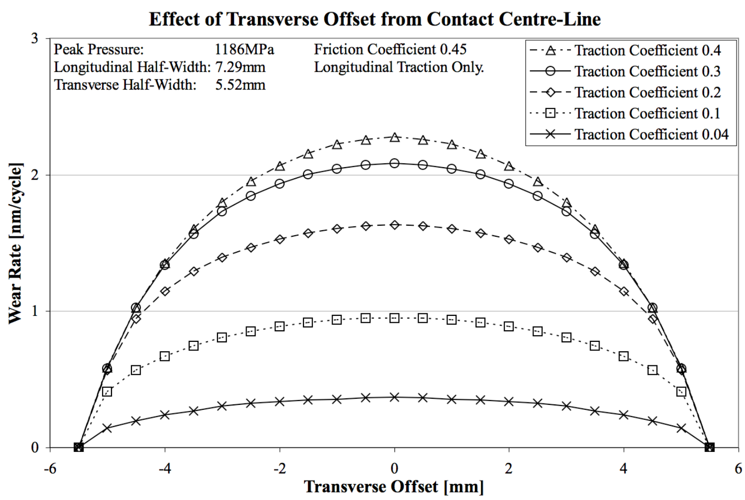

Figure 6-1 *Predicted wear rates, averaged over 100000 cycles, for a range of (longitudinal) traction coefficients (with friction coefficient 0.45) and normal load 100kN. The transverse half-width is 5.52mm, and wear rates are evaluated in 0.5mm intervals from the centreline to the edge of the contact.*

The average wear rate over the first 100000 wheel passes is given by:

$$\bar{w} = 0.2\frac{t_c}{\mu}\left(3-\frac{t_c}{\mu}\right)^2 (2.3226p - 0.6761)$$

where p is peak pressure [in GPa], t_c is the traction coefficient, and $\bar{w}$ is average wear rate [in nm/cycle]; friction coefficient is fixed as μ=0.45, suitable for dry conditions. The asymptotic wear rate (i.e., the 'steady state' wear rate, usually achieved by 100000 cycles) is given by:

$$\underset{\rightarrow}{w} = 0.2\frac{t_c}{\mu}\left(3-\frac{t_c}{\mu}\right)^2 (2.5513p - 0.5579)$$

Both wear rate equations are linear functions of pressure (which is proportional to the cube root of the normal force), for a fixed traction coefficient, so the final wear pattern will be a linear function of pressure. The wear rate equations were used in InnoTrack Deliverable D4.2.3 to predict the pattern of wear at an insulated joint.

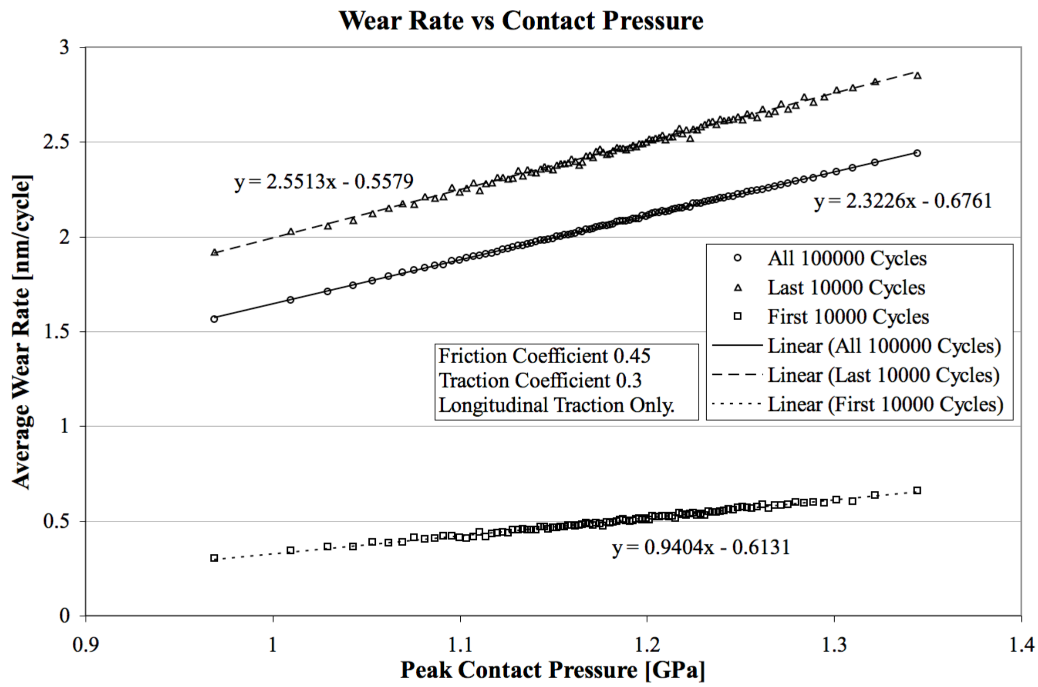

Figure 6-2 Wear rates from simulations over 100000 cycles showing the effect of pressure.

To calculate profile area loss, the wear rate should be multiplied by the width of the contact. Contour plots of profile area loss against traction coefficient and normal load are presented in Figure 6-3.

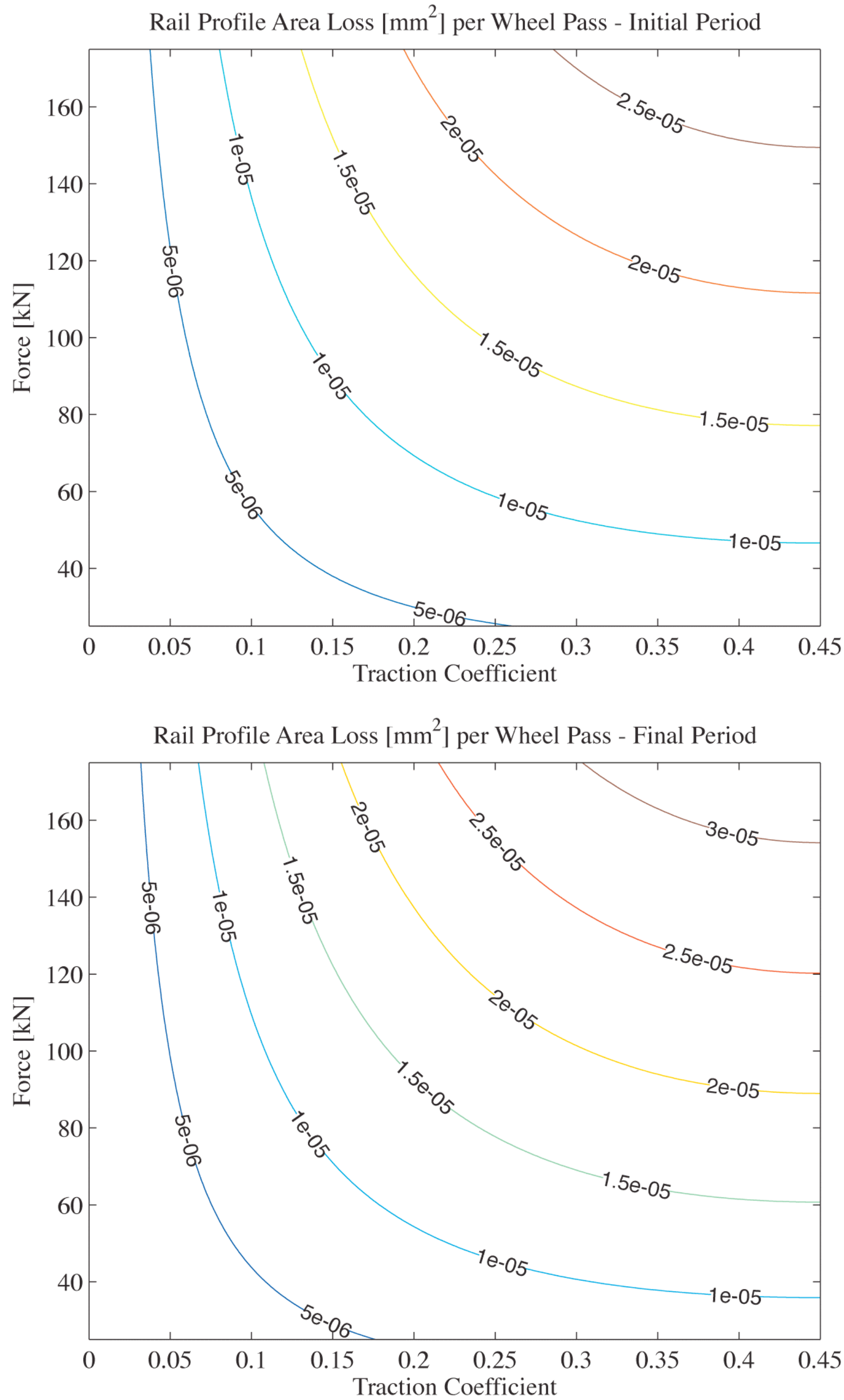

Figure 6-3 Contours of wear rate (profile area loss per wheel pass, in mm2) against traction coefficient (for friction coefficient μ=0.45) and normal load. Above: Averaged over initial 100000 cycles. Below: Averaged over final 10000 cycles of simulations over 100000 cycles.

The equations are based on dry contact and CORUS 260 rail steel. The results are only applicable to head-of-the-rail contact so there will be no curving forces and thus only longitudinal friction forces, usually from locomotives and multiple units, except on approach to stations *where braking is normal and coaches may also therefore contribute significant wear.*

6.3. “Minimum action rules”

Weather is a major factor.

During dry periods (and similarly in tunnels), the coefficient of friction, and thus the available traction, between wheel and rail will be high. Wear rate will be relatively high, and crack initiation at the rail surface will be high also; surface crack length may appear significant, but in the absence of water or other liquid lubricants the cracks will not propagate deep into the rail. Frequent grinding may be necessary to control the profile.

On high-traffic lines through long tunnels, where wear is the dominant factor, wear-resistant premium grade rail steels should be a cost-effective method of extending rail life.

During wet periods the coefficient of friction is typically about half the dry value. This reduces the available adhesion and mainly impacts locomotives. The reduced traction lowers the stress at the rail surface, reducing both wear and crack initiation; however, the subsurface (2-4mm) stresses in the rail are still significant, and existing cracks will continue to grow, assisted by water penetration (water reduces crack face friction, accelerating crack growth in shear, and hydraulic pressurization of the crack can also accelerate crack growth).

The reduced adhesion level means an increased risk of wheel slip, even more so when there is snow or ice (or contaminants such as leaves) on the rails. High-slip contacts can generate high temperatures at the rail surface, causing wear and sometimes also microstructural changes to the steel (e.g., formation of patches of martensite or white etching layer) with the potential for later crack development.

One common method for controlling adhesion is to introduce sand (or similar) into the wheel-rail contact. These hard particles increase the available traction at the contact, increasing the stresses in the rail and thus the potential for wear and RCF, but also add to the abrasive wear at the rail surface.

When the conditions are continuously dry or continuously wet, wear and RCF behaviour are relatively easy to predict. When conditions are mixed the problem is highly complex, which is why weather is a major factor. During a dry spell, there is a gradual build up of short cracks (within about 1mm of the rail surface); during a subsequent wet spell, growth of these cracks is accelerated. A high density of cracks can also increase wear significantly.

6.3.1. Recommended maintenance practice

On routes where harder wheel steels are used, rail profiles should be selected carefully to match the wheel profile – especially where harder rail steels are also used – to ensure optimum system wear performance and reduce the potential for RCF.

For predominantly dry environments, premium grade wear-resistant steels should provide a cost-effective solution for maximizing rail life.

Locations where a long wet spell follows a long dry spell should be inspected more frequently. In regions where weather can be predicted, it is reasonable to schedule the rail grinding at the end of the dry and the beginning of the wet period, to prevent growth of microstructurally short cracks to longer stress-driven cracks which could lead eventually to rail breaks.

In general, when choosing the right rail steel for replacing track, hardness of steel should be considered in conjunction with type of traffic, loads and wheel steels.

New proposed rail steel grades should be tested in the laboratory to calibrate models of wear and RCF for use in rail profile optimization.

Because wear rate is hard to predict precisely, wear should be measured periodically at certain points on the track and recorded in a database, which could be used for validating wear models.

6.3.2. Recommended documentation practice

For proper assessment of rail wear, rail profile measurements (e.g., by MiniProf) should be recorded in a central database. In addition to the profile itself, the following data would be useful:

- name of person taking the measurement
- specific track location and rail identifier
- geographical location (GPS or map coordinates) and date – useful for weather tracking

- track geometry and features (e.g., curve radius, cant, proximity to welds, joints, bridges, etc.)
- rail material and sub-grade type (e.g., ballasted); evidence of sanding or other contaminants
- potential influences from environment (trees, factories, airports, track lubricators)
- initial profile; date of last grinding (if any) and target ground profile
- ID of last record (if any) of profile measurement at the current location
- rail surface inspection (i.e., running band, corrugation, plastic flow, cracks, etc.)
- traffic sequence and type(s) of traffic; wheel material and profile(s); axle loads

6.4. Future work

The wear model and wear equations provide wear rate predictions for specific wheel-rail contacts. To provide a predictive tool of use to infrastructure managers, the wear equations can be incorporated into train-track interaction simulations (e.g., VAMPIRE) to study rail profile evolution, roughness growth and fatigue life.

The test work, metallurgical analysis and wear model development carried out within InnoTrack provides the basis for further development in the immediate future with the following aims for construction of a more general wear equation:

- Calibration and validation of the ratcheting wear model for premium grade rail steels.
- Prediction of wear rates for a range of coefficients of friction and for a range of contact locations across the rail head.
- Study of wear-fatigue interaction for short cracks in standard and premium grade rail steels.
- Study of the effect of variation of transverse location of wheel-rail contact on the wear rate.

Longer-term research and development includes:

- Re-assessment of the material model currently used to predict wear rate of UK 220 Grade rail steel.
- Calibration and validation of the ratcheting wear model for bainitic rail steels and molybdic-alloyed rails.
- Inclusion of thermal effects in the wear model for better prediction of wear in high-slip contacts (e.g., flange contact).
- Study of effect on near-surface stresses of wheel-rail micro-slip and rail surface micro-roughness.

6.5. Bibliography

6.1 INNOTRACK Deliverable 4.2.5 – **Improved model for the influence of vehicle conditions (wheel flats, speed, axle load) on the loading and subsequent deterioration of rails**, 47 pp, and 6 appendices, 47+15+9+22+35+53 pp, 2009

6.2 INNOTRACK Deliverable 4.2.3 – **Improved model for loading and subsequent deterioration of insulated joints**, 19 pp, and 1 appendix, 17 pp, 2009

7. Insulated joints

7.1. Background

Insulated joints electrically insulate two track sections from each other for signalling purposes: A wheelset operating on a track section will short-circuit the rails. By identifying which track section that is short-circuited the position of the train is known.

Insulating joints can be designed in different ways. A normal configuration is that the rail is cut transversally and an insulated polymer layer is placed (glued) in the gap between the rail ends. The joint is assembled using two beams (fishplates) that are bolted to each side of the rail. The joint is often prefabricated and the joint section assembled in the track by welding. Figure 7-1 shows an insulated joint where six bolts are connecting the fishplate to the rail web and where the joint is placed close to the sleeper. Operational designs include also e.g. attachment with four bolts and placement in the middle of the sleeper span.

Specifications of design, mounting and maintenance of insulated joints varies between the different countries in Europe. In the UIC series of technical and research reports, rail corrugation is included under topic A 5 (with the newest report from 1961).

Figure 7-1 A newly installed insulated joint on The West Coast Line in Sweden

Insulating joints are weak points of the rail that frequently cause problems. The joint imposes a sudden variation in track stiffness. Further wheel–rail impact loads are often generated at insulated joints because of a local rail surface irregularity caused by misalignment and plastic deformations of the rail ends. In addition, the insulating layer is very flexible in comparison to the rail. In practice the insulating gap can therefore be considered as free ends of the adjacent rails. This results in a severe stress concentration at the insulating layer.

The study in INNOTRACK focusses on two key issues with insulating joints:

- The wheel–rail contact force during a joint negotiation. High wheel–rail impact forces may damage the insulating joint and adjacent rails, but also wheels and other components such as sleepers.
- Material deterioration of the joint inflicted by the passing wheel with main focus on plastic deformation and related rolling contact fatigue.

In INNOTRACK numerical simulations and field studies have been carried out as described below and with further details in deliverables D4.2.1 [7.3] and D4.2.3 [7.4].

7.2. Influence on wheel–rail contact forces

The imposed variation in track stiffness together with misalignment and/or plastic deformations of the joint ends promotes high wheel rail contact forces at joint negotiations. Numerical simulations were carried out to quantify the influence of vehicle speed and joint dip on wheel–rail contact force magnitudes. Details of the numerical model as well as results from calibration of the numerical model towards field measurements and FE-simulations are presented in [7.5].

In the simulations, the joint dip (at $x=l/2$) is introduced as a relative wheel–rail displacement, x_{irr}

$$x_{irr} = \begin{cases} d\left(1-\cos\dfrac{\pi x}{l}\right), & 0 < x \le l/2 \\ d\left(1+\cos\dfrac{\pi x}{l}\right), & l/2 \le x < l \end{cases} \qquad (7.5)$$

Here *d* is the maximum depth and *l*=1 m the total length of the dipped joint.

Results of the simulations are presented in Figure 7-2. It is seen that the contact force magnitude is significantly influenced by joint depth and vehicle speed.

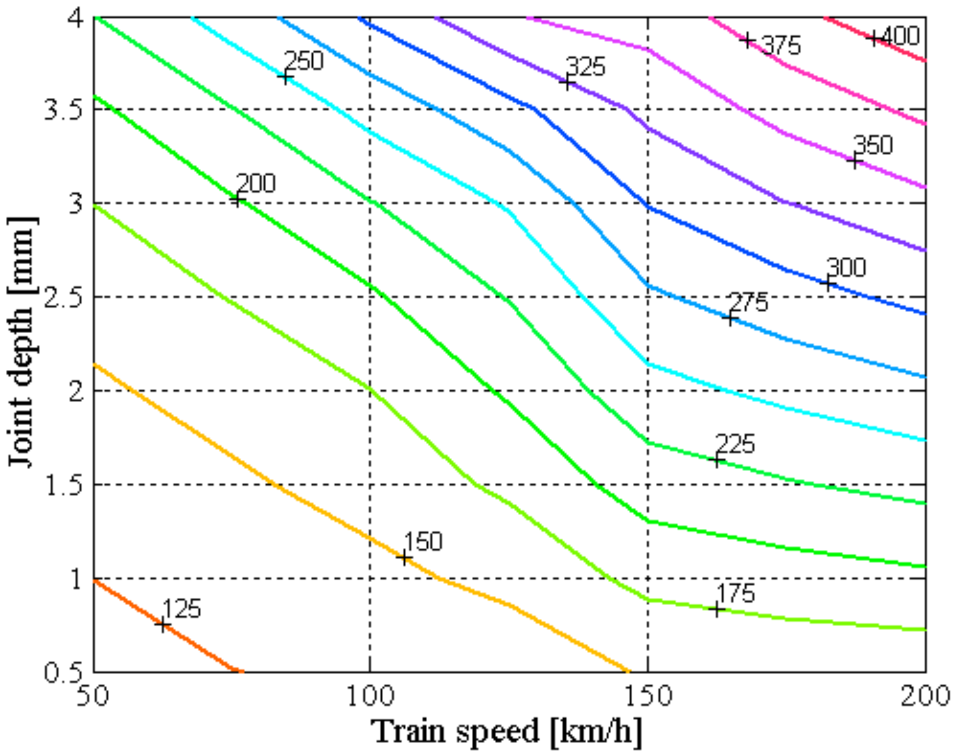

Figure 7-2 Influence of train speed and joint depth on the maximum wheel–rail contact force [kN] at an insulated joint. Axle load 25 tonnes, 90° prefabricated insulated (glued) joint for 50E3 rail with six bolts. From [7.5].

The stiffness variation imposed by the joint will also initiate a transient vibration of the vehicle–track system. Figure 7-3 shows the time history of the wheel–rail contact force. Note the loss of contact at the end of the joint section, after which the contact force oscillates. The latter can be related to the frequent occurrence of corrugation and/or squat patterns in the vicinity of insulated joints.

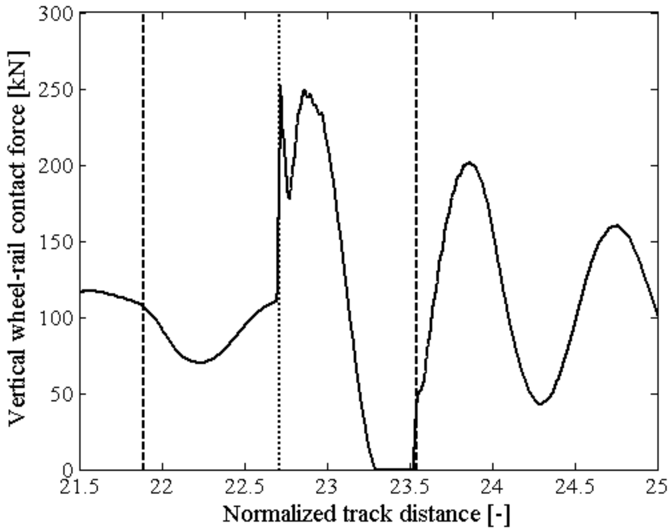

Figure 7-3 Truncated time history of vertical wheel–rail contact force. Dotted line indicates position of insulating layer. Dashed lines start and end of surface irregularity. Insulated joint with l=1 m and d=3 mm. Train speed 125 km/h and axle load 25 tonnes. From [7.5].

7.3. Plastic deformation and crack formation

Owing to the low stiffness of the insulation, there will be a high stress concentration at the rail ends facing the insulating layer. This will promote plastic flow and subsequent crack formation.

To investigate the influence of various parameters on the plastic deformation and rolling contact fatigue, numerical simulations were carried out. The quasi-static simulations consisted of a three-dimensional wheel section traversing the insulated joint. An elasto-plastic material model featuring non-linear hardening was employed for the rail material. Details of the simulations are given in D4.2.3 [7.4] and in [7.6].

Two criteria were employed to quantify fatigue impact:

To quantify ratcheting, i.e. the continuous accumulation of plastic deformation, an effective strain measure was employed as

$$\varepsilon_{\text{eff}} = \frac{\sqrt{2}}{3}\sqrt{\left(\varepsilon_{xx}-\varepsilon_{yy}\right)^2+\left(\varepsilon_{yy}-\varepsilon_{zz}\right)^2+\left(\varepsilon_{zz}-\varepsilon_{xx}\right)^2+6\left(\varepsilon_{xy}^2+\varepsilon_{yx}^2+\varepsilon_{zx}^2\right)} \tag{7.6}$$

The accumulated effective strain during the fourth load cycles (wheel rollover) is taken as a comparative damage measure.

In addition a multiaxial low-cycle fatigue criterion proposed for rolling contact fatigue [7.7] was used. An analysis of the results showed the effective strain measures to give more physically sound results than Fatigue parameter (*FP)*-based predictions. This is presumed to reflect the fact that occurring damage is related to plastic ratcheting.

A further investigation reported in [7.8] (appended to this guideline) indicated that the choice of evaluating the response at the fourth wheel passage is reasonable. However, it was also found that the quasi-static approximation was likely to be a rather crude. Presented results should therefore be used for comparative analyses rather than for quantitative evaluations.

7.3.1. Parametric influences

In the following ε_{eff} magnitudes are evaluated at a point located at a depth of 1.5 mm beneath the top of the rail and at a distance of 1.5 mm from the rail end at the insulation. Parameters considered are vertical load (F_z), lateral load ($F_x=f \cdot F_z$ where a positive f indicates a positive driving torque), maximum coefficient of friction (μ) and insulating gap (δ).

Main results from the parametric study are presented in Table 7-1, Table 7-2 and Table 7-3.

Table 7-1 Influence of maximum coefficient of friction on residual ($\varepsilon_{eff,res}$) and maximum value (ε_{eff}) of the effective strain. F_z=150 kN, f=–0.2, d=4 mm.

μ	$\varepsilon_{eff,res}$ [%]	ε_{eff} [%]
0.25	1.76	2.44
0.5	2.01	2.71

Table 7-2 Influence of joint gap, δ, and vertical load magnitude, F_z. Applied lateral loading is defined by μ=0.25 and f=0.2.

δ	F_z[kN]	$\varepsilon_{eff,res}$[%]	ε_{eff}[%]	
4	150	1.74	2.47	

	200	1.84	2.63	
6	150	1.9	2.67	
	200	2.06	2.92	
8	150	2.05	2.84	
	200	2.11	2.96	

Table 7-3 Influence of lateral loading, F_x. F_z=150 kN, δ=4 mm, μ=0.25 for |f|≤0.2 and μ=0.5 for |f|>0.2.

f	$\varepsilon_{\text{eff,res}}$[%]	ε_{eff}[%]	
-0.3	2.39	3.23	
-0.2	1.76	2.44	
0.0	1.58	2.19	
0.2	1.74	2.47	
0.3	3.08	4.1	

It is seen that the influence of the maximum coefficient of friction is small. To further appreciate the influence of the width of the insulating layer and the magnitude of the lateral load, these results are visualized in Figure 7-4.

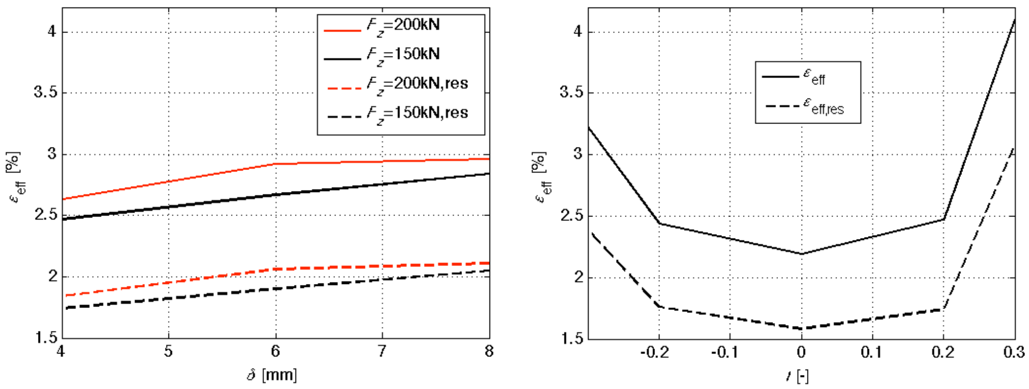

Figure 7-4 Influence of the width of the insulating layer, δ (left) and of the lateral load as defined by f (right). Values adopted from Table 7-2 and Table 7-3.

It is seen that for limited lateral loads (*f* less than about 0.2), the influence of the lateral load is moderate. Higher lateral loads cause a drastic increase in ε_{eff} magnitudes.

Increasing the width of the insulation will cause a more gradual increase in ε_{eff} magnitudes. The saturation for $\delta > 8$ mm is likely to be related to plastic strain redistributions.

Note that failure due to material deterioration of the joint can be related to plastic deformation and cracking in the joint region, but also to bridging of the insulating layer by detached metal chips which cause short-circuiting. This will be discussed further in section 7.4.2 .

7.3.2. Modified joint designs

Non-linear FE-simulations as described above were employed to assess the influence of several modifications of joint design on resulting ε_{eff} magnitudes. The simulations and results are detailed in D4.2.3 [7.4] and [7.8] (appended to the guideline). Here a short summary is given:

Bevelling of the rail head edge

The effect of bevelling was found to be small. This can be interpreted either as that there is no point in introducing bevelling, or that bevelling is a method of increasing the insulating gap (and thereby increasing the gap that must be bridged by a metal chip to cause short-circuiting) without significantly increasing the loading of the joint. Details are provided in [7.6].

Stiffness of the insulating material

Increasing the stiffness of the insulating layer decreases the plastic deformation of the rail, in particular under pure rolling conditions. This comes at the expense of an increased shear stress in the interface between the insulating layer and the rail end. Since already currently used insulating materials are prone to detach from the rail (see figures 4 and 5 in D4.2.3 [7.4]) this implies that stronger glues will be needed. Details on the simulations featuring a stiffer insulating material are provided in [7.8].

Laterally inclined joints

Laterally inclined joints cause increased wheel–rail contact pressures at the insulation. This leads to increased plastic deformation of the rail ends. Further the lateral inclination does not decrease (rather it increases) the shear stresses between the rail edge and the insulating layer. Details are provided in [7.8].

7.4. *Recommendations regarding insulating joints*

The following conclusions and recommendations are valid for the conditions described in this guideline with details in referenced reports. The conclusions may well be valid for other conditions, but this has not been validated in the INNOTRACK study.

7.4.1. Allowed joint dip

Dipped joints will significantly increase peak wheel–rail contact forces during joint negotiation and also induce contact force oscillations after joint negotiation. This will promote plastic deformation and rolling contact fatigue in the rail and (to a lesser extent) in passing wheels. Further it will promote the formation of corrugation and/or squats in the vicinity of the joint. The induced contact force depends significantly on the vehicle speed and joint dip.

Figure 7-2 presents contact load magnitudes related to joint dip and vehicle speed. It is recommended that these results be used as a first indication to prescribe allowed joint dips. For operational conditions (axle load, joint configurations *etc*) that differ from those related to Figure 7-2, modified simulations can be carried out to establish similar response charts if a higher accuracy is needed. Details on the simulation procedure are provided in reference [7.5].

7.4.2. Width of insulating layer

The choice of the insulating layer is a balance between keeping the gap as narrow as possible to minimize the plastic deformation of the rail ends, and to keep it as wide as possible to increase the width a detached metal chip must bridge to cause short-circuiting. Based on the presented analyses the recommended approach is the following:

- On lines where lateral loads are moderate (traction coefficient below roughly 0.2) the insulating gap is made as narrow as possible (4 mm is probably a realistic lower limit). To keep the insulation gap narrow is especially important on lines with high axle loads.
- If the lateral load cannot be sufficiently confined and traffic volumes are relatively high, deterioration of the insulated joint is likely to be such a rapid process that metal chip detachment cannot (with sufficient reliability) be avoided. The insulating

gap can then be increased (or bevelling introduced) to decrease the probability that a detached metal chip bridges the insulation and causes short-circuiting. This is likely to increase the deterioration rate even further. Consequently the increased reliability will come at the expense of more frequent maintenance (but with a shift from unplanned to planned) and a shorter operational life.

An important factor to observe is that use of magnetic rail brakes should be avoided when passing insulated joints to avoid the disposal of metal debris that may cause short-circuiting.

7.4.3. Modified joint design

The study has shown that there is a potential in decreasing joint deterioration by increasing the stiffness of the insulating layer. However this comes at the expense of increasing the stress in the glue that connects the insulating layer and the rail end, which requires an adoption of stronger glues.

The study has shown that moderate bevelling (1 mm) will give negligible influence on the plastic deformation of the rail end.

The study has shown no beneficial effects of laterally inclined joints. Note however that the influence on global bending has not been assessed.

7.5. Bibliography

7.3 INNOTRACK Deliverable 4.2.1 – **Simplified relation for the influence of rail/joint degradation on operational loads and subsequent deterioration**, 22 pp, and 10 appendices, 27+25+10+12+6+8+7+7+25+4 pp, 2007

7.4 INNOTRACK Deliverable 4.2.3 – **Improved model for loading and subsequent deterioration of insulated joints**, 19 pp, and 1 appendix, 17 pp, 2009

7.5 Elena Kabo, Jens Nielsen & Anders Ekberg, **Prediction of dynamic train/track interaction and subsequent material deterioration in the presence of insulated rail joints**, *Vehicle System Dynamics*, vol 44, Supplement, 2006, pp 718–729.

7.6 Johan Sandström & Anders Ekberg, **A numerical study of the mechanical deterioration of insulated rail joints**, *IMechE Journal of Rail and Rapid Transit*, vol 223, no 3, pp 265--273, 2009

7.7 Yanyao Jiang & Huseyin Sehitoglu. **A model for rolling contact failure** *Wear*, vol 224, pp 38–49, 1999

7.8 Jóhannes Gunnarsson, **Numerical simulations of the plastic deformation of insulating joints**, MSc Thesis 2009:15, *Chalmers Applied Mechanics*, Gothenburg, 33 pp, 2009

8. Out of round wheels, rail breaks and crack growth

Historically, fatigue failures in railway rails have taken a wide variety of forms. The once major problem of cracks at fish-bolt holes has been largely mitigated by the introduction of Continuously Welded Rails. Improved steel making techniques mean that manufacturing related defects, for example taches ovales developed from hydrogen cracks, longitudinal-vertical splits etc. are largely a thing of the past. However rolling contact fatigue cracks have become an increasing problem over recent decades and failures originating in the rail foot remain a concern because a high proportion are not detected until after a rail break has occurred.

The reliability of alumino-thermic welds is also an issue: this is addressed elsewhere.

Whilst there has been intensive research on the wheel rail interface in the last few years, research on the effect of wheel irregularities has been sporadic. The next three sections of this report relate principally to this area.

Chapter 9 addresses the problem of relatively short range wheel irregularities, effectively corrugation of the wheel surface. Stress intensity factors are calculated for a head-check type defect using an approximate model, and growth rates are predicted. The influence of the wheel irregularities on growth rate is found to be significantly dependent on wavelength. For irregularities with a wavelength in excess of 20mm it is found that there is no advantage to modelling the detailed pressure variation within a single wheel pass. For shorter wavelengths however, this is non-conservative.

Traditionally the condition of the wheel has been judged visually, and the criterion used to assess whether there is a need for remedial action has commonly been the visible length of a wheelflat. Practically this means that wheels may only be inspected when the vehicle is stationary but the overwhelming disadvantage of this approach is that where the out-of-roundness is not in the form of a traditional wheelflat, it may not be obvious to the naked eye. Such defects, however, can still result in very high wheel-rail forces. Chapter 10 addresses this by focussing on the use of wheel impact force measuring systems as the primary control on wheel out-of roundness i.e. on the direct measurement not of the wheel irregularity, but of its consequences. There is not, however, a simple relationship between impact force measured at one point, and the potential for rail damage, particularly rail breakage. Impact location, track support stiffness etc. will affect the bending moments generated. In addition, if the train speed is varied, the force generated will be affected. A matrix of conditions is therefore evaluated with the intent of developing a 'worst case' wheel-force: rail bending moment relationship.

Solutions for the stress intensity factors of cracks at the corner of the head and of the foot of the rail were developed and used, in conjunction with crack growth rate and toughness data, to evaluate the influence of wheel irregularities on growth rates and the size of defect a fracture. The effect of thermal stresses was also considered. It is concluded that wheel impact loadings have a negligible effect on crack growth rates but a substantial effect on the size of defect at fracture: thermal loading is also significant

Chapter 11 presents a general method of re-assessing minimum action rules using techniques not dissimilar to those in the previous two sections, but combining these with Monte Carlo simulation. This creates a very flexible tool for ‘what if’ simulations, enabling the effect of changes to a wide variety of variables on the fraction of defects that will result in rail breakage to be assessed. Notably it enables the effect of changes to the inspection frequency, the inspection technique and minimum action timescales to be evaluated. The principles behind this work are described in Chapter 11 and to demonstrate the capabilities of the approach, software has been developed with the specific objective of demonstrating the effect of varying impact force control limits on the fraction of foot defects that will result in breakage. Preliminary results have been obtained, but the software is still being validated so that results will not be published until a later date.

9. Growth of small cracks

9.1. *Influence of out-of-roundness*

9.1.1. Influence of periodic pressure variation on crack growth

The crack propagation model developed by Fletcher et al. [9.1] can be used to study the effect of out-of-round (OOR) wheels on crack propagation. The model has been developed to allow cyclic variation of contact pressure with contact location relative to the crack mouth. This is suitable for studying the effect of short-wavelength high spatial frequency pressure fluctuations; longer-wavelength fluctuations (i.e., much longer than the crack size) can be studied effectively using the original model with different (constant) contact pressures.

The effect of periodic variation of wheel-rail contact patch pressure on propagation of semi-circular cracks up to 12mm radius (i.e., penetrating to a depth of about 6mm at 30° angle to the surface) was studied using the '2.5D' Green's-function-based model [9.2]. The following conclusions were reached:

- → *For pressure variations with a wavelength less than about 2mm, the maximum pressure should be used to calculate crack growth rate.*
- → *For pressure variations with a wavelength greater than about 20mm, there is no advantage to modelling pressure variation within a single load pass, and that modelling successive wheel passes with different static pressures would be sufficient.*
- → *Out-of-round wheels with roughness features with wavelengths in the range 2-20mm would accelerate crack propagation, but would require more detailed modelling.*

9.1.2. Short-pitch corrugations on rails and wheels

Rails supported on sleepers have a natural bending frequency in the region of 1kHz, where the wavelength is equal to two sleeper bays; the precise frequency depends on rail section and sleeper spacing. This resonance causes short-pitch rail corrugation, with wavelengths in the centimetre range proportional to train velocity. For example, for a line speed of 72 km/hr and resonant frequency of 1kHz, the corresponding rail corrugation wavelength would be 20mm. A wear mechanism causing growth of short-wavelength corrugation is described by Knothe and Groß-Thebing [9.3], who show that corrugation growth is reinforced only in a wavelength range of 20mm to 100mm. (Note, however, that this is certainly not the only model of rail corrugation growth, and other vehicle-track resonances also affect roughness growth.)

Johansson [9.4] surveyed out-of-round wheels; wavelengths less than 20mm have very low amplitudes, usually less than 1 micron (comparable with new wheels). Tread breaks using cast-iron brake blocks appear to increase roughness amplitude in the range 30-80mm.

The size of the wheel-rail contact is 10-20mm, and this dampens roughness wavelengths (on both wheels and rails) shorter than 20mm.

9.1.3. Influence of periodic pressure variation on wear

The effect of pressure variation (with wavelengths above about 20mm) on rail wear rate was studied (using the wear model in Section §6 above – the simulation, not the wear equation) by considering each wheel pass as an independent event. Wear simulations were thus performed by varying the normal load with each passing wheel, and the predictions compared with the constant average-load case. No significant difference was observed.

→ *Out-of-round pressure variations do not affect rail wear significantly.*

9.2. Minimum action rules

Corrugation patterns on wheels (and rails) have significant amplitudes only for wavelengths longer than about 20mm. Above this, the work in INNOTRACK has shown that there is no need to develop new models for wear and short crack propagation specifically for out-of-round wheels – the contact load varies sufficiently slowly that the variation itself can be ignored. What is important, when examining a particular rail location, is the contact force at that location. Multi-body simulations, which predict wheel-rail contact forces can incorporate these existing models for rail life prediction.

Any corrugation on wheels or rails will lead to increased forces, higher wear and faster crack growth, and at certain speeds may excite resonances in the passing vehicles, further increasing the forces; increasing the vehicle speed will increase the average force [9.5]. Out of roundness will cause the contact force to fluctuate, with peak values 50% higher than the average – and perhaps more, depending on the roughness amplitude and vehicle speed. Chapter 5 above describes this in more detail. The parameter used there is FI_{sub} which is one sixth of the peak pressure, and thus is proportional to the cube root of the normal load, i.e., a 26% increase in FI_{sub} corresponds to a 100% increase in the normal load; Figure 5.3 shows that corrugation can cause FI_{sub} to increase by 30-40%.

In the example of crack growth rates given in D4.2.5 [9.2], the peak pressure oscillates between 1550MPa and 1950MPa (i.e., 11% variation from a mean of 1750MPa) as a result of OOR wheels passing over a crack in a rail. In wet weather, this would result in a 41% increase in crack growth rate – an increase not balanced by a corresponding increase in the wear rate.

Limits are already imposed on OOR roughness amplitudes to limit noise levels [ISO 3095], and Ref. [5.13] presents a limit based on RCF criteria. Minimum action rules for wheel flats, a more severe form of OOR often requiring immediate attention, are discussed in Section §10 below.

9.3. Bibliography

9.1 INNOTRACK Deliverable 4.2.5 – **Improved model for the influence of vehicle conditions (wheel flats, speed, axle load) on the loading and subsequent deterioration of rails**, 47 pp, and 6 appendices, 47+15+9+22+35+53 pp, 2009

9.2 INNOTRACK Deliverable D4.2.1 – The impact of vertical train-track interaction on rail and joint degradation, Annex IX: DI Fletcher, FJ Franklin, A Kapoor, **State-of-the-art report on the effect of material characteristics on material deterioration**

9.3 Knothe, K. and Groß-Thebing, A., **Short wavelength rail corrugation and non-steady-state contact mechanics**, *Vehicle System Dynamics*, vol 46, no 1, pp. 49–66, 2008

9.4 Johansson, A. , **Out-of-round railway wheels – assessment of wheel tread irregularities in train traffic**, *Journal of Sound and Vibration*, vol 293, pp 795–806, 2006

9.5 Johansson, A. and Nielsen, J.C.O., **Out-of-round railway wheels-wheel – rail contact forces and track response derived from field tests and numerical simulations**, *Proc. Instn Mech. Engrs Part F: J. Rail and Rapid Transit*, vol 217, 135–146, 2003

9.6 ISO 3095:2005, http://www.iso.org/iso/catalogue_detail.htm?csnumber=41669.

10. Large cracks: deterministic approach

10.1. Background and limitations

This study aims at quantifying the influence of the main parameters governing crack growth and fracture in rails. The purpose is to establish a scientific foundation for regulations regarding allowed wheel flats and pertinent maintenance practices. Current wheel removal criteria normally relate the alarm limit to the size (length) of a wheel flat. This is not an optimal situation, partly because of workers' safety: it may be both difficult and dangerous to locate and measure the length of a wheel flat during operations. However, there is also a profound scientific argument against such criteria: a wheel flat of a given size will result in different impact load magnitudes depending on, among other things, the type of vehicle, train speed, axle load and track properties.

The aim of this study is to instead base the wheel removal criterion on wheel–rail contact forces, which can be measured by detectors. The study specifically targets the question on how the "severity" of an impact load of a certain magnitude should be quantified. In the current study this is related to the risk of rail breaks. Such a criterion neglects other damage modes, such as sleeper cracking and indentations on the rail surface, etc. This was however deemed acceptable mainly because rail breaks constitute an immediate safety risk, whereas the other damage modes are more benign in that respect. As shown below, the analysis is extremely complicated even with this limitation. It can also be noted that the adopted approach poses no hindrance to parallel studies, e.g. regarding risks for sleeper cracking. Rather, the presented results should be of aid in such a study.

For details on simulations and measurements performed, the reader is referred to INNOTRACK deliverables D4.2.1 [10.1] and D4.2.5 [10.2] and references listed in section 10.9.

Current regulations regarding rail cracks differ significantly between countries throughout Europe as shown in Chapter 3. Rail defects are generally treated in UIC leaflets 712 and 725 and also in the UIC publications "Atlas of wheel and rail defects" (ISBN 2-7461-0818-6) and "An International Cross Reference of Rail Defects" (2-7461-0688-

4). In the UIC series of technical and research reports, topics of interest to the current guideline include A 110, B79, B 169, D 88 and D 141. Details can be found on the UIC website (www.uic.org).

10.1.1. Considered tracks and vehicle

In the following study, three vehicle types are considered, as detailed in Table 10-1 (see also [10.3]).

Table 10-1 Vehicle parameters.

Train type	Axle load (W) [tonnes]	Speed (v) [km/h]	Axle distance L_{12} [m]	Axle distance L_{23} [m]	Axle distance L_{45} [m]
Heavy Haul	30.0	60	1.78	4.40	1.77
Freight	25.0	100	1.80	7.00	3.20
Passenger	21.4	200	2.50	17.50	6.40

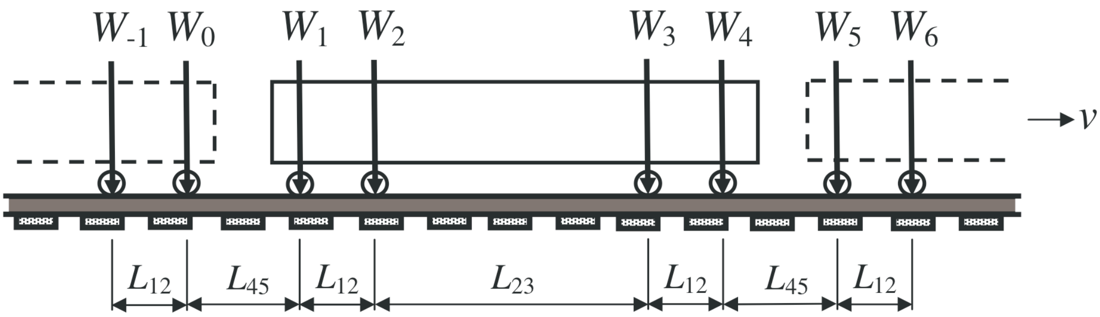

Figure 10-1 Definition of vehicle parameters. From [10.3].

For these vehicles the load has been applied as moving point loads, see section 10.2. In the track model, the stiffness of the rail pad is k_p = 80 MN/m. The ballast stiffness is indicated in connection to simulation results. Details of these simulations are given in [10.3].

In addition full simulations of impacting wheels have been carried out. These feature a bogie with 30 tonne axle load and 1.8 m wheelbase travelling at a speed of 60 km/h. The wheel diameter is 0.90 m and the wheel set mass (including axle and bearings) is 1100 kg. The study concerns 60E1 rails on tangent track with concrete monobloc sleepers (mass 250 kg and centre distances 0.60 m). The ballast stiffness per rail seat is k_b = 140 MN/m and the pad stiffness 120 MN/m. Details of these simulations are given in [10.4].

All simulations of train–track interaction are carried out using DIFF [10.5], which incorporates high-frequency interaction up to some 2 to 3 kHz.

10.1.2. Considered crack types

The study concerns “large” rail cracks in head and foot of the rail with location and geometry corresponding to Figure 10-2. A “large” head crack here denotes a crack that has deviated to a (more or less) transversal growth path and grown out of the contact stress field. From a practical perspective this means that the railhead cracks should be larger than about one centimeter. For foot cracks, the restriction is that theories of large crack linear elastic fracture mechanics growth should be valid. This corresponds to a crack size of some millimeters. Under these presumptions, the global bending of the rail is the main crack driver.

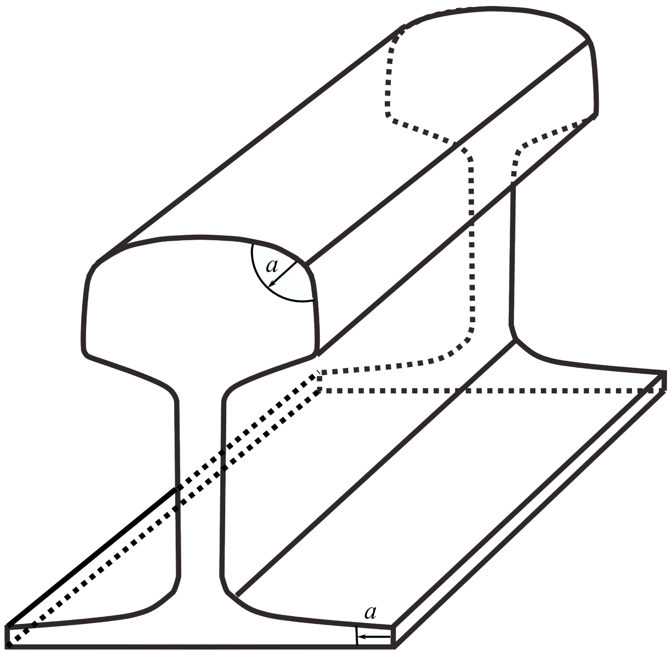

Figure 10-2 Location and size definitions (given by crack length a) of considered cracks.

10.2. Characteristics of wheel flats and wheel rail impact load

Fresh flats, caused by sliding, quickly become rounded. From observations of flatted wheels in operation, the relation between the fresh flat length (l_0) and the rounded flat length (l_r) can be estimated as

$$l_r = 1.5 \cdot l_0 \tag{10.1}$$

Based on measurements it has been found that the geometry can be defined by an irregularity

$$D_{\text{irr}} = \frac{d}{2}\left[1+\cos\left(\frac{2\pi x}{l}\right)\right] \qquad -\frac{l}{2} \le x \le \frac{l}{2} \tag{10.2}$$

Here x is a coordinate along the wheel circumference, l is the flat length and the depth of the flat, d, is given by

$$d = R - \sqrt{R^2 - \frac{l^2}{4}} \tag{10.3}$$

Here R is the wheel radius. Details are found in [10.6].

The resulting wheel–rail impact load has been established from in-field measurements. A numerical model of the impacting wheels has been developed in DIFF [10.3, 10.4, 10.6] and validated against measured wheel–rail contact forces, see Figure 10-3.

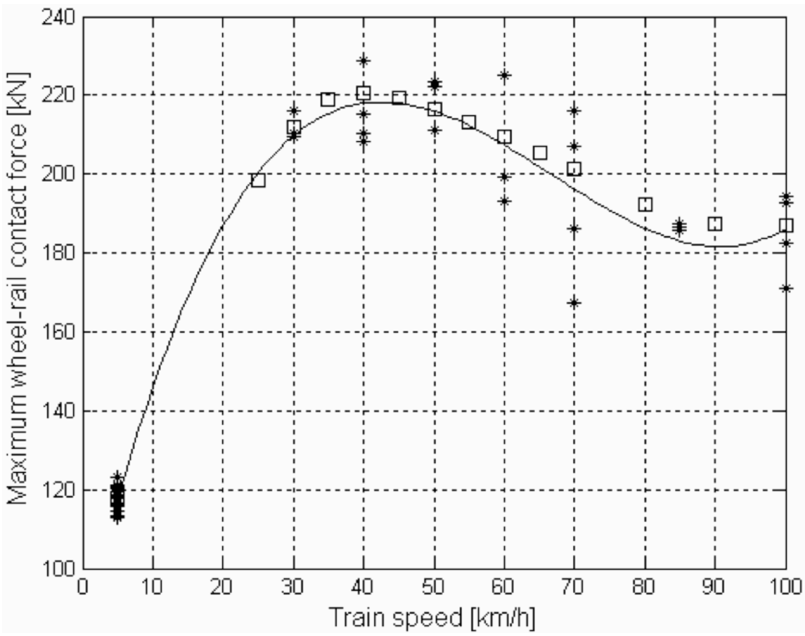

Figure 10-3 Measured (*) and calculated (□) peak wheel–rail contact force versus train speed for a 100 mm long and 0.9 mm deep wheel flat. Axle load 24 tonnes and unsprung wheelset mass 1185 kg. From [10.6].

Simulations featuring a flatted wheel on rail are too computationally demanding for parametric studies. To this end, a simplified contact force evolution has been defined see Figure 10-4. In the simplified model non-damaged wheels are modelled as constant wheel loads.

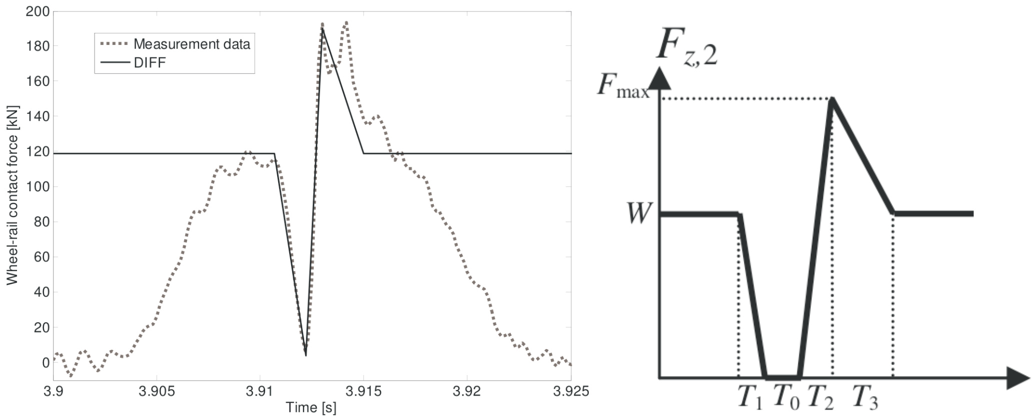

Figure 10-4 Left: Wheel–rail contact force evolution (dotted line) for one wheel passage measured in one sleeper bay section. Simplified load history marked by solid line. Right: Parameterized load history. From [10.3].

The simplified load history can be parameterized, see Figure 10-4. Magnitudes of the four time increments (T_0, T_1, T_2 and T_3 in Figure 10-4) for a "worst case wheel flat" have been evaluated from a factorial design process. These are vehicle and track dependent. Values are given in [10.3].

10.3. Rail bending moments

The ability of the numerical model to evaluate bending stresses in the rail was validated against measurements. As seen in Figure 10-5 the match between measured and simulated magnitudes is very good, especially considering peak magnitudes, which are of most interest.

The magnitude of the bending moment in a certain rail section will depend on the impact position of the wheel flat as discussed below.

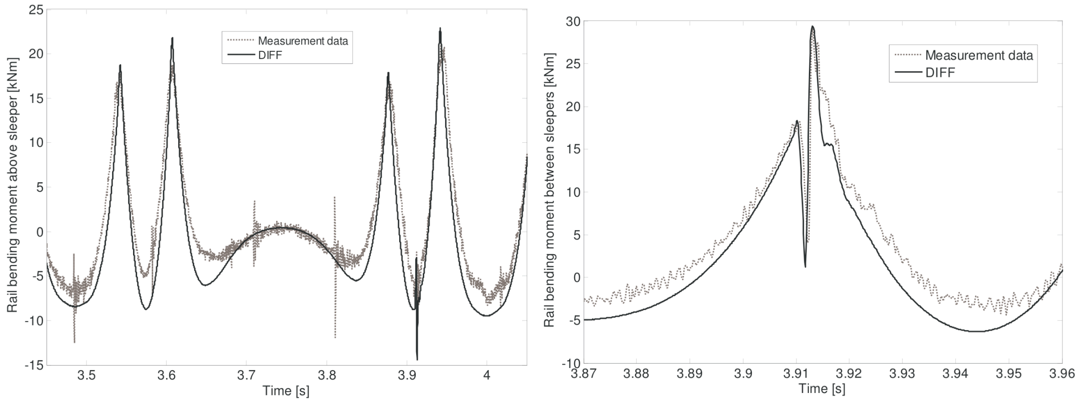

Figure 10-5 *Left: Measured (dotted line) and calculated (solid line) bending moments in the rail above a sleeper located 1.5 sleeper distances away from the impact position of the wheel flat. In the model, wheel flat impact was only applied at 3.91 s.*
Right: Measured (dotted line) and calculated (solid line) bending moment in a sleeper span during wheel flat impact. From [10.3].

10.3.1. Positive bending moments

For positive bending moments (tension in rail foot), the worst case loading is a wheel flat impact in the centre of a sleeper span (with the possible exception e.g. of tracks with hanging sleepers). The extreme bending moment occurs in the rail section of the wheel flat impact. For impact not in the centre of the sleeper span, the corresponding bending moment magnitude in the centre of the sleeper span can be approximated as

$$M_{\max} = kM_{\text{quasi}} \tag{10.4}$$

with

$$k = \begin{cases} 1 + \dfrac{M_{\max} - M_{\text{quasi}}}{2M_{\text{quasi}}}\left(1 + \cos\dfrac{\pi x}{0.6L}\right) & : \quad -0.6L \le x \le 0.6L \\ 1 & \quad\quad |x| \ge 0.6L \end{cases} \tag{10.5}$$

M_{quasi} is the maximum bending moment during a negotiation of a perfectly round wheel. The maximum bending moment at impact loading can be expressed as

$$M_{\max} = \beta_0 + \beta\left(\frac{F_{\max}}{F_{\text{ref}}} - 1\right) \tag{10.6}$$

Here F_{ref} = 250 kN and F_{max} is the impact load from the wheel flat. Equation (10.6) is valid for $F_{ref} \leq F_{max} \leq 350$ kN. Coefficients β_0 and β will depend on vehicle and track configuration.

Values of β_0, β and M_{quasi} (in sleeper span and above a sleeper) for 60E1 rails and varying ballast stiffness per half sleeper (k_b) are given in Table 10-2, Table 10-3 and Table 10-4 for heavy haul, freight and passenger vehicles, respectively. The stiffness of the rail pad is k_p = 80 MN/m. Details and coefficients for 50E3 rails with higher pad stiffness (k_p = 300 MN/m) are given in [10.3]

Table 10-2 Coefficients β_0 and β for heavy haul vehicle, see Table 10-1.

k_b [MN/m]	β_0 [kNm]	β [kNm]	M_{quasi} midspan [kNm]	M_{quasi} above sleeper [kNm]
5	40	40	37	35
10	46	39	34	31
30	48	50	30	27
100	45	48	27	23

Table 10-3 Coefficients β_0 and β for freight vehicle, see Table 10-1.

k_b [MN/m]	β_0 [kNm]	β [kNm]	M_{quasi} midspan [kNm]	M_{quasi} above sleeper [kNm]
5	56	47	36	34
10	51	47	31	28
30	46	47	25	23
100	44	47	23	19

Table 10-4 Coefficients β_0 and β for passenger vehicle, see Table 10-1.

k_b [MN/m]	β_0 [kNm]	β [kNm]	M_{quasi} midspan [kNm]	M_{quasi} above sleeper [kNm]
5	49	39	31	30
10	46	39	27	26
30	42	39	24	22
100	40	39	21	19

10.3.2. Negative bending moments

For negative bending moments (tension in rail head), the worst-case loading is a wheel flat impact in the centre of a sleeper span (with the possible exception e.g. of tracks with hanging sleepers). The extreme bending moment then occurs above the sleeper one and a half sleeper span away. This is normally between the wheelsets in a bogie (see Figure 10-6), but can (depending on the vehicle and track configuration) instead be between two wagons.

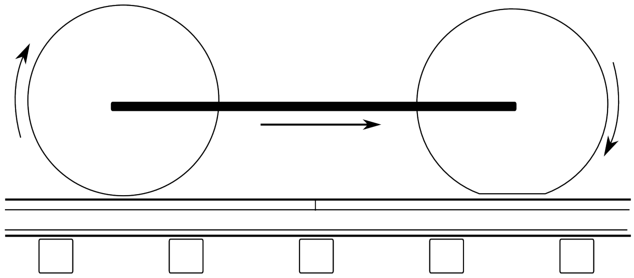

Figure 10-6 Wheel impact position that will induce high negative bending moments in the rail head above the intermediate sleeper (position of high tensile stress marked by a line).

The magnitude of the bending moment will decrease rather significantly if the wheel flat does not impact in the worst case location. The decreased magnitude depends on several factors (axle spacing, ballast stiffness etc), More information is given in references [10.3] and [10.4].

The numerically largest negative bending moment can be expressed as

$$M_{\max} = \gamma_0 + \gamma\left(\frac{F_{\max}}{F_{\text{ref}}} - 1\right) \qquad (10.7)$$

with F_{ref}, $F_{\max}$ and interval of validity as above. Coefficients γ_0 and γ and M_{quasi} (which is here *minimum* bending moment during passage of a round wheel) for 60E1 rails and varying ballast stiffness per half sleeper (k_b) are given in Table 10-5, Table 10-6 and Table 10-7 . Stiffness of the rail pad is k_p = 80 MN/m. Details and coefficients for 50E3 rails (with k_p = 300 MN/m) are given in [10.3]

Table 10-5 Coefficients γ_0 and γ for heavy haul vehicle, see Table 10-1.

k_b [MN/m]	γ_0 [kNm]	γ [kNm]	M_{quasi} above sleeper [kNm]	M_{quasi} midspan [kNm]
5	-44	-18	-26	-25
10	-32	-16	-17	-17
30	-21	-12	-13	-10
100	-18	-12	-12	-10

Table 10-6 Coefficients γ_0 and γ for freight vehicle, see Table 10-1.

k_b [MN/m]	γ_0 [kNm]	γ [kNm]	M_{quasi} above sleeper [kNm]	M_{quasi} midspan [kNm]
5	-39	-11	-25	-23
10	-32	-12	-20	-19
30	-20	-12	-13	-12
100	-17	-13	-9	-8

Table 10-7 Coefficients γ_0 and γ for passenger vehicle, see Table 10-1.

k_b [MN/m]	γ_0 [kNm]	γ [kNm]	M_{quasi} above sleeper [kNm]	M_{quasi} midspan [kNm]
5	-14	-15	-11	-11
10	-18	-15	-10	-8
30	-19	-15	-11	-9
100	-19	-15	-9	-8

10.4. Risks for rail breaks

Rail breaks are governed by tensile stress in the rail at the location of the crack. In addition to tensile stress due to the bending moment, an all-welded rail is also subjected to a tensile stress due to restricted thermal contraction. Further, residual stresses may contribute to rail breaks, but these are not considered in the current study.

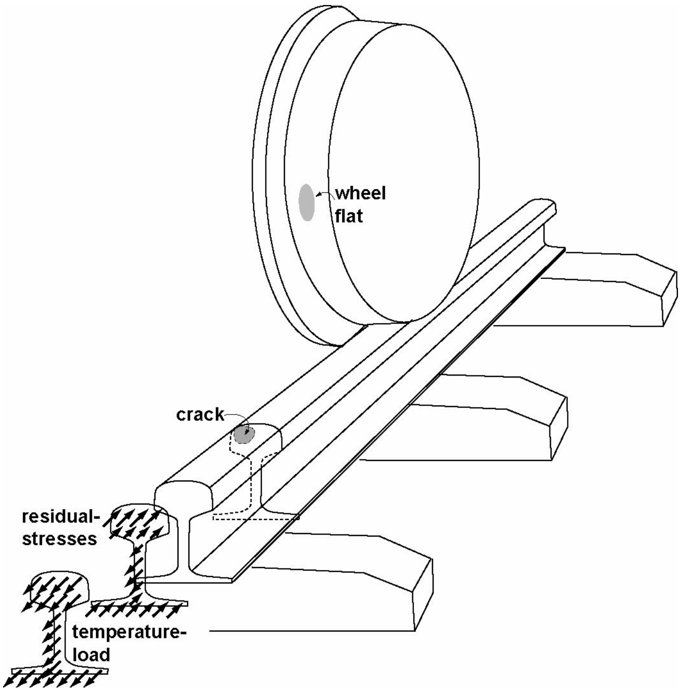

Figure 10-7 Stresses affecting rail breaks: Bending stress induced by a wheel passage (possibly with a flatted wheel), thermal stresses due to restricted contraction and residual stresses. From [10.4].

The loading of the rail crack is quantified by the stress intensity factor

$$K_{\mathrm{I}} = f \cdot \sigma\sqrt{\pi a} \tag{10.8}$$

Here f is a geometry factor, σ the nominal stress and a the crack size as defined in Figure 10-2.

The magnitude of the thermal nominal stress is given as

$$\sigma_{\mathrm{t}} = \alpha E \Delta T \tag{10.9}$$

Here $\alpha = 11.5 \cdot 10^{-6}$ [°C^{-1}], $E = 210$ [GPa] and $\Delta T = T - T_0$ with T being the current and T_0 the stress free temperature.

The nominal bending stress is given as

$$\sigma_{\mathrm{b}} = \frac{M}{I} h \tag{10.10}$$

Here h is the distance from the neutral axis to the top of the rail head (or bottom of the rail foot if foot cracks are considered) and I the area moment of inertia of the rail cross-section.

The geometry factor, f, can for rail foot cracks be approximated as

$$f(a,b) = \frac{\sqrt{\frac{2b_\mathrm{f}}{\pi a} \cdot \tan\left(\frac{\pi a}{2b_\mathrm{f}}\right)}}{\cos\left(\frac{\pi a}{2b_\mathrm{f}}\right)} \cdot \left(0.752 + 2.02\left(\frac{a}{b_\mathrm{f}}\right) + 0.37\left(1 - \sin\left(\frac{\pi a}{2b_\mathrm{f}}\right)\right)^3\right) \tag{10.11}$$

Here a is the foot crack size (see Figure 10-2) and b_f the width of the rail foot (0.150 m for 60E1 rails).

For rail head cracks, the geometry factors for bending and tension were approximated from FE-simulations [10.4] as

$$f_\mathrm{b}\left(\frac{a}{b_\mathrm{h}}\right) = 2.6\left(\frac{a}{b_\mathrm{h}}\right)^2 - 0.97\left(\frac{a}{b_\mathrm{h}}\right) + 0.70 \tag{10.12}$$

$$f_\mathrm{t}(a) = 1.4\left(\frac{a}{b_\mathrm{h}}\right)^2 - 0.16\left(\frac{a}{b_\mathrm{h}}\right) + 0.72 \tag{10.13}$$

Here a is the size of the head crack (see Figure 10-2) and b_h the width of the rail head (0.072 m for 60E1). See [10.4] and [10.7] for details.

Fracture occurs for $K_\mathrm{I} \geq K_\mathrm{Ic}$ where K_I incorporates contributions from both thermal and bending loading.

Given a rail temperature and a crack size, the passage of a flatted wheel will correspond to a risk of rail breakage governed by the impact position of the wheel flat. In Figure 10-8 the probability of rail break due to a rail head crack located above a sleeper is given as a function of wheel flat length and temperature. The fracture toughness K_Ic is taken as 40 MPa·m$^{1/2}$. Details of the simulations are given in [10.4]

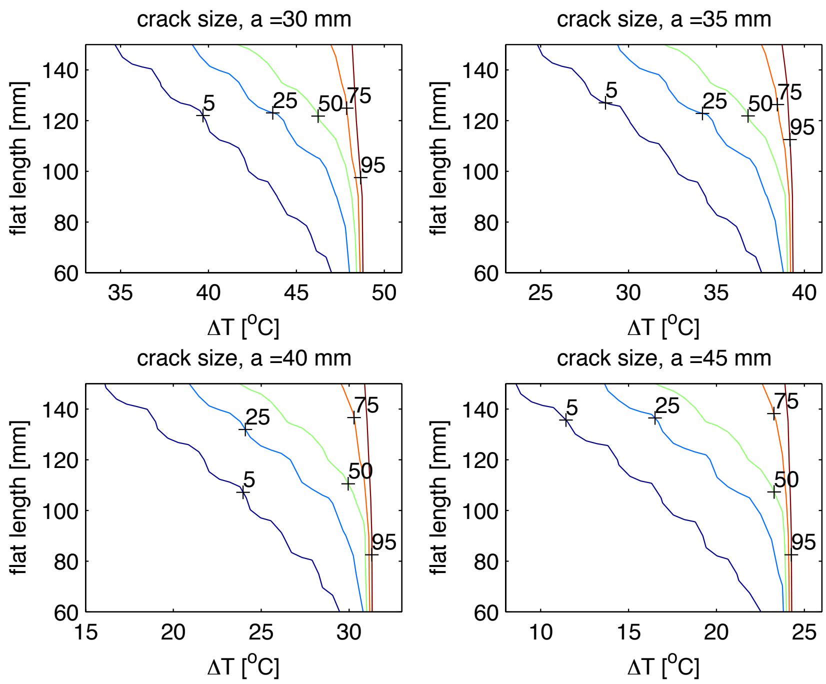

Figure 10-8 Probabilities of rail breaks for varying crack sizes, a, temperature decreases ΔT, and flat lengths, l. The level curves indicate probabilities of 5%, 25%, 50%, 75% and 95 %. Note the different temperature scales. From [10.4].

If the wheel flat is presumed to impact in the worst-case position with respect to a worst-case crack location (mid span for rail foot cracks and above a sleeper for rail head cracks), fracture will occur if the (deterministic) stress intensity factor exceeds the fracture toughness. For our future analyses it is suitable to express the fracture criterion as

$$K_{\mathrm{Ib}} \geq K_{\mathrm{Ic}} - K_{\mathrm{It}} \equiv K_{\mathrm{Ic,red}} \tag{10.14}$$

Here K_{Ib} and K_{It} are stress intensity due to bending and thermal loading, respectively.

Results of such analyses with a fracture toughness, $K_{\mathrm{Ic}} = 40$ MPa·m$^{1/2}$ are presented in Figure 10-9 and Figure 10-10 for rail foot and head cracks, respectively. Fracture is predicted when K_{Ib} (induced by the impact load given on the abscissa) exceeds K_{Ic}–K_{It} (horizontal lines).

Details of simulations and results also for 50E3 rails are given in [10.7] and [10.8].

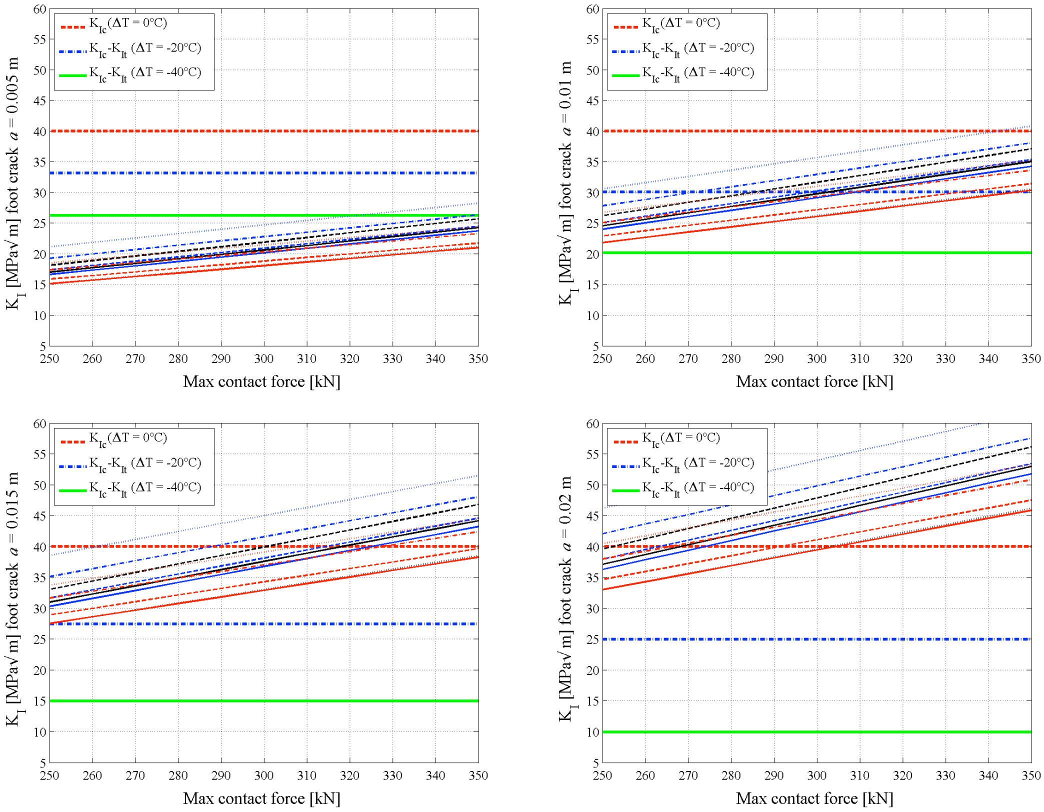

Figure 10-9 Stress intensities in 60E1 rail foot cracks due to impact loads of varying magnitudes. Vehicle type indicated by colour (heavy haul–black; freight–blue; passenger–red). Ballast stiffness indicated by line type (k_b=5MN/m–dotted; k_b=10MN/m–dashed-dotted; k_b=30MN/m–dashed; k_b=100MN/m–solid). Fracture toughness reduced by thermal stress indicated by the horizontal lines. Crack sizes 5 mm (top left), 10 mm (top right), 15 mm (bottom left), 20 mm (bottom right). From [10.8].

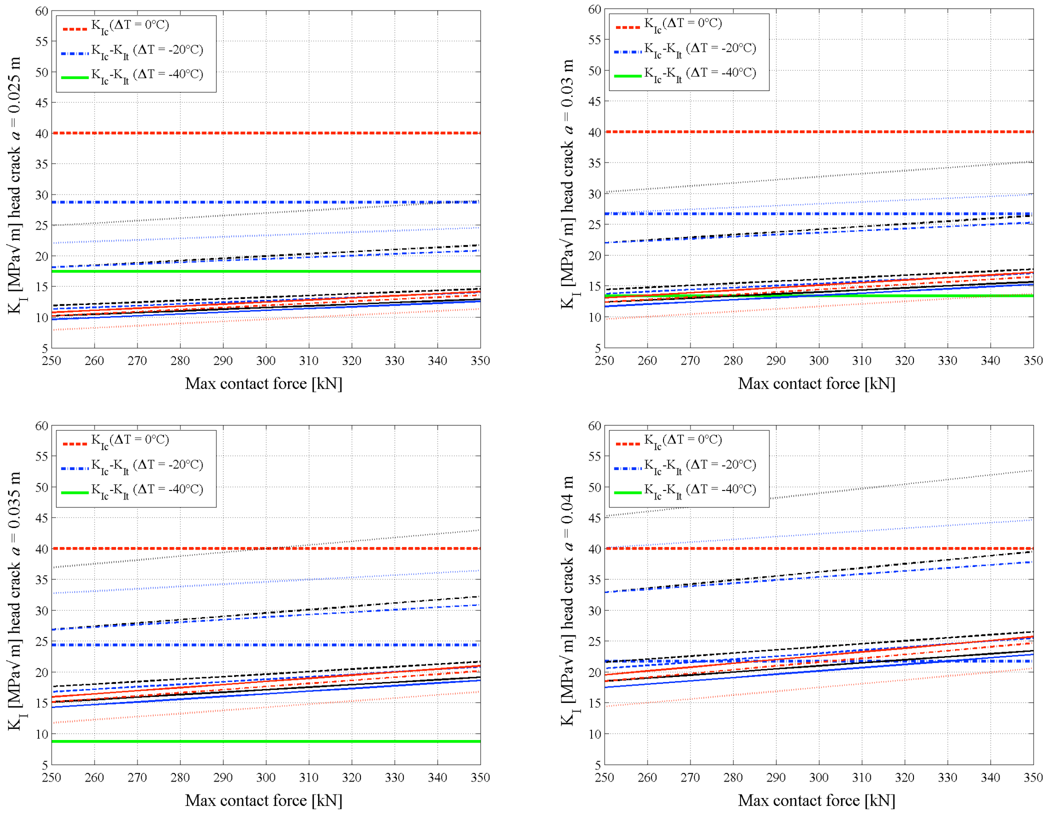

Figure 10-10 Stress intensities in 60E1 rail head cracks due to impact loads of varying magnitudes. Vehicle type indicated by colour (heavy haul–black; freight–blue; passenger–red). Ballast stiffness indicated by line type (k_b=5MN/m–dotted; k_b=10MN/m–dashed-dotted; k_b=30MN/m–dashed; k_b=100MN/m–solid). Fracture toughness reduced by thermal stress indicated by the horizontal lines. Crack sizes 25 mm (top left), 30 mm (top right), 35 mm (bottom left), 40 mm (bottom right). From [10.8].

10.5. Rail crack growth

Crack growth rate may be quantified using the Paris law

$$\frac{\mathrm{d}a}{\mathrm{d}N} = C\left(\Delta K_{\mathrm{I}}\right)^{n} \qquad (10.15)$$

Here da/dN is the crack growth per cycle, and C and n are material parameters; in this study they are taken as $C = 2.47 \cdot 10^{-9}$ and $n = 3.33$ for da/dN in mm/cycle and ΔK in MPa·m$^{1/2}$.

The stress intensity range ΔK can for the current case be evaluated as

$$\Delta K = \max_t\left[K_{\mathrm{Ib}}(t)\right] + K_{\mathrm{t}} - \max\left[\left(K_{\mathrm{It}} + \min_t\left[K_{\mathrm{Ib}}(t)\right]\right)\ ,\ \ 0\right] \quad (10.16)$$

Here t is the time during one wheel passage over the studied crack. As before fracture is presumed for $\max_t[K_{\mathrm{I}}(t)] \geq K_{\mathrm{Ic}}$.

10.5.1. Influence of overloads due to wheel flats

Wheel flats will induce high overloads, which may promote rail breaks. However, since the magnitude of the rail bending moment is so dependent on the impact position, most flatted wheels that pass will give little or no influence on ΔK_{b} and consequently on the rail crack growth.

As seen in Figure 10-11 the influence of flatted wheels on rail crack growth rate is negligible. On the other hand, the influence on rail break (in terms of crack length at fracture) is relatively marked.

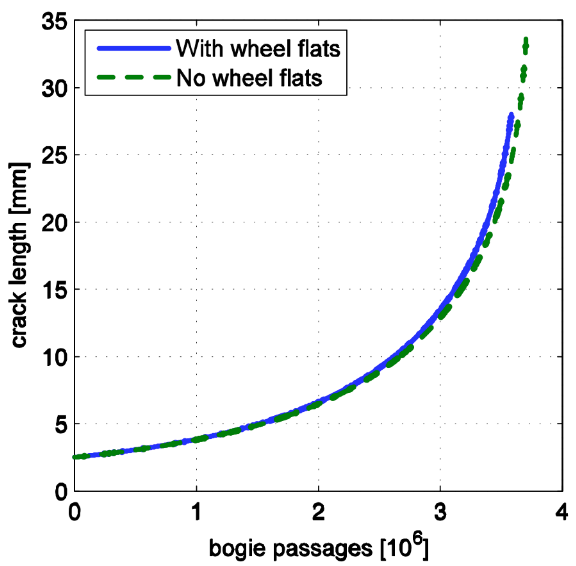

Figure 10-11 Comparison of rail head crack growth between operations with wheel flats (1 wheel out of 100 has a wheel flat of 100 mm length) and with perfectly round wheels. Rail temperature (below neutral) ΔT = 40 °C. The end of the graph corresponds to fracture. From [10.4].

Due to this limited influence of flatted wheels on crack growth rates, employed loads in the crack propagation analyses below are nominal wheel loads, corresponding to bending moments M_{quasi} of perfectly round wheels. Magnitudes of M_{quasi} are listed in Table 10-2 to Table 10-7 above. As an example, the positive and negative bending moments used for an analysis of foot crack growth on a heavy haul line with k_b=5 are 37 kNm and -25 kNm. For a head crack, the corresponding bending moments are 35 kNm and -26 kNm.

10.5.2. Influence of rail temperature

A temperature below the stress free temperature of the rail will induce a constant tensile stress, σ_t (see eq 10.9), resulting in a constant stress intensity factor, K_{It}. This will cause an increase in K_{Imax} leading to an increased risk for rail breaks, but also to an increased ΔK and corresponding crack growth as long as $K_{It} \leq |\min_t[K_{Ib}(t)]|$ (see eq 10.16).

Results from simulations in Figure 10-12 and Figure 10-13 show that the temperature influence is very marked down to a temperature where $K_{It} \leq |\min_t[K_{Ib}(t)]|$ after which it vanishes[1].

[1] This is not entirely true from a physical point of view since there will be a mid stress effect (cf section 10.6). However this effect is limited. Further details are available in textbooks on fracture mechanics.

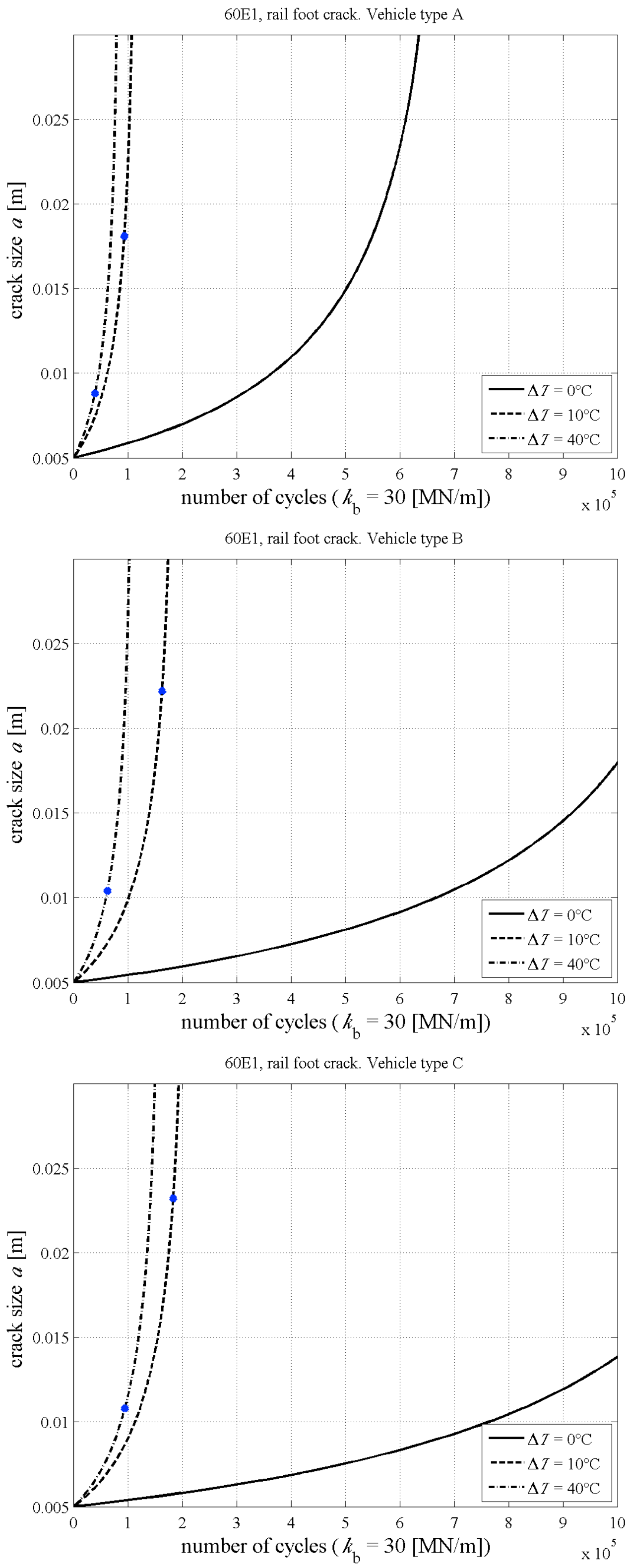

Figure 10-12 Influence of temperature (in terms of degrees centigrade below stress free temperature ΔT) on crack growth for 60E1 rail foot cracks due to nominal wheel loads. Ballast stiffnes k_b = 30 MN/m. Fracture marked by an x. Heavy haul vehicle (top), freight vehicle (mid) and passenger vehicle (bottom). From [10.8].

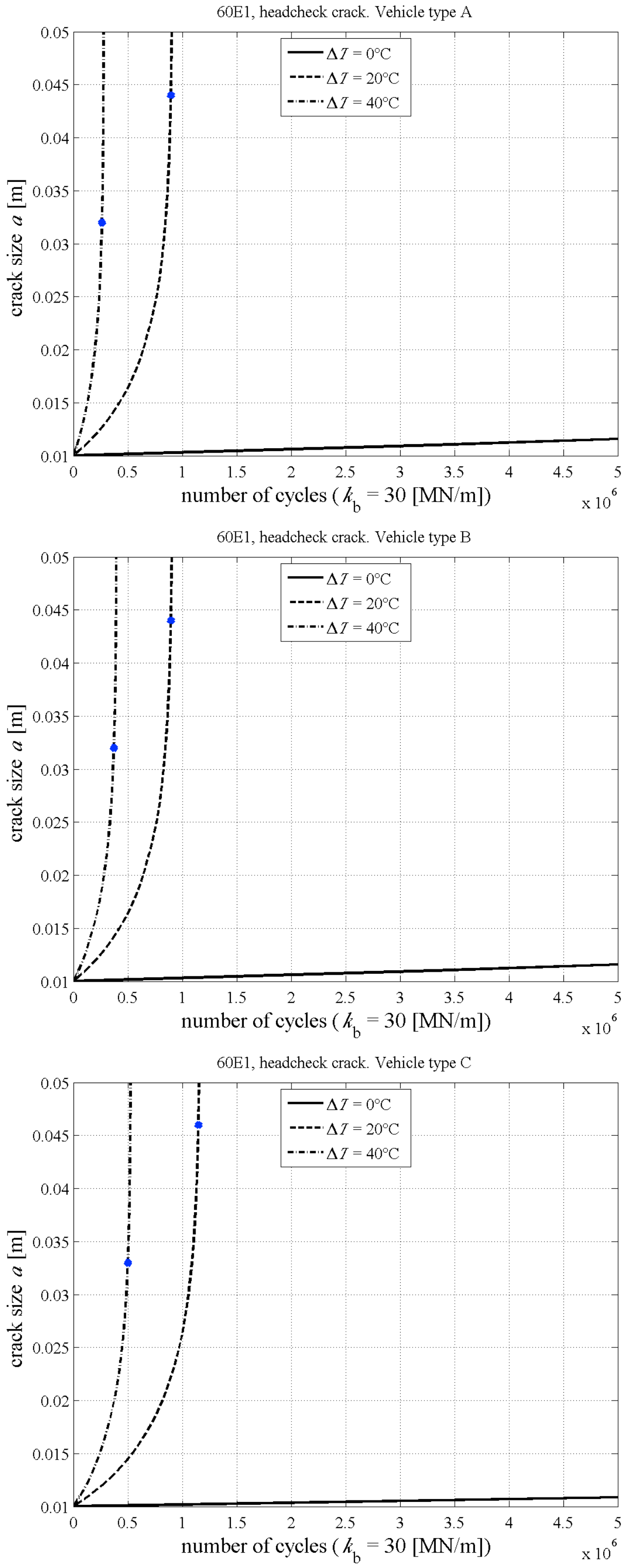

Figure 10-13 Influence of temperature (in terms of degrees centigrade below stress free temperature ΔT) on crack growth for 60E1 rail head cracks due to nominal wheel loads. Ballast stiffnes k_b=30 MN/m. Fracture marked by an x. Heavy haul vehicle (top), freight vehicle (mid) and passenger vehicle (bottom). From [10.8].

10.5.3. Influence of ballast stiffness

Results of crack growth predictions for different ballast stiffnesses are shown in Figure 10-14. Details of the simulations and results also for 50E3 rails are provided in [10.8].

It is seen that low ballast stiffness will increase crack growth rates. Further it is seen that heavy haul traffic corresponds to the highest, and passenger traffic to the lowest crack growth rates. These trends reflect the induced rail bending moments given in Table 10-2 to Table 10-7.

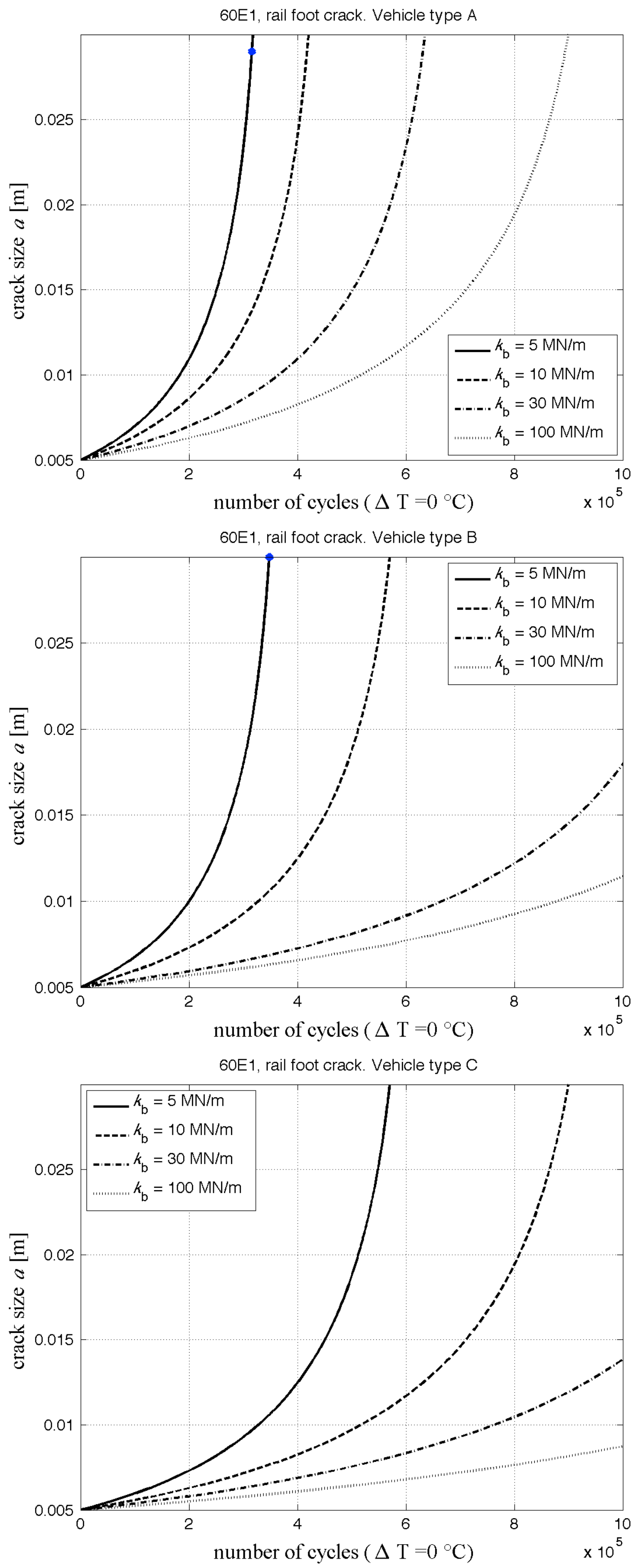

Figure 10-14 Influence of ballast stiffness, k_b, on crack growth for 60E1 rail foot cracks due to nominal wheel loads. Fracture marked by an x. Heavy haul vehicle (top), freight vehicle (mid) and passenger vehicle (bottom). From [10.8].

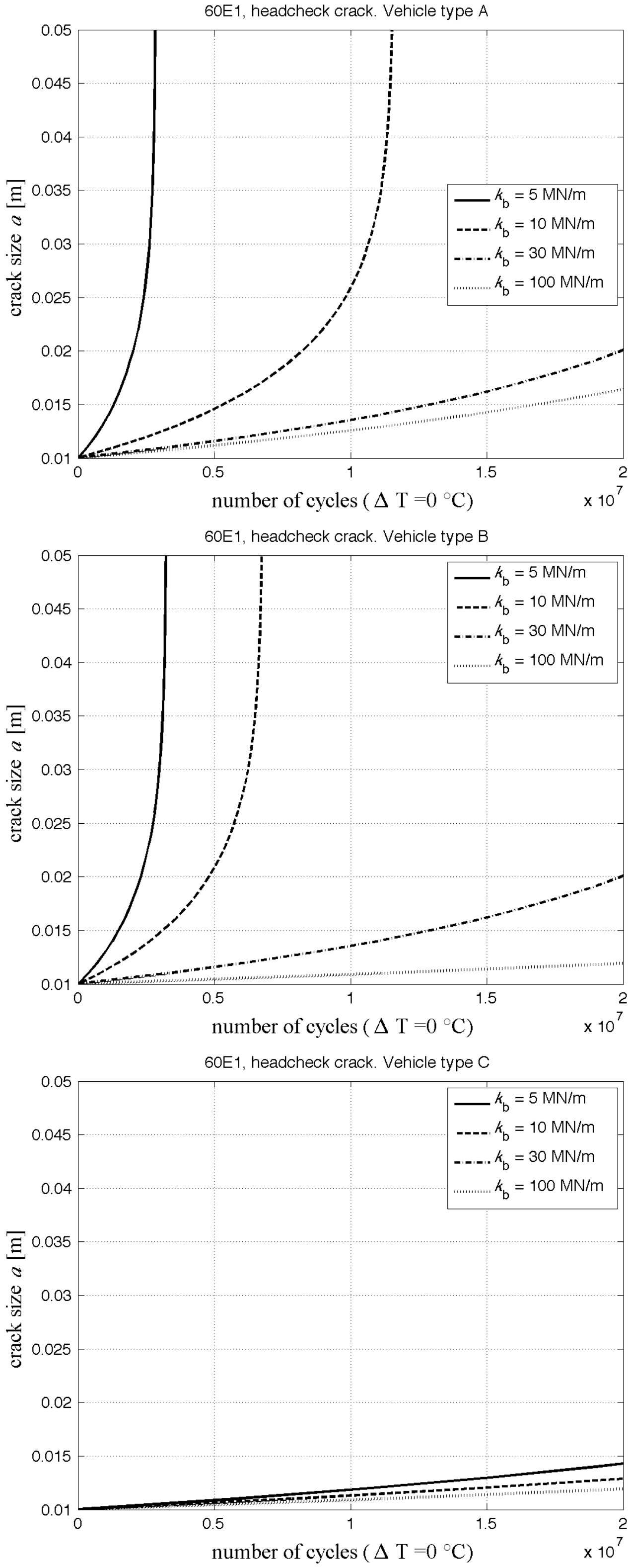

Figure 10-15 Influence of ballast stiffness, k_b, on crack growth for 60E1 rail head cracks due to nominal wheel loads. Fracture marked by an x. Heavy haul vehicle (top), freight vehicle (mid) and passenger vehicle (bottom). From [10.8].

10.5.4. Influence of hanging sleepers

In order to assess the influence of hanging sleepers on rail bending moments (and hence crack growth rates and risks of rail breaks), simulations featuring up to six unsupported sleepers have been carried out. Here the hanging sleepers have a 2 mm gap between the sleeper bottom and the ballast support. Results for "worst-case locations" of the hanging sleepers were identified and are reported in the following. Details of the simulations are provided in [10.3].

Figure 10-16 shows the influence of hanging sleepers on induced bending moments corresponding to an impact load of 250 kN. For comparison, corresponding bending moments for perfectly round wheels (i.e. factors β_0 and γ_0 in Table 10-2 to Table 10-7 above) are given.

It is seen that hanging sleepers will more or less remove the beneficial effect of high ballast stiffness. In particular this seems to be the case for high-speed operations (200 km/h in the current study).

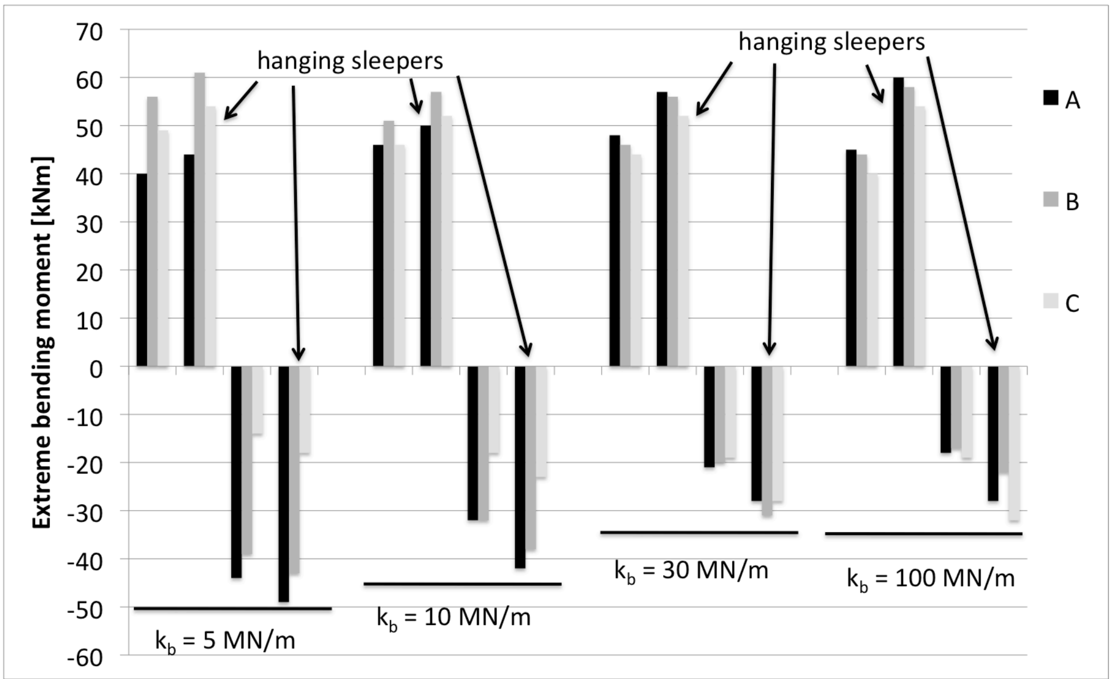

Figure 10-16 Extreme rail bending moments [kNm] due to the impact of a (worst-case) wheel flat with a maximum impact load of 250 kN. A, B and C denote "heavy haul", "freight" and "passenger" vehicles, respectively. Bending moments with hanging sleeper(s) in worst-case location(s) are compared to bending moments induced by "perfectly round" wheels. From [10.8].

The increased magnitude of bending moments due to hanging sleepers will be reflected in a higher crack growth rate and a higher risk of rail breaks. Simulations to exemplify this are presented in [10.8]. Figure 10-17 shows some examples of crack growth curves from [10.8]. The simulations feature wheel impact loads of 250 kN and are thus not comparable to the crack growth curves in sections 10.5.1 to 10.5.3 above. Instead crack growth curves for a wheel–rail contact force of 250 kN and homogeneous ballast stiffness are included in the figures for comparison.

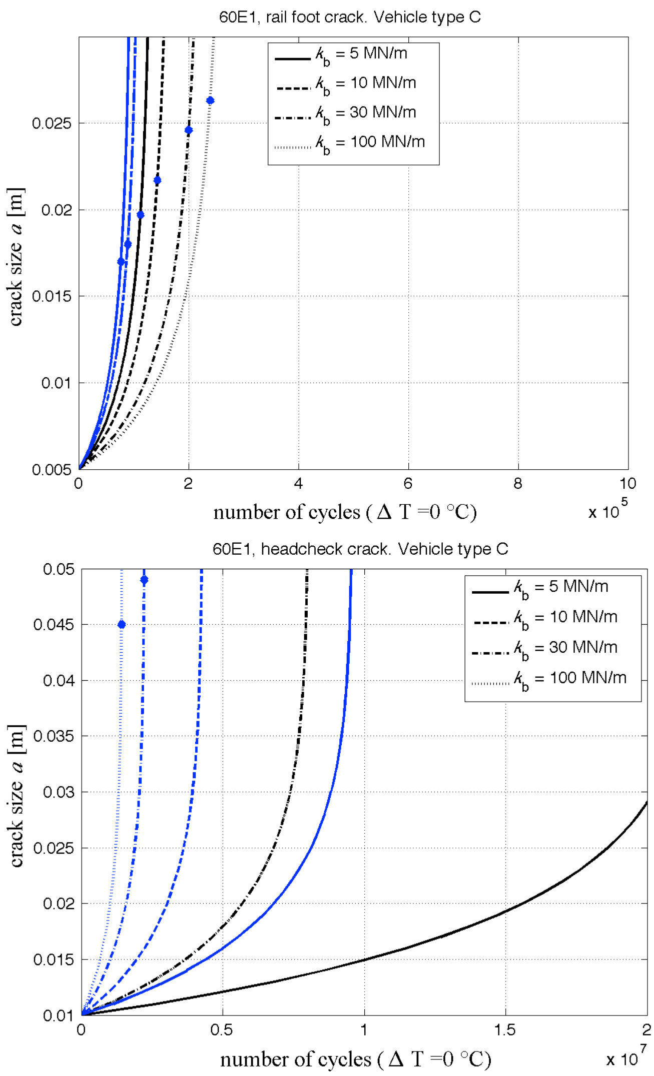

Figure 10-17 Crack growth and fracture (indicated by x) for the case of homogeneous ballast stiffness (black) and hanging sleeper(s) in worst-case position(s). Rail operated by passenger vehicles inducing wheel loads of 250 kN . Growth of rail foot crack (top) and rail head crack (bottom). From [10.8].

10.6. Influence of simulation assumptions

In the current study the material parameters employed for fracture mechanics studies are adopted from [10.9]:

- Fracture toughness, K_{Ic} = 40 MPa·m$^{1/2}$.
- Crack growth parameters: $C = 2.47\cdot10^{-9}$ and $n = 3.33$ for da/dN in mm/cycle and ΔK in MPa·m$^{1/2}$.

Adjustment for altered fracture toughness in the fracture analysis is a straightforward shift of the fracture limits in Figure 10-9 and Figure 10-10. To account for other crack growth parameters requires a re-calculation of the crack growth. In particular the magnitude of n will have a major influence as seen from the example in Figure 10-18.

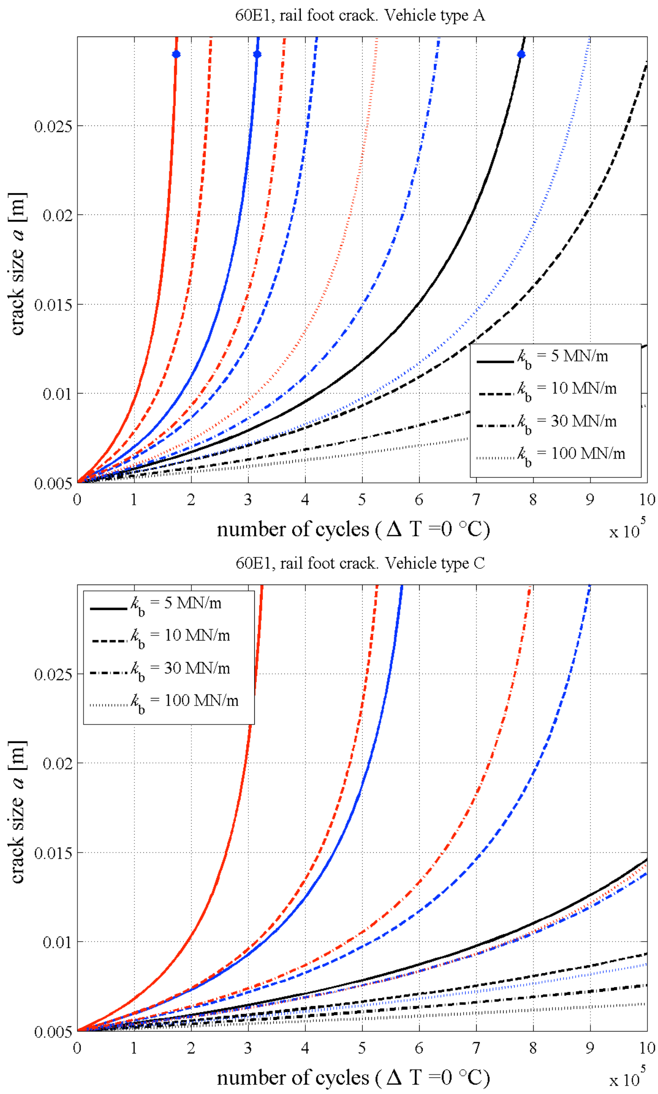

Figure 10-18 Rail foot crack growth due to passing heavy haul vehicles (top) and passenger vehicles (bottom). Crack growth exponent n=3 (black), 3.3 (blue) and 3.5 (red).

The crack growth simulations are non-conservative in that they do not consider any increased crack growth rate due to a positive mean stress (except from any related increase in ΔK), nor the acceleration in crack growth rate close to fracture. The reason these phenomena are not included is that they generally have limited effects and require additional material data that are often not available.

The choice of initial crack size will highly influence predicted number of cycles to fracture. For a head crack the modelling requirements for the crack to have branched transversally and to have grown out of the contact zone govern plausible size in the current study. For a rail foot crack, the choice is more open. The current choice of 5 mm may be overly conservative, but was employed to account for the risk of rails being damaged in service (e.g. due to crow-bar adjustments). For a rail, which is assured to be undamaged, it may be more plausible to presume an initial crack size in the order of 1 mm.

10.7. Conclusions

The following conclusions and recommendations relate to the studied configurations of vehicles and track. Details of these are given above and in INNOTRACK deliverable reports D4.2.1 [10.1] and D4.2.5 [10.2]. The conclusions may be extensible to other operational conditions, but this has not been verified within INNOTRACK.

10.7.1. Characteristics of wheel flats and wheel rail impact load

An analytical expression for wheel flat geometry at initiation and after subsequent flattening during operations has been derived from field measurements. *It is recommended to use the derived geometry as a standard in wheel flat analyses.*

Resulting wheel–rail contact forces have been measured in field. A numerical model has been developed and validated towards field measurements.

A simplified history for wheel–flat impact loads has been developed from measured wheel–rail contact forces and validated to yield accurate predictive results. *It is recommended to use this simplified history as a standard in simplified analyses of dynamic forces due to wheel flat impacts.*

"Worst case" loadings in terms of time parameters of the simplified load history have been evaluated from factorial design. These are vehicle and track dependent.

10.7.2. Bending moments in the rail

Bending moments predicted using the numerical model with simplified loads as described above have been validated against measured rail bending moments from full-scale in-field measurements.

Approximate expressions for quasi-static bending moments (positive and negative) in a rail due to a passing vehicle have been derived for three types of vehicles and four magnitudes of ballast stiffness.

Approximate expressions for extreme bending moments (positive and negative) in a rail due to wheel flat impact have been derived for three types of vehicles and four magnitudes of ballast stiffness. These expressions relate to "worst case conditions" in terms of wheel flat impact position and section of evaluated bending moment.

It is recommended that derived bending moment magnitudes be adopted as standard magnitudes (for relevant operational conditions) in case more detailed knowledge is missing.

10.7.3. Observations regarding crack growth and rail breaks

Approximate expressions for stress intensity factors for rail cracks have been derived. *It is recommended that these be adopted as standard approximations in the absence of more thorough analyses.*

Critical crack sizes (i.e., crack sizes for which fracture is likely) for head and foot cracks in the rail depend significantly on the temperature below the stress-free temperature. For cold conditions, critical crack sizes of roughly 1 and 3 cm are found for rail foot and rail head cracks, respectively. This is of the same order as for observed rail breaks (cf [10.8]).

Low ballast stiffness will lead to higher rail bending moments for nominal loads and normally also for wheel impact loads. Hanging sleepers will remove the beneficial effect of high ballast stiffness and should be avoided. In particular this seems to be the case for high-speed operations (200 km/h in the current study).

10.8. Recommended practices to avoid rail breaks

10.8.1. Establishment of allowable wheel impact loads

1. The operational characteristics of the considered track are established in form of vehicle characteristics, ballast stiffness etc.

2. Bending moments corresponding to nominal and flatted wheels are evaluated. As an approximation relevant bending moments from this report may be applied.

3. Fracture toughness and crack growth data of the rail steel are established. These material data should include a safety factor to account for scatter in material strength according to standard design practice.

4. Stress intensity factors as function of impact load magnitudes are evaluated for various crack sizes and plotted against fracture toughness reduced by the stress intensity due to thermal loading, see Figure 10-9 and Figure 10-10.

5. The allowed impact load magnitude is evaluated based on the condition that a fracture should not occur

   a. for a crack size that may exist in the rail, and

   b. for a temperature that the rail may have.

   Note that a higher alarm limit can be allowed if shorter crack sizes are assured to be detected e.g., by more frequent inspections (see below).

6. In countries where temperatures differ largely between summer and winter it is recommended to impose different allowed wheel impact loads for different seasons.

7. The introduction of multiple alarm levels for wheel impact loads (i.e. “maintenance limit(s)” and “restricted operation limit(s)”) is likely to decrease costs since it will

   a. limit vehicle damage,

   b. limit rail crack growth,

c. facilitate maintenance planning,
d. allow the transition between the different seasonal alarm limits to be carried out over a period and thus decreasing the risk of wheel damage "epidemics" (with related traffic interruptions) when a lower limit is imposed.

10.8.2. Recommended maintenance practices

1. Inspection intervals regarding rail cracks should be based on estimated crack growth rates e.g. those included in this guideline.
2. In such an analysis the initial crack size should be taken as the assured largest remaining crack size after an inspection. For a head crack it must also be assured that the chosen length does not invalidate the simulation presumptions of a limited influence of the contact stress field.
3. Inspection intervals regarding rail cracks should account for the increased crack growth rate during the cold season (as quantified in Figure 10-12 and Figure 10-13) and thus be significantly shorter during these periods.
4. Inspection intervals regarding rail cracks should ideally be chosen so that two inspections are planned before a predicted rail break. In practice this is very cumbersome due to the high uncertainties in operational conditions.
5. Track maintenance should ensure that the specified ballast and pad stiffness is maintained and that hanging sleepers are mitigated. It is recommended that the ballast stiffness per half sleeper should be kept above some 30 MN/m to limit crack growth.
6. Inspection intervals regarding hanging sleepers should be shorter the higher the specified ballast stiffness and speed is. Figure 10-16, Figure 10-17 and Figure 10-18 should be of aid in determining suitable inspection intervals.
7. Mitigation of hanging sleeper(s) and zones with low ballast and/or pad stiffness should be combined with an inspection for rail cracks.

8. Inspection for rail cracks should be carried out before the cold season to minimize the occurrence of larger cracks that may propagate to fracture.

10.8.3. Recommended documentation practices

1. Data that are vital to predicting crack growth and rail breaks and therefore should be documented on a track segment basis include (as a minimum):

    a. Track data: ballast stiffness; rail pad stiffness; rail, sleeper and fastening characteristics; material data for the rail (α, E, K_{Ic}, C, n)

    b. Vehicle data: axle load; axle distance.

    c. Wheel–rail contact forces in terms of maximum, minimum and nominal magnitudes and related vehicle types.

2. If a rail break occurs the above characteristics should preferably be investigated and documented together with crack morphology.

10.9. Bibliography

10.1 INNOTRACK Deliverable 4.2.1 – **Simplified relation for the influence of rail/joint degradation on operational loads and subsequent deterioration**, 22 pp, and 10 appendices, 27+25+10+12+6+8+7+7+25+4 pp, 2007

10.2 INNOTRACK Deliverable 4.2.5 – **Improved model for the influence of vehicle conditions (wheel flats, speed, axle load) on the loading and subsequent deterioration of rails**, 47 pp, and 6 appendices, 47+15+9+22+35+53 pp, 2009

10.3 Jens C O Nielsen, Elena Kabo & Anders Ekberg, **Alarm limits for wheel–rail impact loads – part 1: rail bending moments generated by wheel flats**, *Chalmers Applied Mechanics*, Research report 2009:02, 35 pp, 2009

10.4 Johan Sandström & Anders Ekberg, **Predicting crack growth and risks of rail breaks due to wheel flat impacts in heavy haul operations**, *IMechE Journal of Rail and Rapid Transit*, vol 223, no 2, pp 153–161, 2009

10.5 Jens C O Nielsen & Annika Igeland. **Vertical dynamic interaction between train and track – influence of wheel and track imperfections**, *Journal of Sound and Vibration*, vol 187, no 5, 825–839, 1995

10.6 Jens C O Nielsen, Jonas W Ringsberg & Luis Baeza, **Influence of railway wheel flat impact on crack growth in rails**, *Proceedings 8th International Heavy Haul Conference*, Rio de Janeiro, Brazil, pp. 789–797, June 2005

10.7 Elena Kabo, Anders Ekberg & Jens C O Nielsen, **Analysis of static fractures of rails due to wheel flats**, *Chalmers Applied Mechanics*, Research report 2009:01, 22 pp, 2009

10.8 Anders Ekberg, Elena Kabo & Jens C O Nielsen, **Alarm limits for wheel–rail impact loads – part 2: analysis of crack growth and fracture**, *Chalmers Applied Mechanics*, Research report 2009:03, 53 pp, 2009

10.9 Banverket, **30 ton på Malmbanan – Rapport 4.4: Underhåll, spårmekanisk analys, Appendix 1**, 15 p, 1996 (in Swedish)

11. Large cracks: probabilistic approach

11.1. Motivation for the probabilistic approach

Historic practice in the UK was to base the frequency of ultrasonic inspection on the ‘track category’, this defining, in broad terms, the level of usage and speed of trains over a particular route. The 'minimum actions' however, were the same, regardless of track category. Thus on a rural branch line with a small number of light axle load vehicles per day, the action required, and the timescale for action was the same as that for a heavily used mixed traffic inter-city route. This anomaly prompted British Rail (BR) to initiate a research programme to evaluate the levels of risk implicit in these contrasting situations, with a view to optimising the use of resources – in other words achieving the optimum safety within the constraints of a finite budget.

In principle, this is straightforward. One establishes the crack size at detection, then, using fracture mechanics principles as in section 10, predicts the residual life under a particular traffic pattern. In practice, it is far from straightforward, even if one discounts the effect of wheel irregularities. Within a given track category, there will be a variety of traffic patterns, and thus of force histories on the rail. There will be variations in the rail sections used, and in the rail support stiffness: there will be variations on the crack size at detection, there will be variations in material properties etc., etc.

To make ‘worst case’ assumptions throughout leads to an unworkable situation: one stops the railway! The BR approach was therefore to quantify the risk using 'Monte Carlo simulation'. This approach involves building up a statistical distribution of the critical properties such as rail support stiffness, crack size at detection, libraries of representative traffic patterns etc. These are then sampled and the sample values used to make a deterministic prediction of the residual life of the rail from the time of detection. This process is then repeated a large number of times to produce a distribution of residual lives as a function of track category, thus enabling a comparison to be made of risk in the various situations.

The limitation of this 'first generation' approach was that a necessary input was the distribution of crack sizes at detection. This required the collection of a large number of rail samples for destructive examination. It also meant that the effect of changing the inspection frequency or of improving the method of inspection could not be evaluated. A 'second generation' approach was therefore developed.

This started with the premise that cracks start small, below the threshold of detection. At some point they will pass that threshold, but they will still not necessarily be found. That will depend on when the rail is inspected, which will be a random variable in relation to when the crack started to grow, and on the probability of detection as a function of crack size. The key input for this 'second generation' approach is therefore the probability of detection curve.

It is the second generation approach that has been adopted here. The work however goes beyond that undertaken by BR with the objective of demonstrating the scope of the approach by using it to look at the influence of impact force control limits on the fraction of foot defects that will result in breakage.

The practical limitations of the approach should be noted. The 'second generation' approach cannot be applied when there are large defects already present in the rail as a result of manufacture or installation. For example, whilst Monte Carlo simulation could in theory be applied to establish the distribution of the residual life of defective alumino-thermic welds, you would need to start with a crack size distribution, i.e. apply the 'first generation' approach. (One may also debate whether, in this instance, it would be useful to do this rather than adopt a pragmatic 'clamp and replace' approach).

The 'second generation' approach does not deal with initiation, hence it will predict the fraction of defects that are detected prior to fracture, but it will not predict how many rails will develop cracks. As an example, the method could be used to predict how a change from 50E3 rail to 60E1 would reduce the fraction of rails failing as a result of foot breaks, but it would not predict the change in the total number of defects initiated that might be expected to result from the change. A 'third generation' model, taking account of initiation, would be necessary in this case. Monte Carlo simulation is a very data hungry approach and one has to be aware that such a development would require a lot of additional data collection.

The method requires that there is a robust method of predicting crack growth rates. In the current state of development of our understanding of rolling contact fatigue crack growth, for example, it is very debatable whether this is the case.

A fuller description of the method is given in (Allen, 2007)

11.2. Deterministic prediction of crack growth

Monte Carlo simulation (in this context) involves the repeated execution of deterministic predictions using sampled values of each variable to predict the fraction of defects that will be found before rail breakage occurs and, for those defects that are found, to create a distribution of residual life from the time of their detection. The general principles of this part of the work are the same as those described in chapter 10. However for completeness, and because some details differ, a summary of the process is given here. For the moment, impact loads will not be taken into consideration. This aspect is dealt with in section 11.4.

The traffic history for one day is represented by a sequence of wheel loads and wheel spacings. The Zimmermann equations are used to convert these into a rail foot stress history. This history is then ‘cycle counted’ using the ‘Rainflow’ process to create a matrix containing maximum and minimum values for each of these cycles, and the number of occurrences of each cycle (with the given max. and min. values) in one day's traffic. (Some filtering is now done to eliminate cycles, which would cause negligible damage and so speed up subsequent calculations).

Stress intensity factors are calculated for each maximum and minimum value for the current crack size.

The stress intensity factor associated with the residual stresses in the rail is estimated, for the current crack size, and added to those for the live loads. (In this instance the growth of a defect under the web of the rail is considered: the residual stresses at this location are much more significant than those at the edges of the foot, the case considered in chapter 10). The stress intensity factor associated with thermal loading is also calculated and added to those associated with the live loads. Thus for cycle ‘*i*’ of which there are n_i occurrences

$$K_{\max}(i) = K_{\max}(i_{\text{live}}) + K_{\text{residual stress}} + K_{\text{thermal stress}} \tag{11.1}$$

$$K_{\min}(i) = K_{\min}(i_{\text{live}}) + K_{\text{residual stress}} + K_{\text{thermal stress}} \tag{11.2}$$

The stress intensity factor range is now estimated for each 'live load cycle' as

$$\Delta K(i) = K_{\max}(i) - K_{\min}(i), \quad K_{\max} \geq 0, \; K_{\min} \geq 0 \tag{11.3}$$

$$\Delta K(i) = K_{\max}(i), \quad K_{\max} \geq 0, \; K_{\min} \leq 0 \tag{11.4}$$

$$\Delta K(i) = 0, \quad K_{\max} \leq 0 \tag{11.5}$$

The reason for adding in the static contributions before calculating ΔK may now be clear: the effect of a negative thermal or residual stress may be to reduce radically the stress intensity factor range experienced at the crack tip, and thus the growth rate. The converse will also apply if the residual or thermal stresses are tensile.

The growth rate for each of the 'I' cycles is estimated and the growth increments due to the N_i cycles summed to estimate the growth over the day. The crack geometry is then revised to take account of this, and the process repeated. Constraints are built into the computer code to ensure that, if the extent of growth predicted in any one day is greater than 1%, the growth step is reduced to a fraction of a day to ensure that this condition is complied with. (This '1%' condition ensures that, even though the crack dimensions will change during the period under consideration, the error in the stress intensity factor is negligible).

Stress intensity factors were estimated using the results of Newman and Raju (1979, 1981, see Bibliography) for flat plates in bending. To estimate the stress intensity factors for the overall bending of the rail, the 'plate thickness' was equated to twice the distance from the rail foot to the rail neutral axis, so that the stress gradient matched that in the rail.

On the centre line of the rail, the longitudinal residual stresses are a maximum at the surface and then decay in an approximately linear manner, reaching zero at a depth of the order of 25mm. In this case the stress intensity factors were based on the case of a flat plate of depth equal to twice the depth at which the residual stresses reach zero, again matching the stress gradient in the rail. (It can be shown that an alternative approach gives very similar values.)

Fracture is predicted when any value of $K_{\max}(i)$ exceeds the fracture toughness, K_{Ic} .

11.3. Thermal stresses

Rail temperature varies from minute to minute: indeed the stress free temperature (SFT) is far less a constant than was once thought! This sort of short-term variation would be impractically complex to model, and to some degree it would be so artificial to do so as to be meaningless. The approach adopted has therefore been to sample 'rail temperature' anew for each growth step. Effectively this means that during each day of the simulation the rail temperature is assumed to be constant, but the day-to-day variation of rail temperature matches the overall distribution of rail temperature observed in practice.

Account is also taken of the spatial and temporal variation of SFT, based on the limited data available.

11.4. Application to wheel impact load control

In broad terms, the effect of a wheel irregularity on a rail is comparable with hitting the rail with a hammer. Potentially a broad spectrum of vibration may be induced, but the frequencies of significance are those that correspond to specific vibrational modes in the wheel-rail system.

Historic research identified the low frequency 'P2' force maximum, where wheel and rail move down together, but the movement is increasingly resisted by rail and sleeper bending and ballast compression. This corresponds to frequencies in the range 30 - 100Hz. A 'P1' force maximum was also identified, this being associated with the wheel and rail moving in opposition and compressing the 'spring' that is the contact patch and corresponding to frequencies in the range 200 - 400Hz. At still higher frequencies the movements of the wheel and rail are uncoupled.

The response of the rail to low frequency and quasi-static forces can be predicted with reasonable accuracy by the so-called 'Zimmermann equations' wherein the rail is treated as beam on a continuous longitudinal elastic foundation. However in practice it is found that, when the track is modelled in this way, the effective support stiffness is not constant, but increases linearly with axle load. With this proviso, the Zimmermann equations provide a means for predicting the rail foot stresses under the action of quasi-static loads.

There is no experimental evidence to support the extrapolation of the load dependent stiffness relationships beyond static axle load levels, but this may be used as a working hypothesis for predicting rail bending moments and stresses under low frequency impact loadings.

As the previous section has demonstrated, predicting the response of the rail at higher frequencies requires a substantially more sophisticated and complex model. Whilst in theory there is no problem in building this type of model into a Monte Carlo simulation, in practice it would be very cumbersome to do so. However it is observed that the simple model proposed above, i.e. the prediction of moments and stresses using a force dependent stiffness, results in stress predictions that are in surprisingly good agreement with those measured in track and also those predicted using more sophisticated models. For the present therefore, this simplified approach has been used for the prediction of rail foot stresses as a result of impact loads.

The work reported in chapter 10, indicated that wheel impacts are expected to have a negligible effect on crack growth rates. This justifies a simplification of the process in that the crack growth increment over, say, one day can be estimated and then, as a separate exercise, the risk of breakage as a result of impact loading evaluated for that period.

As indicated in chapter 8, the current situation is that software has been written, implementing the above principles and some initial results have been obtained. It is anticipated that at a later date these will be published and will show how the following factors affect would the breakage rate, to demonstrate the capabilities of the technique:

- impact force control limits
- inspection frequency
- inspection capability
- traffic mix

The results presented will be for a specific site for which impact force data are in the public domain. However the software is still under validation, and it would be premature to present results.

11.5. Bibliography

Ahlbeck and Harrison, 1988	Ahlbeck, D.R. and Harrison, H.D., 'The effects of wheel/ rail impact loading due to wheel trear runout profiles'. Proc. 9th Int. Wheelsets Conference, Montreal, 1988, p. 6.1.1
Allen, 1982	Allen, R.J., 'Stress intensity factors for taches ovales in arbitrary stress fields' British Rail Research Tech. Memo. TM MF 47 (July 1982)
Allen & Sinclair, 1982	Allen, R.J., and Sinclair, J.C., 'The Behaviour Of Short Cracks' Fatigue & Fracture of Engineering Materials and Structures 1982 **5** (4), 343–347
Allen & Pang, 1993	Allen, R.J., and Pang, T.M., 'A Review of the Proposed Type Approval Test for Insulated Joints' BRR Report LM MF 107 (Sept. 1993)
Allen, 2003	Allen, R.J., 'Rail Management: Part 1: Local head Loss' Confidential report to Network Rail, March 2003
Allen, 2004	Allen, R.J., Rail Management: Part 2: 'Rail depth limits'. A review prepared for Network Rail, Jan 2004.
Allen, 2007	INNOTRACK Deliverable 4.2.2, 'Simplified relation for the influence of rail/joint degradation on operational loads and subsequent deterioration', 21 pp, and 4 appendices, 7+1+1+4 pp, 2007
Allen, 2008	Allen, R.J., 'A Scientific Basis for Minimum Actions. Flow Charts' Report prepared for Corus Rail Technologies, Dec. 2008
Anon, 1997	Anon, 'Wheel impact detection systems - the North American Experience' Zeta-Tech Associates, Suite Cherry Hill, New Jersey 1997, quoted by Nielsen and Johansson, 2000
Beagles, M., 1996	Beagles, M., 'Rail defect control: validation of JSTAR live load stresses'. BR Research Report RR-STR-96-020 (April 1996)
Beagles, M., 1996	Beagles, M., 'Rail Defect Control: Methodology for modelling the effects of Ultrasonic Inspection Period'. BR

	Research Report RR-STR-95-115 (April 1996)
Bold, P.E. 1990	Bold, P.E., 'The Calculation of Tache Ovale Growth Rates' Interim Report, Dept of Mechanical and Process Engineering, University of Sheffield, October 1990
Bold, P.E. 1992	Bold, P.E., 'The Calculation of Tache Ovale and Squat Crack Growth Rates'. SIRIUS Final Report, Sept. 1992
Cannon et al. 1972	Cannon, D.F., Walker, E.F., and Barr, R.R. 'The Fracture Toughness of Rail Steels' Iron and Steel Institute conference on Rail Steels, London 23.11.72
Cannon and Sharpe, 1983	Cannon, D.F., and Sharpe, K.A., 'Wheelflats and Rail Fracture'. British Rail Research Tech. Memo. TM MF 70 (Apl. 1983)
Esveld, 2001	Esveld, C., 'Modern Railway Track', 2nd Ed., Publ. MRT Productions, 2001
Hamilton and Watson, 1995	Hamilton, P.N., and Watson, A.S., 'Variation of track stiffness as a function of track type and axle load' BR Research Report RR-STR-95-081 (July 1995)
Hunt, 1996	Hunt, G.A., 'Development of a performance specification for rail pads'. British Rail Research Report RR-TCE-64, July 1996 (Report prepared for Railtrack plc.)
Hunt, 1998	Hunt, G.A., 'Track Engineering Seminar: The Track as a Structure'. AEA Technology Rail Report MR-TCE-036 Issue 1, May 1998
Irwin, 1957	Irwin, G.R., 'Analysis of stresses and strains near the end of a crack traversing a plate' Trans. A.S.M.E. (J. Appl. Mech) 1957 **24** 361
Jenkins et al. 1974	Jenkins, H.H., Stephenson, J.E., Clayton, G.A., Morland, G.W. and Lyon, D. 'The effect of track and vehicle parameters on wheel/ rail vertical dynamic forces' Railway Engineering J. 1974 _ 2 – 16
Matsuiski and Endo, 1968	Matsuiski, M. & Endo, T. (1969) Fatigue of metals subjected to varying stress, *Japan Soc. Mech. Engrg*. (presented at Kyushu branch meeting, March 1968)
Newman and Raju.	Newman, J.C., Jnr and Raju, I.S., 'Analyses of Surface Cracks in Finite Plates under Tension or Bending Loads' NASA

1979	Tech. Paper 1578 (Dec. 1979).
Newman and Raju. 1981	Newman, J.C., Jnr. and Raju, I.S., 'Stress-intensity factor equations for cracks in three-dimensional finite bodies' NASA Tech. Memo. 83200 (Aug. 1981).
Nielsen and Johansson, 2000	Nielsen, J.C.O., and Johansson, A., 'Out-of-round wheels – a literature survey'. Proc. I.Mech.E. 2000 **214 (**Part F) 79
Nielsen and Johansson, 2003	Johansson, A., and Nielsen, J.C.O., 'Out-of-round wheels - wheel-rail contact forces and track response derived from field tests and numerical simulations' Proc. I. Mech. E. 2003 **217** (Part F, J Rail and Rapid Transit) 135
Nielsen et al., 2008	Nielsen, J.C.O., Ekberg, A. and Kabo, E. 'Alarm limits for wheel-rail impact loads - simulation of rail bending moments cause by wheel flats'. Chalmers University draft report, 10.9.08
O'Connor, 1991	O'Connor, P.D.T., 'Practical Reliability Engineering', 3rd Edition, 1991
Paris et al, 1963	Paris, P.C., and Erdogan, F., Trans. A.S.M.E. (J. Basic Eng.) 1963 **85** 528
Roark, 1965	Roark, R.J., 'Formulas for stress and strain', 4th Ed., p. 155, McGraw-Hill Kogakusha, Ltd. 1965
Sandstrom and Ekberg, 2007	Sandstrom, J., and Ekberg, A., 'Predicting crack growth and risks of rail breaks due to wheel flat impacts in heavy haul operation' Chalmers Univ. 2008 (Also submitted for publication as part of the Proceedings of an International Heavy Haul Association specialist technical session, IHHA 2007)
Shah and Kobayashi, 1971	Shah, R.C., and Kobayashi, A.S., 'Stress intensity factor for an elliptical crack under arbitrary normal loading' Eng. Fract. Mech. 1971 **3** 71
Smallwood, 1994	Smallwood, R., 'Variable amplitude fatigue: testing and life predictions'. BR Research Report LR-MF-133, March 1994
Tada et.al. 2000	Tada, H., Paris, P.C., and Irwin, G.R. 'The Stress Analysis of Cracks Handbook', 3rd Edition, p. 52, Publ. ASME, 2000.
Timoshenko	Timoshenko, S., and Langer B.J., Trans. A.S.M.E. (J. Appl.

& Langer, 1932	Mech.) 1932 **54**(23) 277
Toth, L., 2000	Toth, L., 'Fracture properties of rail steels and their practical use'. Proc. Int. Symp. 'Schienenfehler', 16 - 17 Nov. 2000, Brandenburg an der Havel
Walton, 1988	Walton, K., 'Wheel/ rail impact loads'. British Rail Research Internal Memorandum IM MF 041 (April 1988).
Watson, 1990	Watson, A.S., 'The effect of loss of section on rail bending stresses'. BR Research Tech. Memo. TM MF 206 (October 1990)
Watson, 1991	Watson, A.S., 'Measurements of Service Strains in Plain Rail'. British Rail Research Technical Memorandum TM MF 205, March 1991
Watson, 1993	Watson, A.S., 'New criteria for rail renewal in tunnels' British Rail Research Report RR MF 042 (Jan. 1993)

12. Costs and LCC savings

To estimate life-cycle cost (LCC) savings related to the research reflected in this guideline is cumbersome. To a large extent this is due to the nature of the topics addressed: Fatigue phenomena (and to some extent wear) are mainly threshold problems. Up to a certain load level the deterioration is controlled and increases moderately with increased load. However when the threshold is increased the deterioration increases significantly, something often seen as a "failure epidemic". Loading should here be interpreted in a very broad sense.

The main challenge addressed in this guideline is to keep operational conditions as well as inspection and maintenance efforts balanced so that the condition of the railway is as close to the threshold as possible without exceeding it. In doing so, LCC savings may be obtained in several fields, some of which are (in increasing difficulty of quantifying costs):

- The lifetime of the components may be maximized
- Inspection and maintenance costs may be reduced by optimization (inspecting/maintaining the right thing at the right time), but also by a shift from corrective to pro-active maintenance.
- The reliability of the system will increase leading to higher traffic volumes and improved marketing opportunities.
- Cost of failures may be decreased regarding direct costs (damages, needed repairs etc), indirect costs (traffic interruptions etc) and long-term costs (decreased trust in the railway system).

As an example of the difficulty in assessing LCC costs it can be noted that the cost of a failure can range from more or less zero up to millions of Euros.

The issue of detailing LCC savings will be further addressed in the INNOTRACK sub-project 6 – LCC and RAMS assessment. To give some ideas of the costs involved, the sections below give an overview of costs mainly related to preventive grinding from DB's and ProRail's perspective.

12.1. Cost and LCC savings from DB's perspective

With the increase of traffic loads and train speeds, surface cracks occurred. First head checks at DB have been detected in the early nineties, only a few years after the first locomotive with three-phase asynchronous motors started operation. Since that time to date head checks became more and more a problem in track maintenance. Today, removal and prevention of head checks causes more than 90% of the rail grinding program of DB, which amounts to 40 Mio. EUR per year since 2007. Adding the remedy costs for failure removal by short segment rail replacement and the costs for long rail renewal due to severe head checks or squats, RCF causes maintenance costs of approximately 150 Mio. EUR per year.

While there is no natural balance between crack growth and material wear, artificial wear by cyclic grinding is the only possibility to prevent RCF. Therefore DB implemented a preventive grinding strategy in 2007 to minimise rail failures and to prolong rail life. Since then, rail grinding is an integral part of the overall maintenance and renewal strategy of DB. Main task of this strategy is the prolongation of track life in order to minimise Life-Cycle-Costs. With cyclical grinding, rails on tangent tracks and mild curves are supposed to reach a total lifetime of about 40 years, which is equal to the lifetime of sleepers and ballast. Due to a doubling of the grinding budget from 20 Mio. EUR in 2006 to 40 Mio. EUR per year since 2007 DB expect a significant cost reduction for short segment rail replacement and long rail renewal in the next years.

12.2. Cost and LCC savings from ProRail's perspective

ProRail maintenance budget increased by 4 times from 2001 till 2005 because of Head Checks and Squats. Too many small and unplanned renewals occured because of severe rail defects by RCF cracks. The main problem was a big increase of traffic (more than 7% per year) and new rolling stock (double deck trains).

On a yearly budget ProRail needs 60 Mio EUR for maintenance by grinding and renewals to manage RCF defects. Around 20 Mio EUR is needed for grinding actions. A grinding overview of different processes of grinding can be seen in Figure 12-1. Corrective RCF grinding and cyclic grinding are typically for RCF maintenance. Corrugation grinding is just a small budget. The idea is that cyclic grinding is the ultimate answer to manage an optimized budget to prevent RCF. Preventive grinding is needed to refurbish new rails to clean the rolling skin and building in defects etc.

ProRail grinding policy was born in 2005 and implemented since 2006. If ProRail had not used the current grinding policy, the RCF budget would have increased to more than 80 Mio EUR per year. Grinding is beneficial in matters of RCF and is proven in practice.

Programs to save budgets are still possible. To plan in a longer time span it is possible to combine small renewals in a bigger scope and savings can be made. Even grinding with smaller equipment (hand grinding machines) is possible. Some pilot tests have already been done. This will save more than 15% of the renewal budget for rail defects for ProRail.

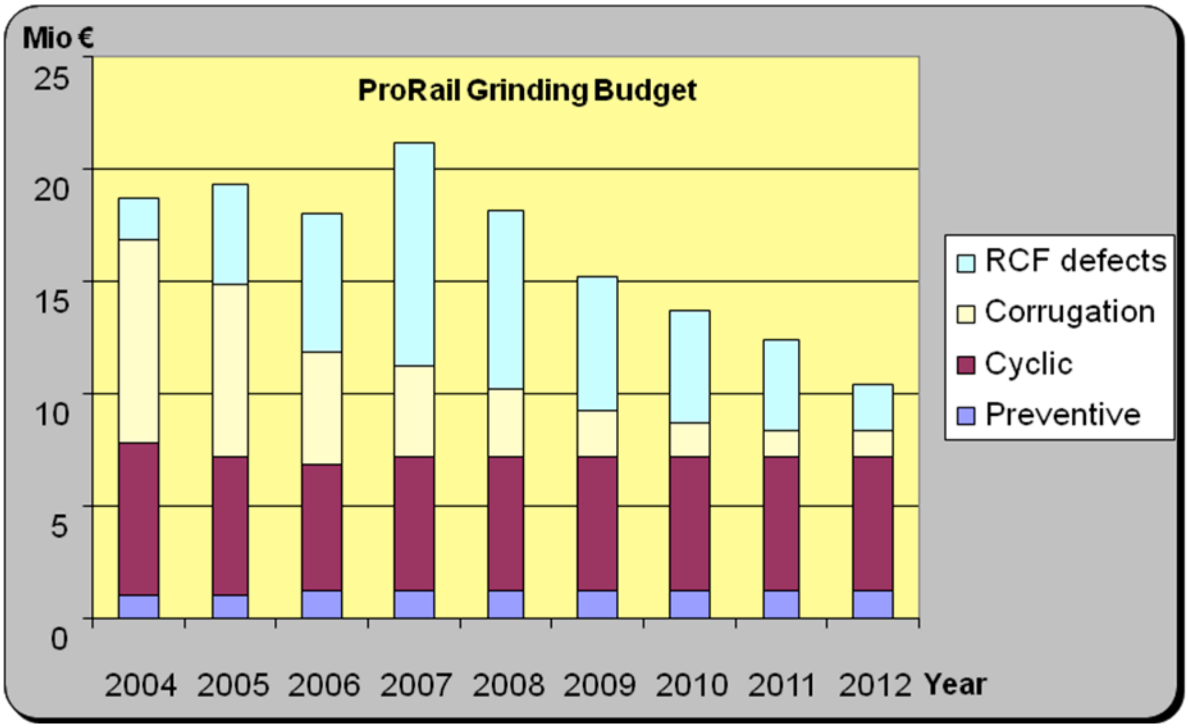

Figure 12-1 ProRail grinding budget for the near future.

13. Concluding remarks

This guideline is targeted towards implementation. It contains a basis for future handbooks, codes, leaflets and norms. Recommendations in the guideline are general, but often based on generic and/or selected operational conditions. To translate the recommendations into national and/or European practices and regulations there is therefore a need to reformulate the recommendations based on national conditions. To aid in this work, the guideline and references contain detailed backgrounds to the recommendations.

From a European perspective it can be noted that even for the rather similar railways investigated the current minimum actions differ significantly. Consequently any step towards harmonisation has to be based on a scientific basis such as provided in this guideline since the only alternative would be futile debates on which practices that are the “best”.

14. Annexes

1. Z. Li., X. Zhao, M. Molodova, & R. Dollevoet, **The validation of some numerical predictions on squats growth**, Proceedings *8th International Conference on Contact Mechanics and Wear of Rail/Wheel Systems*, Florence (Italy), September, 2009, vol 1, pp 369–377.

2. M. Molodova, Z. Li & R. Dollevoet, **Simulation of dynamic responses of vehicle-track system for detection of track short wave defects**, Proceedings *8th International Conference on Contact Mechanics and Wear of Rail/Wheel Systems*, Florence (Italy), September, 2009, vol 3, pp 1121–1128.

3. Z. Li, X. Zhao, and R. Dollevoet, **The determination of a critical size for rail top surface defects to grow into squats**, Proceedings *8th International Conference on Contact Mechanics and Wear of Rail/Wheel Systems*, Florence (Italy), September, 2009, vol 2, pp 379–388.

4. X. Zhao, Z. Li and R. Dollevoet, **Solution of the wheel-rail rolling contact in elasticity and elasto-plasticity using a transient finite element model**, Proceedings *8th International Conference on Contact Mechanics and Wear of Rail/Wheel Systems*, Florence (Italy), September, 2009, vol 3, pp 871–879.

5. Jens C O Nielsen & Anders Ekberg, **Acceptance criterion for rail roughness level spectrum based on assessment of rolling contact fatigue and rolling noise**, Proceedings *8th International Conference on Contact Mechanics and Wear of Rail/Wheel Systems*, Florence (Italy), September, 2009, vol 2, pp 409–418.

6. Jóhannes Gunnarsson, **Numerical simulations of the plastic deformation of insulating joints**, MSc Thesis 2009:15, *Chalmers Applied Mechanics*, Gothenburg, 2009, 33 pp